NAZARBAYEV UNIVERSITY

DEVELOPMENT OF CELL-PENETRATING NANOPARTICLES FOR DRUG DELIVERY

by

Balnur A. Zhaisanbayeva

Submitted in partial fulfilment of the requirements for the degree of Doctor of Philosophy in Science Engineering and Technology

Date of Completion

March, 2024

Development of cell-penetrating nanoparticles for drug delivery

by

Balnur A. Zhaisanbayeva

Submitted in partial fulfilment of the requirements for the degree of
Doctor of Philosophy in Science Engineering and Technology

School of Engineering and Digital Sciences
School of Sciences and Humanities
Nazarbayev University

Supervised by
Prof. Gonzalo Hortelano
Prof. Ivan Vorobyev
Prof. Ellina Mun
Prof. Vitaliy Khutoryanskiy

March, 2024

Declaration

I, Balnur A. Zhaisanbayeva, declare that the research contained in this thesis, unless otherwise formally indicated within the text, is the author's original work. The thesis has not been previously submitted to this or any other university for a degree and does not incorporate any material already submitted for a degree.

Signature: 

Date: 11.06.2024

BLANK

ABSTRACT

Recently, there has been a growing interest in nanoparticle-related pharmaceutical and biomedical research. Anticipated outcomes of such applications include the development of *in vitro* and *in vivo* diagnostics kits, improved biocompatible materials production, and advancing drug delivery systems.

In the realm of inorganic nanoparticles, silica or materials coated with silica exhibit potential for biomedical applications due to their small size, stable chemical structure, colloidal stability, and high surface reactivity. Despite the growing interest in silica nanoparticles, little is known about their toxicity resulting from the various synthesis methods; thus, recent findings often contradict each other. Moreover, most synthesis studies need more information about nanoparticle behaviour in the physiological environment, making it challenging to understand the biological effects of these nanoparticles for further clinical trials. Therefore, a newly emerging approach, safe-by-design, is starting to play a crucial role in developing nanoparticles for biomedical sciences.

This dissertation explores organosilica nanoparticles synthesised from 3-mercaptopropyltrimethoxysilane (MPTS) for potential biomedical applications as a drug delivery system. The work involves extensive characterisation and toxicological evaluation of organosilica nanoparticles with thiol groups on the surface. The experiments have underscored the safety of organosilica nanoparticles through comprehensive *in vitro* and *in vivo* assessments. The further potential use of these nanoparticles was explored by covalently attaching cell-penetrating peptide (TAT) and anticancer drugs (doxorubicin). The findings of this work demonstrated that the functionalised nanoparticles changed the function of thiolated nanoparticles, and conjugated drugs continued to be effective and retain their properties.

BLANK

ACKNOWLEDGEMENTS

My sincere appreciation goes out to the supervisory committee - Professor Vitaliy Khutoryanskiy, Professor Ivan Vorobyev, Professor Gonzalo Hortelano, and Dr Ellina Mun— I have been incredibly fortunate to receive their support and guidance throughout my PhD journey. Professor Vitaliy Khutoryanskiy allowed me to train in his laboratory, culminating in this PhD thesis, and introduced me to the captivating realms of nanoparticles and polymers. Professor Ivan Vorobyev guided me into the world of microscopy and offered crucial support at the outset of my PhD endeavour. Professor Gonzalo Hortelano consistently provided guidance and advice during my research journey, believing in me as an independent scientist. Dr Ellina Mun allowed me to work in her group, offering endless support in my research and the challenges of PhD life. I would like to convey my appreciation to the research group for their invaluable support in conducting the experiments, and I give special thanks to Alua Imantay and Nariman Mashurov.

My appreciation is also extended to professors from the Biology Department, SSH —Dr. Tri Pham guided and taught me to enhance my microscopy and laboratory skills. I sincerely appreciate Dr Sholpan Askarova's laboratory, particularly Dr Bauyrzhan Umbayev and Dr Farkhan Olzhayev, for their invaluable assistance during the *in vivo* experiments. I especially want to thank Dr. Bauyrzhan Umbayev for generously sharing his expertise in *in vivo* imaging, animal handling, and histology.

I thank the Nazarbayev University Core Facilities for granting me access to top-notch equipment. It was a pleasure to work and learn from the Core Facility staff, particularly Dr. Aleksandr Arbuz and Nurgul Daniyeva, who provided training on TEM and SEM and supported me as a young researcher. I appreciate the Department of Material Science's assistance with XPS measurements and the Chemistry Department's support with NMR and TGA.

My family and friends have consistently supported and believed in me throughout my academic journey. I dedicate this work to my mother for her tireless support in all my decisions.

Contents

LIST OF TABLES

LIST OF FIGURES

LIST OF ABBREVIATIONS

NP	Nanoparticle
DDS	Drug Delivery Systems
TEOS	Tetraortosilicate
APTES	(3-aminopropyl)triethoxysilane
MPTS	3-mercaptopropyltrimethoxysilane
DMSO	Dimethyl sulfoxide
PEG	Polyethylene glycol
DTNB	5,5-dithio-bis-(2-nitrobenzoic acid)
PBS	Phosphate-buffered saline
AFM	Atomic Force Microscopy
SEM	Scanning Electron Microscopy
TEM	Transmission Electron Microscopy
XPS	X-Ray Photoemission Spectroscopy
FTIR	Fourier-transform infrared spectroscopy
GA	Glutaraldehyde
NHS	N-hydroxysuccinimide
TGA	Thermogravimetric analysis
DLS	Dynamic light scattering
SDS-PAGE	Sodium Dodecyl Sulphate-Polyacrylamide Gel Electrophoresis
NMR	Nuclear Magnetic Resonance
Dox	Doxorubicin
DAPI	4′,6-diamidino-2-phenylindole
MSN	Mesoporous silica nanoparticles
CTAB	Cetrimonium bromide
FDA	Food and Drug Administration
TME	Tumour microenvironment
EPR	Enhanced permeability and retention
EM	Extracellular matrix
MONs	Mesoporous organosilica nanoparticles
GSH	Glutathione

BLANK

CHAPTER 1. INTRODUCTION

Cancer is a widespread health condition characterised by abnormal cell division and the second-largest cause of mortality globally (Siegel, Miller and Jemal, 2020). Carcinogenesis arises when healthy cells accumulate mutations that disrupt the growth, metabolism and death of cells. The following hallmarks can distinguish cancer cells: deregulation of growth factors, insensitivity to anti-growth signals, avoidance of cell death pathways signalling, angiogenesis, metastasis, altered energy metabolism to support cancer cell growth, and evasion from the immune response (Hanahan and Weinberg, 2011). Those cancer cell hallmarks act as targets in developing treatment methods. Current treatment protocols involve precise staging of cancer, which is followed by the prescription of radiotherapy, chemotherapy, surgery and hormonal therapy depending on the type of cancer (Hanahan and Weinberg, 2011). However, radiotherapy and chemotherapy cause various side effects, such as fatigue, weight loss, and different health conditions that deteriorate patient compliance. The main reason for the side effects is the effect of therapeutic agents on healthy cells surrounding tumour sites. To reduce the side effects and improve the activity of the chemotherapeutics, precise delivery of the drug should be carried out. As one of the most promising emerging fields, nanomedicine is bringing about a profound change in the fight against cancer. Growing interest is shown in new drug delivery systems (DDS), particularly those based on nanoparticles. Due to their high drug-loading capacity, specialised release properties, and a variety of engineered uses, synthetic nanoparticles (NPs) are being researched and made more well-known

1.1. CANCER AND DRUG DELIVERY SYSTEMS

Cancer is a genetic disease that arises from cellular DNA corruption, resulting in abnormal gene expression. The accumulation of mutations is the primary mechanism of change, though non-mutational (epigenetic) changes are increasingly recognised as necessary. Tumour suppressor genes and oncogenes, which both have vital roles in healthy cells, are the two gene classes that cause cancer. Activating mutations in proto-oncogenes are responsible for uncontrolled cell division, improved survival (even after anti-cancer treatment), and the spread of cancer. When a gene gets duplicated numerous times on a chromosome but maintains its original sequence, it is known as an oncogenic mutation (N-MYC, also called MYCN in neuroblastoma).

In cancer, mutations that activate proto-oncogenes result in unregulated cell division, increased cell survival (even following anti-cancer treatments), and metastasis. In 2000, Hanahan and Weinberg outlined six essential alterations (such as independence from growth factors, evasion of growth inhibitors, resistance to cell death, angiogenesis, preservation of replicative capacity, invasion, and metastasis) that predominantly account for the malignant characteristics of cancers. (Douglas Hanahan and Robert A. Weinberg, 2000). In 2011, two more new cancer hallmarks were described - reprogramming energy metabolism and avoiding immune destruction, which enables the common cancer traits such as genomic instability and inflammation (Hanahan and Weinberg, 2011).

Genetic instability and inflammation are two pivotal enabling traits fundamental to the progression of cancer. Genomic instability denotes the state wherein cancer cells relinquish control over their genetic material, accruing a myriad of mutational alterations that continuously reshape their biology and foster the hallmark features of cancer. The inherent conditions prevailing within the tumour microenvironment and the impacts of external anticancer treatments like radiotherapy, chemotherapy, targeted therapies, and immunotherapies contribute to the selection of cancerous cell clones. Intratumoral immune heterogeneity poses a substantial obstacle to current cancer therapies, as it furnishes tumours with a means to acquire resistance to treatments. Inflammation commonly arises as premalignant and malignant lesions induce an inflammatory milieu by attracting and activating immune system components. Nuclear factor kappa B (NFκB) has emerged as a pivotal mediator linking inflammation and cancer. NFκB is critical in tumour-associated macrophages and senescent cells, perpetuating and fostering tumour progression (Hanahan and Weinberg, 2011; Nenclares and Harrington, 2020).

Surgical and radiation therapy treatments are effective and efficient methods to treat non-metastatic cancers, but they are not effective when the cancerous cells has circulated to other parts of the body. Chemotherapy and hormone therapy are the most commonly prescribed treatments for metastatic cancers due to their ability to get to every organ in the body through the cardiovascular system. Chemotherapy medications generally exert their effects by inhibiting the rapid multiplication of cancer cells through the use of chemical substances. Nevertheless, they also interfere with the rapid growth required to maintain hair follicles, bone marrow, and gastrointestinal tract cells, causing unwanted side effects. This unspecific and, therefore, less strategic approach was changed after the discovery of cell signalling networks involved in regulating cell proliferation and differentiation in the late 1990s. This enabled the development of drugs that targeted

these networks and led to targeted therapy. (Pérez-Herrero and Fernández-Medarde, 2015).

1.2. NANOMEDICINE

Nanomedicine is a scientific area that uses nanotechnology for medical applications. This field involves using nanoscale materials, devices, and techniques to diagnose, treat, and prevent diseases. Nanoparticles' distinguished properties, including their high surface area-to-volume ratio and ability to cross biological barriers, make them promising tools for medical applications (Burgess, 2012).

Nanomedicine is an emerging field in medical society. Therefore, a proper definition of the term was required. In 2004, the European Science Foundation put forward a description of nanomedicine as the discipline encompassing the science and technology involved in diagnosing, treating, and preventing diseases and injuries, alleviating pain, and safeguarding and enhancing human health through the utilisation of molecular tools and insights into the molecular workings of the human body. (Sweeney, 2015). Since the emergence of nanomedicine, several drugs in the nanoscale have made it to clinics. Two of the first nanoparticle-based drug delivery systems were Doxil and Abraxane. However, many more studies are in the clinical studies stage and are being developed in laboratories worldwide (Dang and Guan, 2020; Rodríguez *et al.*, 2022).

Considering the extremely small size of nanoparticles and their ability to be modified to target particular sites, the benefits of nanoparticles cannot be denied. Moreover, in clinical practice, patients also benefit from the reduced toxicological side effects. That said, the proportion of nanomedicine that completed clinical trials was much lower than that of those being developed each year. Complex biological, pharmaceutical, and translational barriers can explain that. The main biological barriers include understanding the tumour, the permeability and penetration of particles and, importantly, the targeting mechanisms. Another difficulty arises in nanomedicine production: a researcher must consider many different aspects, such as the stability of composite in the bloodstream, biodistribution, the drug release kinetics and biodegradation of a carrier.

Some examples of nanomedicine applications include precision medication delivery, imaging, and sensing. Targeted drug delivery involves using nanoparticles to deliver drugs to specific sites in the body, such as tumours, while minimising the side effects on healthy tissues. Imaging applications include using nanoparticles as contrast agents for medical imaging techniques, such as magnetic resonance imaging (MRI) or

computed tomography (CT). Sensing applications involve using nanoparticles to detect biomolecules or other biological markers in the body, which can aid in diagnosing diseases.

Nanomedicine is a rapidly growing field with the potential to revolutionise healthcare by providing more effective and targeted therapies for various diseases. However, there are concerns about nanomedicine's safety and long-term effects, as well as ethical and regulatory issues surrounding its use.

1.3. STRUCTURE AND PROPERTIES OF ORGANOSILICA NANOPARTICLES

Silicon is among the prevalent elements on Earth, and the most frequent mineral in the Earth's crust is crystalline silica in quartz. Silicon is recognised as an essential nutrient, but adverse health effects have been linked to dust inhalation (Mebert *et al.*, 2017). Numerous studies have been conducted on the impact of silica exposure, especially crystalline silica (0.5–10 nm), on human health. Workers who are exposed to crystalline silica at work develop silicosis, a fibrotic lung disease that has been connected to pulmonary tuberculosis, emphysema, and lung cancer. However, because the toxicological potential of silica has been associated with its crystallinity up to this point, natural amorphous silica is widely considered less dangerous. (Murugadoss *et al.*, 2017).

Due to their natural abundance and biocompatibility, several materials containing silica and its oxides (e.g., silica, silicon dioxide, SiO_2) have been studied as nanostructures for biomedical applications. Silica is considered "generally safe" and the United States Food and Drug Administration (FDA) granted approval for use in the food industry as an adjuvant (Ways *et al.*, 2020).

The surface of inorganic silica nanoparticles contains silanol groups, enabling the formation of unstable hydrogen bonds with some pharmacological moieties. Nevertheless, because these associations are weak, they do not offer sufficient regulation over the release of drugs. Hence, current research aims to enhance silica nanoparticles by incorporating organic constituents into their framework (Xiong and Qiao, 2016; Yu *et al.*, 2018). Many researchers turn to so-called two-step synthesis to form organosilica nanoparticles. Tetraethyl orthosilicate (TEOS) is used as the nucleus in this procedure, and then organosilanes are added either throughout or following the synthesis to integrate organic groups (Roy *et al.*, 2005; G. *et al.*, 2014; Cheng *et al.*, 2019; Tsai *et al.*, 2019).

This approach is also employed to modify the outside surface of nanoparticles for functional purposes, enabling subsequent alteration with ligands or drugs.

Interestingly, organosilanes are rarely used as the sole source for synthesising silica nanoparticles. However, there is a potential in using organosilanes as a single source for nanoparticle production through a straightforward one-pot synthesis method, allowing for incorporating organic functional groups into their structure. One such instance is exemplified by nanoparticles synthesised from thiol-containing organosilanes, such as 3-mercaptopropyltrimethoxysilane (MPTS), as demonstrated by Nakamura et al. (Nakamura and Ishimura, 2007) and Irmukhametova et al. (Irmukhametova, Mun and Khutoryanskiy, 2011). Moreover, by altering the thiol-organosilane, such as 3-mercaptopropyltriethoxysilane (MPTS) or 3-mercaptopropylmethyldimethoxysilane (MPDMS), as well as the solvents and catalysts used, it becomes feasible to regulate the charge, shape and size of nanoparticles (Nakamura and Ishimura, 2008; Nakamura *et al.*, 2011; Al Mahrooqi *et al.*, 2018a). These nanoparticles are distinguished by thiol groups on the surface and in bulk, further linking various molecules to thiol groups.

The chemistry behind the synthesis of organosilica nanoparticles is a bottom-up approach based on sol-gel chemistry. Upon hydrolysis of silica precursor, silanol groups (-Si-OH) are formed, which further undergo condensation with other silanols of silanes ($Si(OX)_4$, where X represents ethoxy or methyl ester functional group) or organosilanes ($[Si(OX)_3]_n$-R, where R is an organic group). Upon condensation, the so-formed siloxanes (Si-O-Si) further grow into oligomers and aggregate, forming organic-inorganic material of silsesquioxane framework. Organic groups within the framework and outer surface of nanoparticles can be used to conjugate drugs or ligands through covalent, electrostatic and hydrogen bonds (Nakamura, 2018; Pietschnig, 2018; Cheng *et al.*, 2020).

Despite growing interest in the application of silica nanoparticles, their toxicity is not well understood, and recent findings often contradict each other. Several studies have investigated the toxicity of SiNPs *in vitro* and *in vivo*. SiNPs have been shown *in vitro* to cause oxidative stress, inflammation, and apoptosis throughout different cell types, including lung, liver, kidney, and skin cells (Yang *et al.*, 2009; Passagne *et al.*, 2012; Mendoza *et al.*, 2014; Guo *et al.*, 2015; Hadipour Moghaddam, Yazdimamaghani and Ghandehari, 2018; K. I. Lee *et al.*, 2020; Ahmadi *et al.*, 2022). However, the toxicity of SiNPs appears to be affected by several factors, encompassing surface charge, shape, size, concentration and cell type.

1.4. OBJECTIVES AND STRUCTURE OF THE THESIS

This project aims to formulate an organosilica-based nanoparticle functionalised with cell-penetrating peptides and anticancer drugs to facilitate cellular penetration into targeted cells while minimising cytotoxicity to other cells.

The objectives necessary to achieve the aim of this work are:

1. Review of the toxic effects of thiolated organosilica nanoparticles and evaluation of the impact of PEGylation. This chapter is a part of the published article in the “International Journal of Pharmaceutics”.

2. Development of a method for peptide conjugation to nanoparticles and methods to characterise functionalised nanoparticles.

3. Development of a protocol for conjugating anticancer drugs to organosilica nanoparticles and evaluate their properties.

The dissertation comprises six chapters, organised according to the tasks performed.

Chapter 1 briefly overviews current advances in nanotechnology in cancer therapy.

Chapter 2 discusses the role of organosilica nanoparticles in current cancer therapy and outlines their future potential in the biomedical field.

Chapter 3 presents the synthesis and characterisation of organosilica nanoparticles, along with their extensive *in vitro* and *in vivo* examination.

Chapter 4 reveals the successful conjugation of the cell-penetrating TAT peptide to the nanoparticle's surface.

Chapter 5 describes the effective conjugation of doxorubicin to the surface of nanoparticles through disulphide bridge formation.

Chapter 6 concludes the results from previous sections and discusses future perspectives and drawbacks of this study.

1.5. ROLE OF COLLABORATORS

The present dissertation represents a multidisciplinary study on developing novel safe-by-design organosilica nanoparticles for targeted cancer therapy. This research received support from the Ministry of Science and Higher Education of the Republic of Kazakhstan, Project Grant No. AP13068353.

All aspects of this thesis underwent a thorough review by the supervisory team, which includes Professor Vitaliy Khutoryanskiy, Professor Ivan Vorobyev, Professor Gonzalo Hortelano, and Dr. Ellina Mun.

Several components of this work were conducted in collaboration with Nazarbayev University (NU) members and the National Laboratory Astana. All *in vivo* experiments were carried out at the National Laboratory Astana under the supervision of Dr. Bauyrzhan Umbayev and Dr. Farkhad Olzhayev. Dr. Tri Pham performed AFM and live cell imaging experiments.

This thesis results from my work, and I am the sole author. Individual contributions are detailed in the author's contribution section, where applicable.

1.6. THESIS OUTPUT

Throughout the span of this study, a number of significant contributions were made.

- Establishment of toxicological profiles of thiolated organosilica nanoparticles and effect of PEGylation.
- Synthesis of drug-conjugated organosilica nanoparticles with glutathione-dependent drug release kinetics.
- Synthesis and characterisation of peptide-conjugated organosilica nanoparticles.

Journal Articles

Zhaisanbayeva, B. A. et al. (2024) ‘In vitro and in vivo toxicity of thiolated and PEGylated organosilica nanoparticles’, International Journal of Pharmaceutics. Elsevier B.V., 652(January), p. 123852. doi: 10.1016/j.ijpharm.2024.123852.

Conference Presentations

Balnur A. Zhaisanbayeva, Ellina A. Mun, Ivan A. Vorobjev, Gonzalo Hortelano, Vitaliy V. Khutoryanskiy. “Evaluation of cytotoxicity of thiolated organosilica nanoparticles and the effect of PEGylation on toxicity reduction”. NanoMedicine International Conference 2021. Online, October 2021 (Abstract).

BLANK

CHAPTER 2. LITERATURE REVIEW

2.1. CANCER AND CURRENT TREATMENT

Cancer, ranked as the second leading cause of death worldwide, presents a significant and pressing issue in the field of public health (Siegel, Miller and Jemal, 2020). There is a substantial financial, psychological, and physical cost associated with cancer, which affects not only people but also families, communities, and healthcare systems globally. Social and economic disparities arising from variations in income, education, housing, employment, dietary habits, cultural factors, gender, ethnicity, and environmental conditions exacerbate this burden. Populations encountering social and economic disadvantages face inferior outcomes, as they are more prone to developing treatable cancers diagnosed at advanced stages, resulting in poorer prognoses and restricted access to treatment options (André Ilbawi, 2020).

In order to effectively fight cancer, it is essential to have a thorough understanding of the fundamental processes that contribute to its formation. Cancers arise from somatic cells with genetic defects that disrupt the usual mechanisms regulating DNA replication and cell division. Although malignant cells possess complex genetic characteristics, they exhibit a typical phenotype that allows for differentiation between various kinds of disease. The most prominent feature of cancer is its uncontrolled proliferation, which sustains its invasive capacity and lethality. Most cancer cells include metabolic alterations that enable survival in hostile settings that are typically lethal to normal cells. This adaptation allows cancer cells to proliferate continuously (R A Cairns, I Harris, S McCracken, 2011).

2.2. TARGETING DRUG DELIVERY SYSTEMS

Targeted drug delivery systems involve administering medications to particular organs, tissues, or cells. These systems aim to enhance the effectiveness of pharmaceuticals and minimise adverse effects by administering drugs specifically to the affected region instead of the entire body. Nanoparticles have been studied for multiple administration routes based on the physiological and biochemical properties of the drug and nanocarrier. Each route of administration has unique properties and barriers that can be overcome by precise nanoparticle design. Traditional drug delivery methods include oral, parenteral, nasal, pulmonary, transdermal, and rectal or vaginal routes (Figure 2.1.).

Depending on the route of administration, the pharmacokinetics of the drug may vary; moreover, the absorption and bioavailability of the drug may also be influenced by the composition of the target site (Eun Ji Chung, Lorraine Leon and Carlos Rinaldi, 2020; P. V. Mohanan and Sudha Kappalli, 2023). To address these issues, nanoparticles can be designed to achieve passive or active targeting systems.

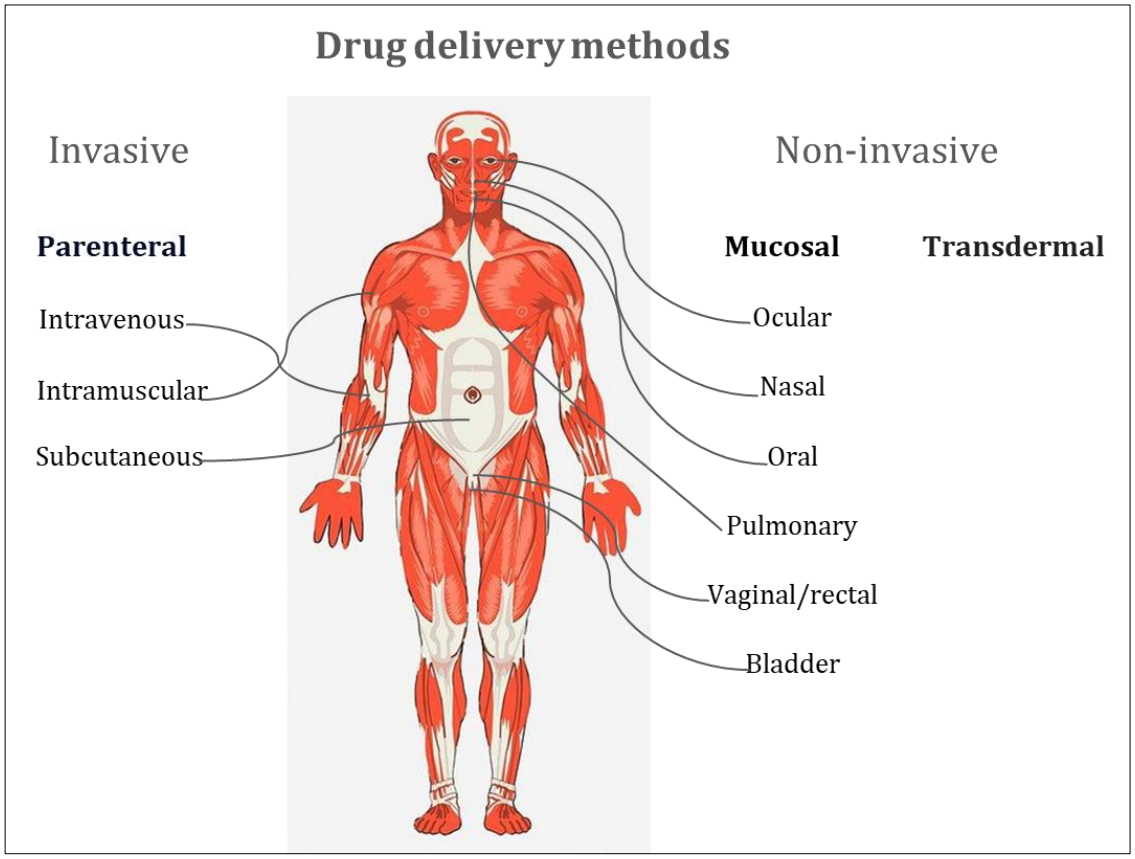

Figure 2.1. Routes of drug administration.

Passive targeting relies on the drug's physical and chemical properties, allowing it to accumulate in specific cells or tissues, such as hydrophobic drugs in fatty tissues. Active targeting employs ligands or antibodies attached to the drug delivery system to target cells or tissues specifically. Triggered targeting releases drugs at specific sites triggered by external stimuli, like light or heat, suitable for hard-to-reach areas like tumours. A localised targeting approach directly delivers medications to the affected area, as seen in administering drugs to incision sites during surgery.

Nanoparticles are excellent carriers for delivering chemotherapeutic drugs due to their characteristics, including poor solubility, enhanced toxicity, short lifetime when administered, accumulation on healthy organs, unspecific action, and multidrug resistance (Golombek *et al.*, 2018). Encapsulation of chemotherapeutic agents into nanoparticles prolongs blood circulation time, increasing treatment efficiency. Modifying

the surface of mesoporous silica nanoparticles (MSNs) allows for the modulation and control of biodistribution and localisation. This, combined with reduced doses and administrations, can significantly reduce the toxic adverse consequences of chemotherapy and ameliorate patient compliance (Aminu *et al.*, 2020).

Specific delivery can be achieved by increasing the circulation time of nanoparticle-drug conjugates; however, it is crucial to manage the medication's release method. Precise drug delivery can be achieved through passive and active targeting.

Passive targeting relies on specific properties of the tumour microenvironment (TME). Inflammation and hypoxia on the tumour site induce disruptions in the endothelium of blood vessels, making them more permeable due to hypoxia and the need for oxygen and nutrients for a tumour to grow and spread from new vessels or engulf existing ones. Newly organised vessels characterised as chaotic, with a high number of pores, allow the penetration of large molecules of size more than 40kDa (Attia *et al.*, 2019). Moreover, TME has an abnormal lymphatic drainage system, contributing to nanoparticle accumulation on a tumour site. However, small-sized drug molecules can easily wash out from the site; thus, drug encapsulation may prolong active molecules' activity (Golombek *et al.*, 2018). This enhanced permeability and retention (EPR) effect is a possible way of nanoparticle accumulation in TME.

Furthermore, due to the defective function of a lymphatic drainage system, elevated angiogenesis with leaky vessels and fibrosis of the interstitium in solid tumours evolve high interstitial fluid pressure (IFP). The range of IFP in normal tissue is from -3 to 3 mmHg and is regulated by stromal cells and extracellular matrix (EM), while the IFP of a tumour can be from 2 to 10 times higher (Heldin *et al.*, 2004; Böckelmann and Schumacher, 2019). Usually, high IFP develops in the core of the tumour; thus, delivery specificity increases only by 20-30% compared to healthy organs (Attia *et al.*, 2019). High IFP leads to the return of the nanoparticles/drugs to the capillaries or the areas with low IFP. Moreover, this pressure difference causes metastasis development (Heldin *et al.*, 2004; Golombek *et al.*, 2018). Nonetheless, this obstacle can be overcome by reducing IFP, for example, with taxanes (Griffon-Etienne *et al.*, 1999), thus improving perfusion and allowing NP delivery to the core of the tumour.

The targeting strategy depends on nanoparticles' physicochemical properties and TME characteristics, as different tumour types have different pore sizes, permeability, and leakage processes, and some lack the EPR effect (Attia *et al.*, 2019). Besides, nanoparticles may be phagocytised by macrophages or form a protein corona (an

aggregation of plasma proteins on the NP's surface), which can change the behaviour of the NP. To avoid these issues, coating nanoparticles with polyethylene glycol (PEG) is highly practised (Zhang *et al.*, 2018; Li, H., Raehm, L., Charnay, C., Durand, J. O., & Pleixats, 2020). Besides, PEGylation can enhance passive targeting as PEG is a hydrophilic and biocompatible molecule that prevents nanoparticles from aggregating. Moreover, nanoparticles with sizes ranging from 20 to 100 nm have demonstrated better targeting of the tumour microenvironment (TME) (Kim *et al.*, 2014; Han *et al.*, 2020; J. G. Lee *et al.*, 2020). Several formulations relying on the enhanced permeability and retention (EPR) effect have received FDA approval, with Doxil, a liposome-encapsulated doxorubicin, being the first NP-drug conjugate approved in 1995. Other formulations, including Arbaxane, Myocet, DaunoXome, and Oncaspar, have also been approved or are under clinical trials (Pillai, 2014; Rosenblum *et al.*, 2018). However, passive targeting may not be the ideal approach for all tumours, prompting the exploration of active targeting.

Recognising the limitations of passive targeting, nanoparticles can be adorned with disease-specific ligands to facilitate active targeting. This involves attaching ligands to overexpressed receptors on the tumour cell membrane, such as transferrin, folate, and growth factor receptors, commonly used to target tumour cells (Pillai, 2014). Active targeting is crucial for delivering drugs, genes, and proteins to tumour cells while minimising the impact on normal and healthy cells. During the design of the delivery system, specific ligand parameters must be investigated, including targeting affinity, molecular weight, and biocompatibility.

2.3. ORGANOSILICA NANOPARTICLES AS DRUG DELIVERY SYSTEMS

Due to their straightforward and easily scalable synthesis method, the scientific community has expressed significant interest in silica, mostly in mesoporous silica nanoparticles (MSNs). This method produces nanoparticles with a large surface area, a well-organized structure, and a pore size that can be adjusted. Large volumes of therapeutic chemicals can be encapsulated in MSNs due to their unique pore shape, which protects them from early breakdown and prevents them from interacting with healthy cells (Wu *et al.*, 2016; Yu *et al.*, 2018). In addition, pore gatekeepers, such as polymers, enable the creation of a drug delivery system that precisely controls the release of drugs, hence improving the efficacy of anti-tumour therapy. Before the widespread use of MSNs in

drug administration, there are still significant issues that need to be addressed entirely regarding their biodegradation, biosafety, and excretion. Scientists have explored the potential for integrating organic components into the inorganic silica (Si-O-Si) matrix due to the advantageous properties of the organic drug delivery system, which exhibits both biological compatibility and biodegradable properties to the systems, such as micelles. Solid-lipid nanoparticles and liposomes (Yang, Chen and Shi, 2019a; Song *et al.*, 2022; Picchetti *et al.*, 2023). The diverse range of organosilane precursors provides extensive opportunities to tailor and enhance nanoparticle physicochemical characteristics and biological efficacy. Numerous hybrid silica structures have been created as a consequence of this investigation. They can be divided into two main categories: mesoporous organosilica nanoparticles (MONs), which combine both conventional silica and organosilica precursors, and periodic mesoporous organosilica (PMO), which is produced solely using organosilica precursors (Yang, Chen and Shi, 2019b; Li, H., Raehm, L., Charnay, C., Durand, J. O., & Pleixats, 2020; Tamanoi *et al.*, 2021).

Organosilica nanoparticles have specified pore sizes, a porous structure, and a size that can be controlled. Higher concentrations of medicinal agents, such as chemotherapeutic medicines, as well as more giant molecules, such as genetic material and proteins, can be loaded because of the enormous pore volume and changeable pore size (Yanjun Jiang, Huan Liu, Lihui Wang, Liya Zhou, Zhihong Huang, Li Ma, Ying He, Lujing Shi, 2019; Salekdeh *et al.*, 2021; Zhang *et al.*, 2021; Picchetti *et al.*, 2023). The specificity of treatments can be improved by using a stimuli-sensitive particle degradation mechanism regulated by the organic contents on the particle matrix. This prevents the therapeutic agents from degrading quickly inside the body (Guimarães *et al.*, 2020; Song *et al.*, 2022). Regulating the rate at which particles degrade improves the ability to manage the lifespan and elimination rates of nanoparticles of organosilica in the human body, thereby enhancing the safety of these drug delivery systems (Hadipour Moghaddam *et al.*, 2017; Luo *et al.*, 2019). Additionally, the structural adaptability of organosilica nanoparticles can be adopted to incorporate novel features into nanoparticles, such as photodynamic capacity, fluorescence and tumour targeting (Figure 2.2.) (Yu *et al.*, 2018; Feng *et al.*, 2022). One more benefit is the availability of many precursors for commercial use, making the synthesis technique easily scalable for large-scale production.

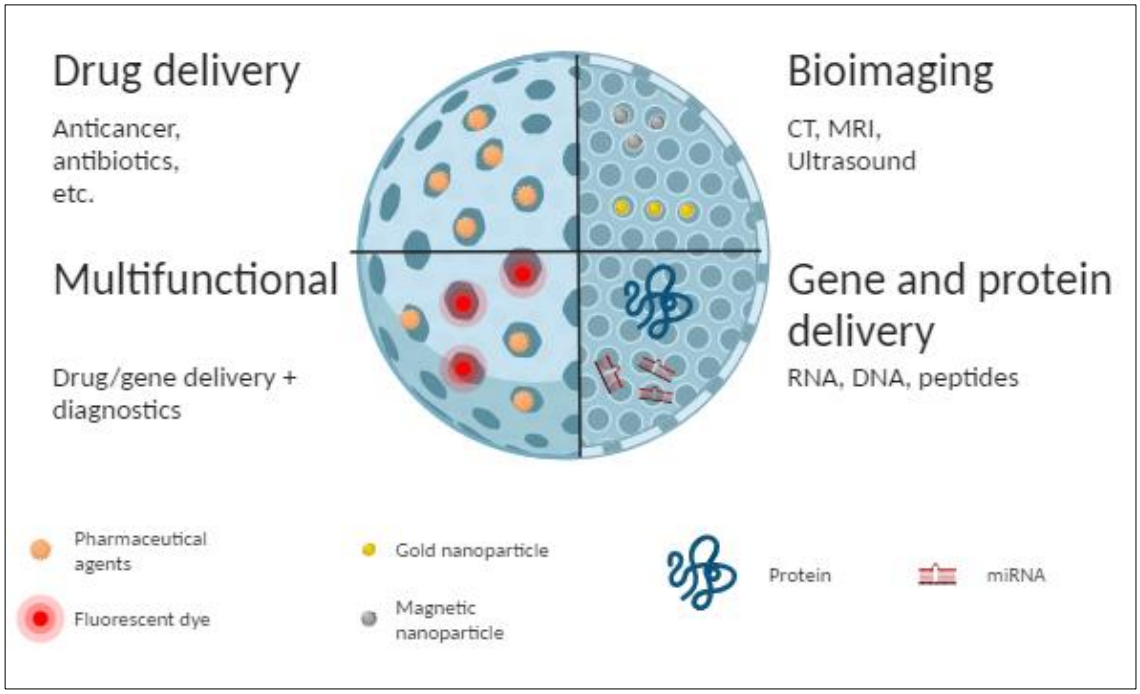

Figure 2.1. Modifications of mesoporous organosilica nanoparticles.

The presence of organic bridges notably alters the chemical characteristics of the silica matrix. Encapsulation of drugs within the pores of organosilica nanoparticles can be achieved using methods that disperse the nanoparticles and the drug, stimulating hydrophobic/hydrophilic or electrostatic interactions between the cavities of nanoparticles and therapeutic compounds (Mai *et al.*, 2023; Teng *et al.*, 2023). Conversely, identical organic bridges can facilitate the regulated drug release from organosilica nanoparticles by responding to specific stimuli, including temperature, redox potential, and pH. These stimuli can induce the disintegration or destruction of nanoparticles. Furthermore, the exterior of organosilica nanoparticles can be customised by attaching stimuli-responsive components that function as agents to block the pores and control the release of drugs when exposed to a particular stimulus (Guimarães *et al.*, 2020).

2.4. FUNCTIONALISATION OF ORGANOSILICA NANOPARTICLES

The nanoparticle's surface chemical composition significantly influences nanoparticles' toxicity and biological response. Several studies showed that Stöber silica nanoparticles induce ROS (reactive oxygen species), which generated cytotoxicity in vitro studies; also, the cytotoxicity is size- and time-dependent. For example, Si NPs induced the production of cytochrome *c* in the cytoplasm, which is the trigger of

apoptosis, increased ROS production and reduced expression of caspase-12, which triggers ER stress-induced cell death of alveolar epithelial cells (K. I. Lee *et al.*, 2020). Also, the concentration of silanol groups affects the cytotoxicity level of nanoparticles, ROS generation and hemolysis of red blood cells(Murugadoss *et al.*, 2017; Rubio *et al.*, 2019); therefore, controlling the silanol content or masking it with other organic reactive groups can be a safer approach in designing nanoparticles for drug/gene delivery. Moreover, functionalising the nanoparticles' surface allows us to control their action by modifying biological activity, including blood circulation time, targeting specific cells/organs, hemocompatibility, and reducing systemic toxicity. There are two main features of NP modifications:

a) External surface modification is usually used to graft nanoparticles with various polymers (polyethylene glycol, chitosan, etc.), antibodies, peptides and other targeting ligands. This technique mainly stabilises nanoparticles in biological fluids and induces targeted delivery for therapeutic or diagnostic applications.

b) Internal surface modification is used with mesoporous or hollow nanoparticles. Here, therapeutic peptides, proteins, antibodies, drugs, or imaging agents are bound within the nanocomposite's pores to deliver therapeutic agents or be used in diagnostic imaging.

Preceding conjugation with different compounds onto the exterior of the silica nanoparticles usually functionalises with alkoxysilanes or/and aminosilanes that covalently bind by siloxane bonds during the condensation reaction. There are several common strategies used to implement this functionalisation:

1) The post-grafting method is also known as the classic technique of NP functionalisation. It employs several synthesis steps, the first being the synthesis of nanoparticles, usually from TEOS, and then the addition of functional organosilanes. However, this method was reported to form polydispersed nanoparticles with uncontrolled silane groups (Von Baeckmann *et al.*, 2018). Tsai et al. reported a synthesis of mesoporous silica nanoparticles for the simultaneous delivery of a DNA plasmid and cisplatin for hepatocellular carcinoma; their synthesis comprises two steps and several stages for surface modifications. Overall, nanoparticles were synthesised from TEOS in a CTAB-containing solution, then the product was purified, and the next step of functionalisation was performed with 3-(trihydroxy silyl)propyl methyl phosphonate (THPMP); formulated nanoparticles showed polydispersed distribution in size compared to non-functionalized nanoparticles (Tsai *et al.*, 2019). Similar polydispersion was

revealed after the functionalisation with (3-aminopropyl)triethoxysilane (APTES) in nanoparticles of 50 and 160 nm (Bouchoucha *et al.*, 2017a).

2) Co-condensation is a single-step synthesis technique in which a precursor of silica nanoparticles (TEOS) is combined with organosilanes, forming nanocomposites with functional groups. However, this approach also has a drawback: Some functional groups are located inside the silica core and are not active. Also, it is challenging to control the distribution of desired functional groups on the outer surface of MSN (Von Baeckmann *et al.*, 2018).

3) Kecht et al. introduced the delayed co-condensation method (Johann Kecht, Axel Schlossbauer, 2008). Here, organosilanes were added after the TEOS introduction. Therefore, the spatial location of functional groups can be maintained by the variation of the time when organosilanes should be introduced (Von Baeckmann *et al.*, 2018). Usually, functionalised nanoparticles involve two-step synthesis in one pot, first to formulate mesoporous structure micelle forming reactants such as Aerosol-OT and 1-butanol mixed in solution to create a template for the nanoparticles; the next step includes synthesis of mesoporous core silica nanoparticles. Roy et al. (Roy *et al.*, 2005) used vinyltriethoxysilane (VTES) as a precursor and, after 30 minutes, added APTES to form amino groups on nanoparticles; the amount of the amino groups correlates with the added APTES concentration. Formed amino groups were used to attach DNA molecules and dyes to track the delivery of nanoparticles in vitro; moreover, the immobilisation of plasmids protects DNA from digestion by DNase 1 (Roy *et al.*, 2005). By now, the delayed co-condensation technique has become frequently used. Firstly, TEOS nanoparticles are synthesised in a CTAB solution. After some time (from 20 minutes to several hours), alkoxysilanes or/and aminosilanes are added, forming nanoparticles with various functional groups on the surface (Souris *et al.*, 2010; Yang *et al.*, 2019) or, in some cases, vinyltriethoxysilane (VTES) used as a silica precursor, and APTES added to produce amino groups on the surface of the nanoparticle for further modifications (Kumar *et al.*, 2010).

2.5. FUNCTIONALISATION OF SILICA NP WITH PEPTIDES AND ANTIBODIES

The peptides used in functionalised mesoporous silica nanoparticles (MSN) can be categorised into the following groups: targeting, stimuli-responsive, and multifunctional, chimeric peptides.

Targeting peptides assists in drug delivery to the disease site. Minimising the accumulation of nanoparticles with drugs in healthy tissues or organs before exposure to tumour sites is essential, thus decreasing potential side effects. Targeted peptides also play a role in reducing the drug dosage and improving the effectiveness of treatment.

One of the most common and proven peptides in tumour cell membrane targeting is RGD, arginine-glycine-aspartic acid tripeptide, which is applied not only for MSN but also for liposomes, micelles, and other kinds of nanoparticles. It works by binding to the integrin receptor, which is overexpressed in tumour cells, and the cyclic form of RGD was shown to have stronger binding (since linear ones exhibited many different conformations in solutions). Other targeting peptides of silica nanoparticles include IL-13 (interleukin-13), T22 peptide analogue P, and SP94 peptides. Another aspect that needs to be considered for targeted delivery is the destination to the nucleus, where the tumour's genetic material can be destroyed. For this, TAT peptide is commonly used as a nuclear localisation signal (NLS) to target the nuclear pore complex (NPC) of tumour cells by binding with import receptors as importin α and β, also referred to as karyopherins (Pan, He, Liu, Chen, Ma, *et al.*, 2012; Hu, Xiao and Zhang, 2016). Since importin is present in healthy and cancer cells, it is crucial to use multistage targeted delivery by functionalising nanoparticles with several different peptides, such as the combination of RGD and TAT (Hu, Xiao and Zhang, 2016).

Stimuli-responsive peptides avoid premature drug outflow and fall into three major types: enzyme-responsive, pH-responsive, and temperature-responsive. Chimeric peptides represent the combination of several peptide fragments that exhibit different biological activity.

Silica nanoparticles exhibit an advantage in surface functionalisation by being efficiently functionalised with amino and carboxyl groups (Kardys, Bharali and Mousa, 2013). This is performed by a modified Stober process of hydrolysis of tetraethyl orthosilicate (TEOS) and 3-aminopropyl triethoxysilane (APTES) within the presence of ethanol as an organic solvent and ammonium hydroxide (Kardys, Bharali and Mousa, 2013; Hu, Xiao and Zhang, 2016). Generally, the most straightforward method of attaching peptides, dyes, drugs, and other organic molecules to silica is forming a siloxane bond. Occasionally, multistep conjugation is applied, where the silica surface needs to be functionalised with appropriate reactive groups, such as thiol, azide, maleimide, alkyne, or others. Before this, hybrid silylated precursors must be formed in a derivative form of alkoxysilane or dichlorosilane (Maurel *et al.*, 2021). MSN can be functionalised with

peptides by forming disulfide bridges. Xiao et al. (2013) report the formation of pH and redox-responsive MSN, where they were functionalised with RGDFFFFC with azide group tumour targeting peptide by forming the disulfide bridges. Four phenylalanines act as gatekeepers blocking the pores by hydrophobic interactions between benzene rings. Before this, MSN was also functionalised with the thiol group through 3-mercaptopropyltrimethoxysilane (Xiao *et al.*, 2014).

Besides peptides, antibodies are also frequently applied in cancer cell targeting, and currently, there are nine antibody-drug conjugates that the FDA approves for clinical applications. Different conjugation methods fall into covalent and non-covalent attachment categories, as well as the usage of adaptor molecules (e.g., biotin). Non-covalent binding commonly includes ionic adsorption, where antibodies are attached via electrostatic interactions, yet the result lacks stability and reproducibility. Adaptor molecules, such as the avidin-biotin complex, also exhibit some limitations in terms of pH. The covalent attachment comprises click-chemistry, maleimide chemistry, and carbodimide chemistry, which are more favourable. The nanoparticle surface is commonly functionalised with amino, carboxyl, or maleimide groups, which can further conjugate with the antibody's amino acid side chain. Yet covalent conjugation also has some obstacles to tackle, such as avoiding antibody oligomerisation and catalyst usage, which may add to nanoparticle toxicity (Van Zundert *et al.*, 2021).

A recent study by Zundert (2021) and her colleagues introduced a copper-free click-chemistry strategy for antibody conjugation with MSN. First, MSN was coated with polyethyleneimine (PEI), which acted as a basis for nanoparticle functionalisation with the amine group through the covalent attachment of azide (N_3) moiety. The Azide group was attached by NHS ester coupling, whereas dibenxocyclootyne (DBCO) was also attached to lysine residues of antibodies by NHS ester coupling reaction. Through the click chemistry reaction between the nanoparticle-attached azide group and DBCO-bonded antibodies, the desired antibody-conjugated MSNPs were obtained. In this study, they successfully demonstrated targeting of CD44 (Cluster of Differentiation 44) and EGFR (Epidermal Growth Factor Receptor) overexpressing tumour cells. A significant advantage of this method is the absence of any catalyst. Authors suggest that this method of antibody-conjugation can be applied to other types of nanoparticles as well, provided that they have an amino group present (Van Zundert *et al.*, 2021).

In a research study by Bouchoucha et al. (2013), MSNs were conjugated with the blood-brain barrier (BBB) targeting monoclonal Ri7 antibody through PEGylation. The

BBB prevents therapeutic medicines from reaching the CNS, posing a significant barrier to the treatment of a variety of neurodegenerative illnesses. Nanoparticle models targeting brain micro-vessel endothelial cells (BMEC), the constituent of the main BBB constituent, via the transferrin receptor (TfR), have shown preclinical effectiveness. The enormous density of transferrin receptors in the endothelial cell membranes of the blood-brain barrier is particularly interesting. Due to the significant accumulation of the rat Ri7 anti-mouse TfR antibody in brain microvascular endothelial cells (BMEC) through a transferrin receptor mechanism, this antibody has undergone comprehensive research to develop technologies for targeting the blood-brain barrier (BBB). Firstly, MSN was also functionalised with an amino group by the reaction with APTES. Subsequently, MSN was further functionalised with a gadolinium chelating agent, DTPA, to generate a significant contrast enhancement effect, allowing them to be seen in an MRI. Then, Maleimide-PEG-N-Hydroxysuccinimide (MAL-PEG-NHS) was linked to the Ri7 antibody via a reaction between maleimide groups and the Ri7 antibody's thiols. By traditional NHS reaction, the antibody-PEG-NHS molecule was attached to the accessible amine groups on the exterior surface of MSN-DTPA(Gd) nanoparticles. MSN was able to bind the TfR at the cell surface and stimulate TfR-mediated endocytosis after being conjugated to Ri7 antibodies. So, the resulting Ri7-conjugated MSN demonstrated high targeting capability and affinity for BMEC, which pose a severe obstacle to many drugs reaching the brain (Bouchoucha *et al.*, 2017b).

The orientation of the antibodies must be carefully considered in antibody conjugation to the nanoparticle. The specificity of protein modification especially needs to be considered since improper specificity may hinder or block the orientation of the antigen-binding domain (Spicer *et al.*, 2018).

2.6. FUNCTIONALISATION WITH DRUGS

Various methods exist for loading pharmaceuticals into mesoporous silica nanoparticles (MSNs), which vary in terms of the drug-loading technique, the composition of the MSNs, and their functional groups. Scientists are working on synthesising the MSNs that display optimal loading capacity and site-specific release of the drug with minimum cytotoxic effects on the surrounding environment. One such system was proposed by Tien et al., who developed pH-dependent aldehyde-functionalized dendritic mesoporous silica nanoparticles (DMSNs-CHO) for protein drug delivery. In the study, DMSNs were functionalised with aldehyde groups to form

DMSNs-CHO and bovine serum albumin (BSA) was used as a model protein drug (Tian, Xu and Zhu, 2017). Since protein drugs frequently contain primary amine groups, BSA was loaded into DMSNs-CHO nanoparticles by creating imine linkages, which connected the aldehyde groups of DMSNs-CHO to the primary amines of BSA. As the pH of the intracellular environment is lower than that of the extracellular environment, the fall in pH causes the intracellular release of BSA (Tian, Xu and Zhu, 2017). *In vitro* experiments showed that BSA release from DMSNs-CHO/BSA nanoparticles was significantly higher at pH 6.0 compared to pH 7.4 due to the pH-labile imine bonds; thus, this study developed a protein drug delivery system with pH-dependent release response (Tian, Xu and Zhu, 2017). In another study by Shinde and Prasad, hydrophobic drugs were delivered by MSNs amino-group functionalised drug delivery system (Shinde and Prasad, 2021). They synthesised MSNs featuring hydrophobic opening and hydrophilic functional groups on its external surface to deliver hydrophobic drug proflavine. Furthermore, to analyse the impact of functional groups on drug uptake and release, the outer surface was modified by propargyl alcohol, trimethylene glycol, and PEG (2000) via azide–alkyne click-chemistry (Shinde and Prasad, 2021). It was found that hydrophilic functional groups on the outer surface could assist with MSN dispersion in an aqueous environment, while hydrophobic drugs could be loaded into hydrophobic pores (Shinde and Prasad, 2021). The loading and release efficacy is studied using two approaches: first, modification of the surface with one of the alkynes followed by drug loading or vice versa with surface functionalisation afterwards(Shinde and Prasad, 2021). Compilations of the *in vitro* studies showed that bulkier functional groups lower the loading capacity and proflavine release from the amino-functionalised MSNs (Shinde and Prasad, 2021).

In one of the *in vitro* studies, Xu and his colleagues synthesised gelatin-coated MSNs for cancer treatment (Xu *et al.*, 2013). It is known that matrix metalloproteinases (MMPs), members of the protease family, are upregulated in cancer cells, and several drug delivery systems were proposed to reduce their effect. However, most showed nonspecific release and high toxicity levels to normal cells. They used gelatin as a site-specific drug release substrate, which is biocompatible, non-immunogenic and could be degraded by MMPs that are upregulated in tumour tissues (Xu *et al.*, 2013). Doxorubicin was expected to be released from MMPs-degradable gelatin-coated MSNs (MSNs-Gel) in response to the tumour microenvironment. The mice receiving DOXMSNs-Gel showed a more significant decrease in the size of a tumour compared with body weight stability with those receiving free DOX and DOXMSNs without gelatin. This effect is

explained by the on-demand drug release and accumulation of DOX at tumour sites by enhanced permeability, retention effect, degradation of gelatin by MMPs and site-specific accumulation of DOX in the nucleus of tumour cells (Xu *et al.*, 2013). Another way to deliver anticancer drugs was demonstrated by Tran and his colleagues, who synthesised doubly decorated mesoporous silica nanoparticles to transport cisplatin drug molecules (Tran *et al.*, 2018).

2.7. TOXICOLOGICAL STUDIES ON ORGANOSILICA NANOPARTICLES

Silicon is one of the most prevalent elements on our planet, the Earth's mantle contains the highest concentration of crystalline silica in quartz. Silicon is acknowledged as a necessary nutrient, but there have also been reports of harmful health effects linked explicitly to dust inhalation (Murugadoss *et al.*, 2017).

The versatile chemical and physical properties of silica nanoparticles have broadened their usage in medicine, cosmetics, and the food industry (Niu *et al.*, 2016). Nevertheless, there is a dearth of comprehensive research on the relationship between organosilica nanoparticles and biological systems. Recent studies have released toxicity data regarding silica nanoparticles synthesised using tetraethyl orthosilicate (TEOS). Despite varying data, there is a consensus that nanoparticles' size, charge, functionalisation, and shape directly impact toxicity. Furthermore, silica nanoparticles can be classified into crystalline and amorphous. Crystalline nanoparticles are associated with the development of silicosis, a fibronodular lung disease, in mining workers (Leso *et al.*, 2019), while the effect of amorphous silica on humans remains unclear.

Amorphous colloidal silica nanoparticles have been shown in recent studies to be cytotoxic *in vitro*, causing oxidative stress-mediated apoptosis in a concentration- and size-dependent manner. It has been discovered that some nanoparticles compromise membrane integrity, which increases cytotoxicity. In general, toxicity levels were higher for smaller nanoparticles (10–20 nm) than for bigger ones (more than 50 nm) (Murugadoss *et al.*, 2017). When comparing nanoparticles of different sizes, it was observed that those measuring 50, 100, and 150 nm exhibited lower toxicity levels in human corneal epithelial cells and did not cause any damage to the cell membrane (Park *et al.*, 2016).

Although drawing definitive conclusions from the data is challenging due to higher nanoparticle concentrations causing overload within cells, *in vivo* studies on rats

and mice revealed no toxicity when nanoparticles were administered orally and topically, regardless of shape and size. Most administered nanoparticles were cleared through the gastrointestinal and urinary tracts. Nevertheless, it is difficult to affirm that the nanoparticles supplied were higher than those encountered through human breathing (Murugadoss *et al.*, 2017). In other studies, nanoparticles grafted with chitosan and polyethylene glycol showed no cytotoxicity and apoptosis (Moodley and Singh, 2019). In spite of the fact that silica nanoparticles are frequently referred to as "highly biocompatible," there is a dearth of information regarding their hemocompatibility (Pamukcu, Kaba and Karaman, 2019). Studying the compatibility of silica-based nanosystems with the bloodstream is crucial in establishing an effective method for intravenous drug delivery. In general, there is a lack of conclusive information about the toxicity of silica nanoparticles, and there is an insufficient amount of data regarding the impact of silica nanoparticles on human health. The existing data on the toxicity of silica mainly characterises nanoparticles produced from TEOS. To our knowledge, there is no data on the toxicity profiles for thiolated and PEGylated organosilica nanoparticles synthesised from 3-mercaptopropyltrimethoxysilane (MPTS).

Conversely, a significant amount of research has been conducted on mesoporous silica nanoparticles. Various nanoparticle systems have been designed through research efforts spurred by the possible applications of MSNs in biological systems and nanomedicine. There have been worries regarding their potential toxicity in living organisms throughout the advancement of these nanosystems. Despite multiple studies confirming the safety of silica-based materials, particularly MSNs, there remains a lack of consensus about the biosafety of these nanoparticles due to conflicting experimental evidence (Wang *et al.*, 2018; Ko *et al.*, 2020). Nevertheless, by making relatively straightforward adjustments, the biocompatibility and overall behaviour of MSNs can be enhanced based on existing information. This is because they depend on physical and chemical characteristics, such as shape, surface features, crystal structure, pore size, particle size, and other factors related to interactions between nanomaterials and biological systems (Farjadian *et al.*, 2019).

Silica nanoparticles have not yet been thoroughly described in terms of their characteristics and cytotoxic effects (Singh, Shi and Goel, 2023). The evaluation of the biosafety of SiNPs for biomedical purposes, as well as the examination of their distribution within the body and their toxicity in living organisms, is still being carefully studied (Ko *et al.*, 2020; Solorio-Rodríguez *et al.*, 2021; Shabbir *et al.*, 2023). Therefore,

a significant amount of clarification is necessary, particularly regarding the impact of SiNPs on living organisms. The cytotoxicity of NPs raises substantial problems, such as the potential for inhibiting and altering cell activity, leading to severe damage.

CHAPTER 3. THIOLATED ORGANOSILICA NANOPARTICLES BASED ON MPTS AND THE ROLE OF PEGYLATION ON TOXICITY

3.1. INTRODUCTION

Nanoparticles have become more important in the biomedical industry, particularly in developing medication and gene delivery systems and diagnostic instruments. The primary advantages of nanoparticles in drug delivery systems (DDS) lie in their diminutive size and expansive surface area, which enable precise regulation of the release kinetics and behaviour of the nanoparticles. Additionally, nanoparticles exhibit an enhanced permeability and retention effect. These properties make nanoparticles highly attractive for drug delivery systems (Vega-Vásquez, Mosier and Irudayaraj, 2020). Silica nanoparticles are considered potential candidates for drug delivery systems (DDS) because of their biocompatibility, hydrophilicity, and ability to be functionalised (Xiao *et al.*, 2014; Mebert *et al.*, 2017; Castillo, Lozano and Vallet-Regí, 2020). Silica nanoparticles can be categorised into two distinct groups: inorganic and organic. Inorganic nanoparticles are often produced using tetraortosilicate (TEOS) and consist of a silica framework with silanol groups on the surface (Nakamura, 2018). In 1968, Stöber et al. pioneered the sol-gel technique for synthesising inorganic silica nanoparticles from tetraethyl orthosilicate (TEOS) through self-condensation in ethanol, using ammonia as a catalyst (Stöber, Fink and Bohn, 1968).

Organosilica nanoparticles, composed of a silica framework, possess carboxyl groups inside and outside the nanoparticle's core (Nakamura, 2018). Furthermore, to achieve advanced surface modification, some researchers incorporate thiol and amine groups into nanoparticles by adding an extra step during production. The functionalisation process involves the utilisation of organosilanes, such as (3-aminopropyl)triethoxysilane (APTES) (Zhang *et al.*, 2014; Chen *et al.*, 2017) or 3-mercaptopropyltrimethoxysilane. The grafting of organosilanes can be carried out in two ways: by adding them after synthesising TEOS-based nanoparticles or by including them during the synthesis as a second step. Both approaches possess certain drawbacks, primarily the challenge of effectively managing organic entities' dimensions and spatial positioning.

Nakamura et al. developed a method to create organic silica nanoparticles using a single source of organosilane. The nanoparticles were produced using the Stober

synthesis technique with a size range of 350 to 1200 nm. Additionally, the nanoparticles have thiol groups on their surface (Nakamura and Ishimura, 2008).

Later, Irmukhametova et al. (2011) suggested employing sodium hydroxide as a catalyst, DMSO as a solvent, and MPTS as a precursor to create a novel technique for creating organosilica nanoparticles. The nanoparticles obtained are less than 100 nm and exhibit a high density of thiols on their surface (Irmukhametova, Mun and Khutoryanskiy, 2011).

In Professor Khutoryanskiy's studies, organosilica nanoparticles were synthesised using this method with slight modifications, and their properties have been thoroughly investigated and reported by our research group (Irmukhametova *et al.*, 2012; Mun, Williams and Khutoryanskiy, 2016; Al Mahrooqi *et al.*, 2018b; Ways *et al.*, 2018). The synthesis of organosilica nanoparticles comprises three key steps: hydrolysis, then the methoxysilane groups undergo condensation, resulting in the formation of a cross-linked nanoparticle structure by the use of methoxysilane and disulfide bridges..

This chapter will describe the toxicological profile of MPTS-based organosilica nanoparticles in an aprotic solution. Additionally, a subset of thiolated organosilica nanoparticles will undergo PEGylation with polyethylene glycol (PEG) of varying molecular weights.

The process of attaching or binding PEG or PEG-containing copolymers to the surface of nanoparticles significantly increases the duration of their presence in the bloodstream by several orders of magnitude. This mechanism creates a water-attracting protective coating, which prevents opsonin proteins from recognising it by using steric repulsion forces. Furthermore, PEG exhibits little negative effects when tested in living organisms and has been authorised for intravenous use in humans (Farjadian *et al.*, 2019).

Despite the recent recognition of silica nanoparticles' prospects in biomedicine and the numerous opportunities they offer, several challenges remain. One notable challenge is the incomplete understanding of organosilica nanoparticles' toxicity and biocompatibility profiles. This gap in knowledge underscores the need for further investigation and exploration in this area. The extensive examination of the cytotoxic effects on biological entities is necessary due to the abundance of diverse silica-based nanoparticles.

3.2. MATERIALS AND METHODS

Table 3.1. List of consumables, Chapter 3.

Name	Abbreviation	CAS-number	Manufacturer
(3-Mercaptopropyl)trimethoxysilane	MPTS	4420-74-0	Sigma-Aldrich
Sodium hydroxide	NaOH	1310-73-2	Sigma-Aldrich
Dimethyl sulfoxide	DMSO	67-68-5	Sigma-Aldrich
Dialysis tubing cellulose membrane	n/a	n/a	Sigma-Aldrich
Atto 488 maleimide	A488	n/a	Sigma-Aldrich
Methoxypolyethylene glycol Maleimide, 5000 Da	PEG5000	99126-64-4	Sigma-Aldrich
Methoxypolyethylene glycol Maleimide, 750 Da	PEG750	99126-64-4	Sigma-Aldrich
Alexa Flour-750 C5 maleimide	A750	n/a	Fisher
5,5-dithio-bis-(2-nitrobenzoic acid)	DTNB	69-78-3	Sigma-Aldrich
L-cysteine hydrochloride monohydrate	n/a	52-89-1	Sigma-Aldrich
CellTiter Non-Radioactive Cell Proliferation Assay	MTT	n/a	Promega
DAPI	n/a	28718-90-3	Sigma-Aldrich
Alexa Fluor-555 Phalloidin	A555	n/a	Fisher
Paraformaldehyde	PA	30525-89-4	Sigma-Aldrich
Osmium tetroxide solution	n/a	20816-12-0	Sigma-Aldrich

3.2.1. Synthesis and Characterisation

Thiolated nanoparticles were synthesised according to the protocol developed by Irmukhamedova et al. (Irmukhametova, Mun and Khutoryanskiy, 2011). Briefly, 0.750 mL MPTS was added to 20 mL DMSO, followed by 0.5 mL of 0.5M NaOH, which was mixed and agitated at ambient temperature for a duration of 24 hours while air was continuously introduced. After 24 hours, dialysis purified nanoparticles against ddH_2O for eight water changes (5 L) in 12-14 kDa cellulose membrane dialysing tubing (Sigma-Aldrich). The produced nanoparticles were maintained in a sealed container in a liquid state at a temperature of +4°C in a refrigerator.

Synthesis of fluorescently labeled nanoparticles

Thiolated nanoparticles were conjugated with fluorescent dyes Atto-488 maleimide (Sigma-Aldrich) and Alexa Flour-750 C5 maleimide (Fisher) for *in vitro* and *in vivo* experiments. The ratio of dye to the thiol content on the nanoparticles' surface was 1:20. So, to 10 mL of nanoparticles suspension, 50 µL of Atto-488 maleimide and 40 µL of Alexa Flour-750 C5 maleimide, samples were stirred at room temperature for 16 hours followed by dialysis as described above at dark condition. Nanoparticle suspensions were stored in the fridge at 4°C in the dark.

Synthesis of PEGylated nanoparticles

Thiolated and fluorescently labelled nanoparticles were further PEGylated with methoxypolyethylene glycol maleimide with molecular masses of 750Da and 5000Da according to the protocol published by Mun et al. Shortly, 10 mL of nanoparticle suspension, 100 mg and 50 mg of PEG with molecular masses of 750Da and 5000Da were added and stirred for 16 hours at room temperature. This was followed by purification with dialysis against ddH_2O, as described above.

Measurement of dynamic light scattering and zeta potential

The nanoparticles' suspension was 100x times diluted in ultrapure water before analysis. Diluted nanoparticles were analysed for size and zeta potential using Nano-S Zetasizer at 25°C; each batch was measured three times in three repeats, and the mean value with standard deviation was calculated.

Ellman' assay

The Ellman's test was employed to quantify the thiol content, utilising 5,5-dithiol-bis-(2-nitrobenzoic acid) (DTNB) to determine the concentration of free sulfhydryl groups on the surface of nanoparticles. Before the experiment, nanoparticles underwent freeze-drying. A suspension of nanoparticles (10 mL) was weighed and placed in a freezer at -20 °C overnight. Frozen nanoparticles were then dried on Lyotrap freeze-drier for three days after the weight of the powder was measured to calculate the concentration of nanoparticles (w/v).

Lyophilised nanoparticles (3 mg) were hydrated in 10 mL of 0.5 mol/L PBS (pH 8) for 1 hour, and 3 mg of DTNB dissolved in 10 mL 0.5 mol/L PBS (pH 8). After one hour, 0.5 mL of nanoparticle suspensions were combined with 0.5 mL of DTNB solution and kept in a dark environment for 2 hours. Subsequently, the mixture was subjected to centrifugation at a speed of 13000 rotations per minute for a duration of 6 minutes. The liquid portion was transferred onto 96-well plates, and the amount of light absorbed was measured at a wavelength of 405 nm using Varioscan. The thiol concentration on

nanoparticles was determined using a calibration curve of L-cysteine hydrochloride monohydrate, with concentrations ranging from 0.004 to 0.644 µmol/mL.

RAMAN spectroscopy

FT-RAMAN spectra of nanoparticles were measured using Horiba LabRam Evolution. Before the measurement, nanoparticles were freeze-dried at the Lyotrap freeze dryer. Nanoparticle powder was evenly placed on a glass slide and measured by excitement with a 532 nm laser.

Transmission electron microscopy

TEM images of thiolated and PEGylated nanoparticles were obtained with JEOL JEM - 1400 Plus at an acceleration voltage of 120 kV. Samples were prepared: nanoparticles were diluted to a 1:10 ratio in ultrapure water and dropped onto a 400 mesh carbon-coated Cu grid. They were then washed in ultrapure water to remove excess unattached nanoparticles and stained with Uranyl Acetate-Zero non-radioactive electron microscopy stain for 1 minute, air dried at room temperature on filter paper.

Nanoparticle stability in physiological media

The nanoparticles were evenly distributed at a 100 µg/mL concentration in three different substances: deionised water, a solution of 0.9% NaCl, and a cell culture medium containing 10% FBS. The solution underwent filtration using a syringe filter with a pore size of 0.44 µm. The hydrodynamic size of the particles was determined in the solution by DLS over a period of five days. In order to investigate the impact of salt content on the aggregation of SiNP-SH, we conducted measurements of the hydrodynamic size of nanoparticles in NaCl solutions ranging from 100 mM to 6 mM.

3.2.2. *In vitro* toxicity

MTT assay

Cell viability was assessed using the CellTiter Non-Radioactive Cell Proliferation Assay (MTT) from Promega, USA. Prior to conducting the studies, the nanoparticles were diluted in a cell culture medium to concentrations ranging from 0 to 1000 µg/mL. The HEK293, MCF7, and HPF cell lines were placed in a 96-well plate with a density of $5*10^4$ cells per well. They were then cultured at 37°C with a 5% CO_2 atmosphere overnight until they reached confluency. Once the cell culture reached the desired density, the previous cell media (consisting of DMEM+10%FBS+1% PenStrep antibiotics) was removed and replaced with a fresh solution containing nanoparticles at concentrations of 10, 50, 100, 200, 400, 800, and 1000 µg/mL. The cells were then incubated 24, 48, and

72 hours in a humidified atmosphere at 37°C with 5% CO_2. The cells exposed to cell medium without nanoparticles were designated as the negative control. After the nanoparticles were incubated, 15 µl of MTT dye solution was added to each well and incubated for 4 hours. Then, 100 µl of solubilisation solution was added to dissolve the formed formazan crystals. The measurement of absorbance was conducted using a plate reader at a wavelength of 570 nm (Microplate reader Varioscan, Thermo Scientific, USA). The formula provided below is used to determine the vitality of cells:

$$Cell\ viability\ \% = \frac{Absorbance\ of\ treated\ cells}{Absorbance\ of\ negative\ control} * 100\%$$

Hemolysis Assay

The nanoparticles' hemolytic capabilities were evaluated using hemolysis analysis. Three healthy persons were used to obtain blood samples, which were collected using K2-EDTA vacutainers manufactured by Ayset, Turkey. The samples were then centrifuged at a speed of 1000 rpm for 10 minutes. The plasma and buffy coats were removed, leaving just the red blood cells (RBCs). The RBCs were diluted in PBS to create a 2% (v/v) RBC solution. The nanoparticles were solubilised in phosphate-buffered saline (PBS) at 0, 50, 100, 200, 400, 600, 800, and 1000 µg/mL concentrations. Afterwards, 0.2 mL of a suspension containing nanoparticles was mixed with 0.8 mL of a solution containing red blood cells in an Eppendorf tube. The mixture was then incubated for 1 hour at 37°C. The tubes underwent centrifugation at a force of 2500 g for 6 minutes, and 200 µl of the resulting liquid above the sediment was moved to a 96-well plate. Measurements of absorbance were recorded at wavelengths of 541 nm and 655 nm. Water and PBS were used as the positive and negative controls, respectively. The hemolysis percentage was determined using the following formula.

$$Hemolysis\ \% = \frac{Absorbance\ sample - Absorbance\ \ negative\ contr}{Absorbance\ \text{positive contr} - Absorbance\ \text{negative contr}} * 100\%$$

Cell stiffness analysis

A549 cells were seeded on Corning® 35 mm TC-treated culture dishes for Atomic Force Microscopy (AFM) for 24 hours in a humidified atmosphere at 37°C with 5% CO_2. Four hours before the experiment, cells were treated with 200 µg/mL nanoparticles (SiNP-SH, SiNP-PEG750, and Si NP-PEG5000). After 4 hours of incubation with nanoparticles, the cell media was changed. Atomic Force Microscopy was employed to quantify the cell stiffness of the treated cell lines, while Zeiss Axiovert was utilised for

visualisation. The AFM B300 tip was used as an indenter, possessing a clearly defined spherical shape, to penetrate the cell. Before experiments, the B300 tip was calibrated using the Force Spectroscopy mode. This calibration involved a contact-based approach to ensure that the tip sensitivity and spring constant remained unaffected.

The Young's moduli of cells were quantitatively calculated by fitting the force-indentation curves to the Hertz model. The GraphPad Prism 5 Software was used to analyse and visually show the cell stiffness data. The results were compared using a one-way variance analysis (ANOVA) and Kruskal-Wallis tests.

3.2.3. *In vitro* localisation

Uptake of nanoparticles within cells

Prior to conducting the studies, the nanoparticles were labelled with Atto-488 maleimide. MCF7 cell lines were cultured in 6-well plates with collagen-coated cover glass of thickness number 1. The cells were seeded at a density of 50000 cells per well. The cells were cultured until they reached the necessary level of confluency and attached to the coverslip overnight in a humid environment at 37°C with 5% carbon dioxide. Subsequently, traditional media was substituted with a cellular medium that included thiolated and PEGylated (PEG750 and PEG5000) nanoparticles, which were fluorescently labelled. The nanoparticles were present at 200 µg/mL concentrations and were subjected to incubation for 2, 4, 6, and 24 hours. The cells that were incubated were rinsed with PBS three times, then treated with a fixative and stained with DAPI and Alexa Fluor-555 Phalloidin. The coverslips were moved to a glass slide using mounting material (Fluoromount) and let to dry in the air for the entire night. The dried slides were examined using a laser scanning microscope (LSM-780, Cals Zeiss, Germany) equipped with an oil immersion objective lens with a magnification of x63. Using the same laser powers, a Z-stack was captured for each image with a step size of 0.28-0.30 µm.

Scanning electron microscopy of erythrocytes

The interaction of red blood cells with nanoparticles was evaluated with SEM. Blood samples were obtained from three healthy individuals in a K2-EDTA vacutainer (Ayset, Turkey) and proceeded as above to collect RBC. Then, RBS was diluted to the 2% (v/v) solution in PBS and fixed with 2% glutaraldehyde. Next, RBCs were placed onto glass coverslips coated with 20 nm golden film and incubated with thiolated and PEGylated nanoparticles at 200 µg/mL concentration for 1 hour at 37°C. After incubation, RBC and nanoparticles were fixed in 2% paraformaldehyde, stained with 4%

osmium tetroxide, and gradually dehydrated in ethanol. Samples were left overnight to dry, then spattered with 15 nm gold (spattering) and visualised on Crossbeam 540 scanning electron microscopy at 5kV electron high tension voltage.

3.2.4. *In vivo* biodistribution and toxicity

Animal and treatment

All animal work was conducted according to the laws and regulations of The Institutional Animal Care and Use Committee at Nazarbayev University (NU-IACUC). Upon the start of experiments, research team members working with animals obtained NU-IACUC 17/30112020 ethical approval.

Thirty-four female BALB/c mice aged 6-8 weeks were obtained from the National Centre of Biotechnology (Astana, Kazakhstan) and housed at the Laboratory of Bioengineering and Regenerative Medicine (National Laboratory Astana) in a temperature-controlled room with food and water supply. Mice were divided into three groups, containing nine animals per group. Mice in the control group were injected with saline buffer (300 μL) intravenously (IV) to the tail vein; animals in group 2 were injected IV with thiolated nanoparticles, and in group 3 with nanoparticles PEGylated by PEG with molecular mass 5000 Da. All experiments were conducted in triplicates.

Evaluation of biodistribution

The organosilica nanoparticle distribution was evaluated on SiNP-SH and SiNP-PEG5000 nanoparticles. Before the experiments, both nanoparticles were fluorescently labelled with Alexa Fluor-750. Nanoparticles were administered to mice intravenously to the tail vein at a concentration of 7 mg per kilo of animal. At particular time points post injection (2 hours, days 3, 7, 14 and 28), animals were deeply anaesthetised and sacrificed for organ collection (brain, lungs, heart, spleen, kidneys, liver, intestines and stomach) to visualise on IVIS spectrum imaging station (PerkinElmer, USA).

TGA evaluation

After imaging, animal organs were collected in tubes with ultrapure water for thermogravimetric analysis to confirm the presence of Si derivatives in organs. Collected organs were sonicated at a pulse ratio for 5 seconds with 90% amplitude for ten cycles (Fisher Scientific, USA). Grounded organs were freeze-dried, and powdered organs were analysed on TGA (STA 6000, PerkinElmer, USA) at 30 - 950°C with nitrogen flow.

Histology

To evaluate the pathological effect of nanoparticles, animals on days 7 and 28 were sacrificed, and major organs (lungs, liver, kidney, spleen, column and stomach) were fixed in 10% formalin. Further organs were paraffin fixated and sectioned on a glass slide.

Parafilm-embedded organ sections were stained with haematoxylin and eosin and further viewed by Acioscope 5 (Carl Zeiss, Germany).

3.3. RESULTS AND DISCUSSION

Silica nanoparticles are widely used in biomedical research, including drug delivery systems and diagnostic tools. Most studied nanoparticles are synthesised from tetraethyl orthosilicate (TEOS) and covered by silica precursors containing organic compounds within the core (Figure 3.1.).

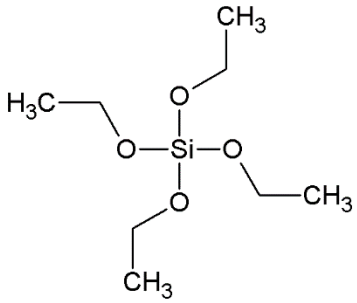

Tetraethyl orthosilicate (TEOS)

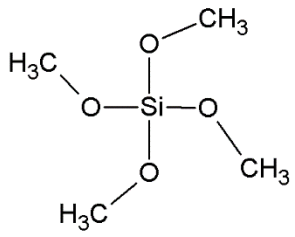

Tetramethyl orthosilicate (TMOS)

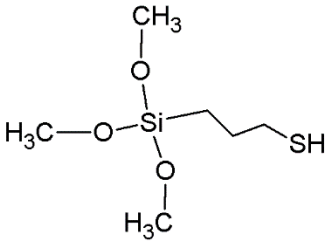

(3-Mercaptopropyl)trimethoxysilane (MPTS)

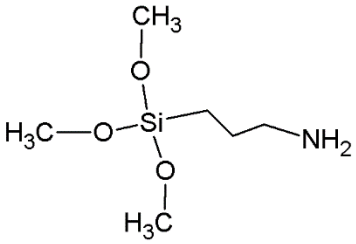

(3-Aminopropyl)triethoxysilane (APTES)

Figure 3.1. Precursors to silica and their chemical structure.

In our work, we skipped forming an inorganic core and formed a nanoparticle from 3-mercaptopropyltriethoxysilane (MPTS). The advantage of these nanoparticles is that they will form nanoparticles with degradable organic structures within the core and thiol groups on the surface.

As was previously indicated, thiolated organosilica nanoparticles (SiNP-SH) produceduction comprises of the procedure involving the self-condensation of 3-mercaptopropyl)trimethoxysilane (MPTS) in an aprotic solution, catalysed by NaOH (Mun *et al.*, 2014). The synthesis consists of the steps that coincide with the progress of synthesising nanoparticles from TEOS. The first step is the hydrolysis of the methoxysilane group in a nucleophilic reaction, followed by the condensation of deprotonated silanol species, creating coupling of monomers up to the level when they rich supersaturation; at this step, the nucleation of primary products occurs when the structure becomes insoluble. Then, the aggregation of primary particles reaches the level of rich colloidal stability, followed by particle growth forming stable nanoparticles (Figure 3.2.). In addition, the -SH group in MPTS is essential for nanoparticle formation, as it forms disulfide bonds upon oxidation (Irmukhametova, Mun and Khutoryanskiy, 2011). The disulfide bridge makes these nanoparticles more desirable, as it is another benefit for proper NP degradation upon reaching suitable conditions (Mekaru *et al.*, 2019).

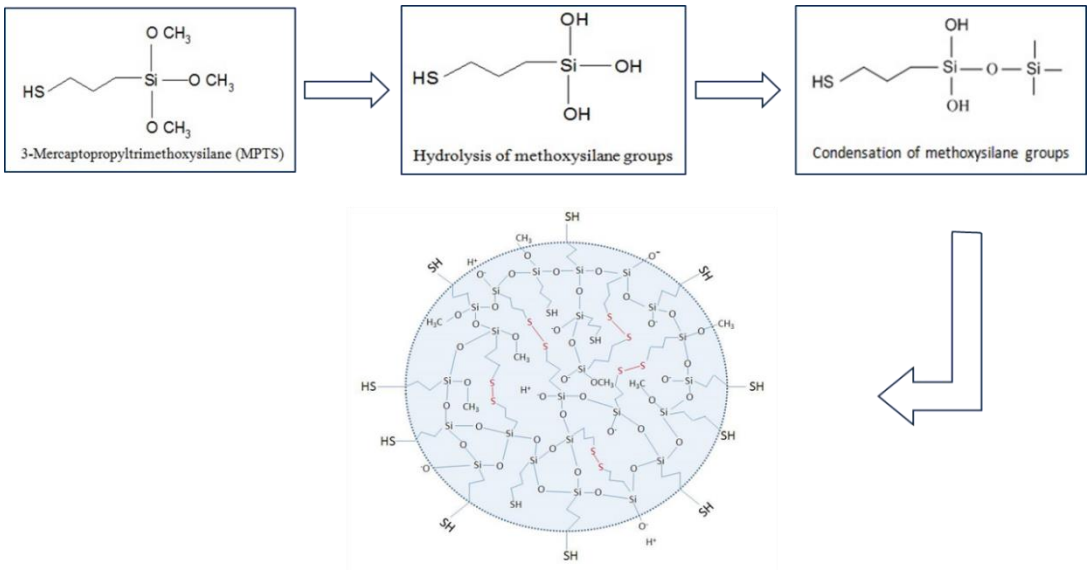

Figure 3.2. Schematic representation of thiolated organosilica nanoparticles synthesis from MPTS (Al Mahrooqi *et al.*, 2018a).

The thiolated nanoparticles were characterised using Ellman's test and dynamic light scattering. In addition, a portion of thiolated nanoparticles was acquired for modification using polyethylene glycol with molecular weights of 750 Da (SiNP-PEG750) and 5000 Da (Si NP-PEG5000). The PEGylated nanoparticles were evaluated using Ellman's test and Dynamic Light Scattering (DLS). The nanoparticles underwent a substantial increase in size as a result of PEGylation using PEG5000.

In addition, the quantity of thiol groups in SiNP-PEG750 and SiNP-PEG5000 decreased, as shown in Table 3.2. Analysis of hydrodynamic diameters indicates that PEGylation resulted in bigger nanoparticles, as seen in Figure 3.3-C. Conjugating with PEG of greater molecular weight augmented the nanoparticles' size.

Table 3.2. DLS and Ellman's assay results of thiolated and PEGylated nanoparticles.

	SiNP-SH	**SiNP-PEG750**	**Si NP-PEG5000**
Hydrodynamic diameter, nm	56±1	55±1	63±1
Diameter, nm (TEM)	29±4	28±5	28±6
PDI	0.140±0.010	0.127±0.008	0.135±0.009
ξ-potential, mV	-45.4±3.0	-34.9±10.8	-28.9±6.5
SH group content, µmol/g	481±79	364±56	228±99

In addition, the PEGylation method changed the surface charge of the nanoparticles, which resulted in a lower negative charge than the thiolated particles. This result aligns with the idea that sulfhydryl groups decrease after PEGylation. Table 3.2 demonstrates a decrease in sulfhydryl group concentration for nanoparticles coupled with PEG of 750 Da and 5000 Da. Specifically, the concentration reduced from 481±79 µmol/g for SiNP-SH to 364±56 µmol/g and 228±99 µmol/g for SiNP-PEG750 and SiNP-PEG5000 correspondingly. Figure 3.3-D demonstrates how the Raman spectroscopy analysis verified the decrease in thiol group concentration by lowering the peak associated with the S-H stretch (at 2570 cm^{-1}) after PEGylation.

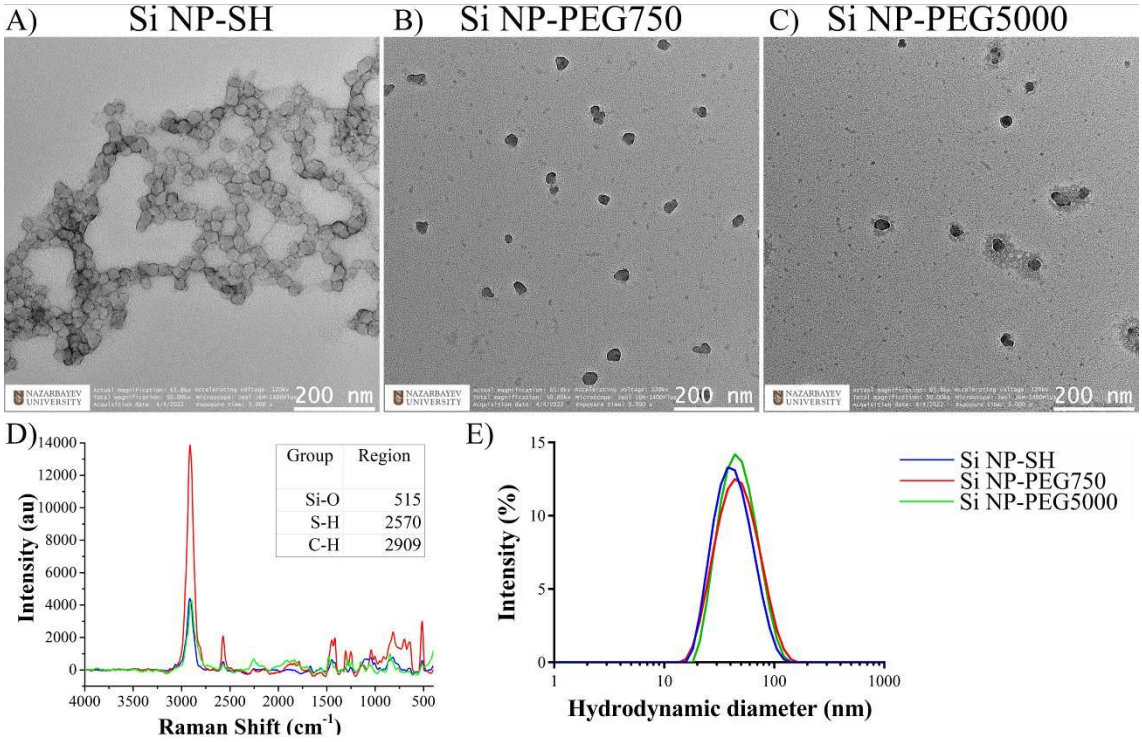

Figure 3.3. The physical and chemical properties of PEGylated and thiolated organosilica nanoparticles. Images from Transmission Electron Microscopy (TEM) of A) SiNP-SH, B) SiNP-PEG750, C) Si NP-PEG5000, D) Raman spectroscopy of nanoparticles, and E) the hydrodynamic size distribution of the nanoparticles in water.

In order to provide additional understanding on the discrepancy in the physical and chemical characteristics of the nanoparticles, we run experiments using transmission electron microscopy (TEM) to analyse the structural properties of the PEGylated and thiolated nanoparticles. The TEM pictures revealed that the size of the dry nanoparticles is approximately half the hydrodynamic diameter of the particles determined by DLS. Surprisingly, we observed that PEGylated nanoparticles had a low aggregation, which may be due to the PEG-corona surrounding nanoparticles (Figure 3.3-C). On the other hand, the transmission electron microscopy (TEM) images of thiolated nanoparticles showed interconnected structures that resembled chains, which had been previously observed by Irmukhametova et al. (Irmukhametova, Mun and Khutoryanskiy, 2011). The chains are most likely formed through the intermolecular interactions of SH-groups on the surface of nanoparticles, resulting in the creation of disulfide bridges (Figure 3.3-A). PEGylation with PEG5000 eliminated the creation of a linear arrangement. In this study, we will explore the impact of PEGylation on *in vitro* investigations.

The aggregation of nanoparticles in biological fluids is well acknowledged to cause changes in their properties and, more importantly, can lead to severe harm or even

death (Mohammadpour *et al.*, 2019; Avsievich *et al.*, 2020; Li *et al.*, 2020). In order to analyse the variations in nanoparticle sizes in different substances and assess the effects of PEGylation, we performed measurements on SiNP-SH, SiNP-PEG750, and SiNP-PEG5000 in three specific substances: cell culture medium with 10% FBS, 0.9% NaCl solution and deionised water. Figure 3.4 demonstrates that the size of nanoparticles remained consistently unchanged over a period of five days. The hydrodynamic size of all types of nanoparticles in all solutions, with the exception of SiNP-SH in saline, remained within an acceptable range.

SiNP-SH was seen to undergo substantial aggregation in the saline solution, which continued to occur even after filtering. This phenomenon can be ascribed to the catalytic impact of NaCl and the sensitivity of sulfhydryl groups on the surface of the nanoparticles, similar to the observed action in proteins that contain sulfhydryl groups (Kang *et al.*, 2021). Measurements of the hydrodynamic size were undertaken at various concentrations to examine the relationship between SiNP-SH aggregation and salt content. The salt concentration has a substantial impact on the aggregation state of SiNP-SH. Stability is attained at a concentration of 25 mM; at this point, the nanoparticles cease to agglomerate, and their polydispersity index (PDI) remains consistent (Figure 3.4).

Our observations indicate that SiNP-SH nanoparticles are larger than PEGylated nanoparticles in cell culture media. This disparity can be attributed to the development of a protein corona on the thiolated nanoparticles' surface, and PEGylation constrains the attachment of proteins to nanoparticles.

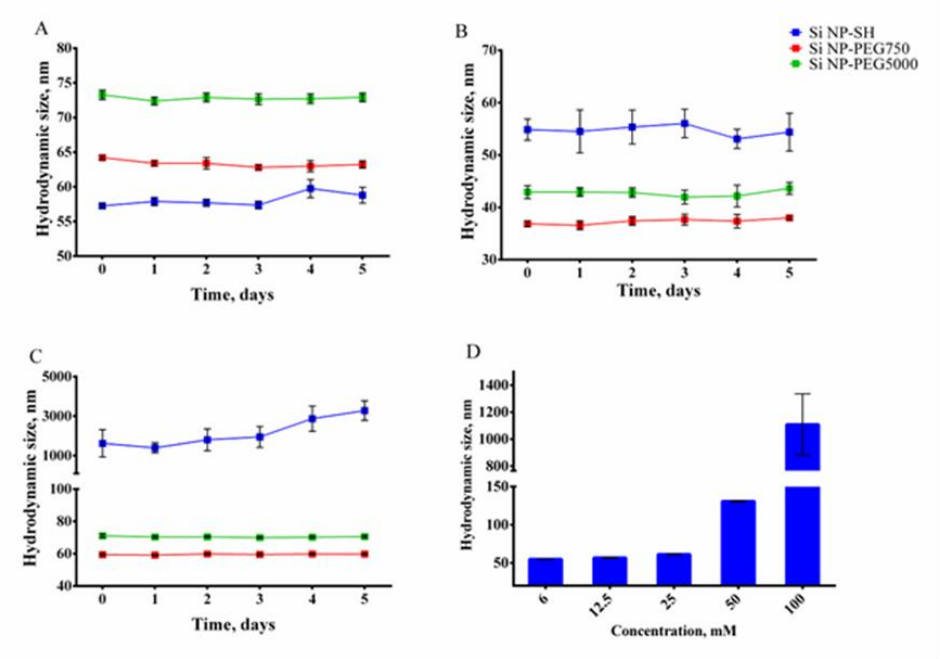

Figure 3.4. The hydrodynamic diameter of thiolated and PEGylated nanoparticles was assessed over five days in A) deionised water, B) cell culture medium, and C) 0.9% sodium chloride solution. D) the SiNP-SH size dependence at different sodium chloride concentrations.

The next stage of this investigation was to evaluate the cytotoxic effects of the organosilica nanoparticles on four different cell lines, including malignant ones and those that were not. These cell lines included A549 lung carcinoma epithelial cells, MCF-7 breast cancer cells, HEK293 human embryonic kidney epithelial cells, and human lung fibroblasts (HPF). The cells were exposed to SiNP-SH, SiNP-PEG750, and SiNP-PEG5000 at doses ranging from 10µg/mL to 1000 µg/mL for 24, 48, and 72 hours. Our observation revealed that nanoparticles induced toxicity in a manner that was dependent on the dosage and the specific cell line. An observed decrease in viability below 70% indicates that the material is unsuitable for biomedical application, as stated in the ISO 10993-5:2009(en) standard (*ISO 10993-5:2009(en), Biological evaluation of medical devices — Part 5: Tests for in vitro cytotoxicity*, 2009). This decrease was observed in all analyzed cell lines after 24, 48, and 72 hours when exposed to high SiNP-SH concentrations (800 - 1000 µg/mL). Nevertheless, the A549 cell line exhibited greater sensitivity to SiNP-SH than other cell lines. Specifically, after 48 and 72 hours, cell viability started to decline at doses of 200 µg/mL and 100 µg/mL, respectively (Figure 3.5). The cell lines treated with SiNP-PEG5000 displayed a dose-dependent effect, with viability dropping below 70% at 800 µg/mL concentrations and 1000 µg/mL. Once again, the A549 cell line showed a higher vulnerability to the nanoparticles. Furthermore, the

deleterious impact of SiNP-PEG5000 was found on HEK293 cell lines at doses of 400 µg/mL and above (Figure 3.5). SiNP-PEG750 showed higher toxicity in comparison to the other two nanoparticle variants. The impact of SiNP-PEG750 on A549 cell lines had a comparable outcome to the other two. However, during 48 and 72 hours of treatment, viability declined at 200 µg/mL and 50 µg/mL concentrations, respectively (Figure 3.5). Furthermore, the MCF7 cell line, which showed resistance to SiNP-SH and Si NP-PEG5000, decreased viability at concentrations of 400 µg/mL and 10 µg/mL after 48 and 72 hours, respectively.

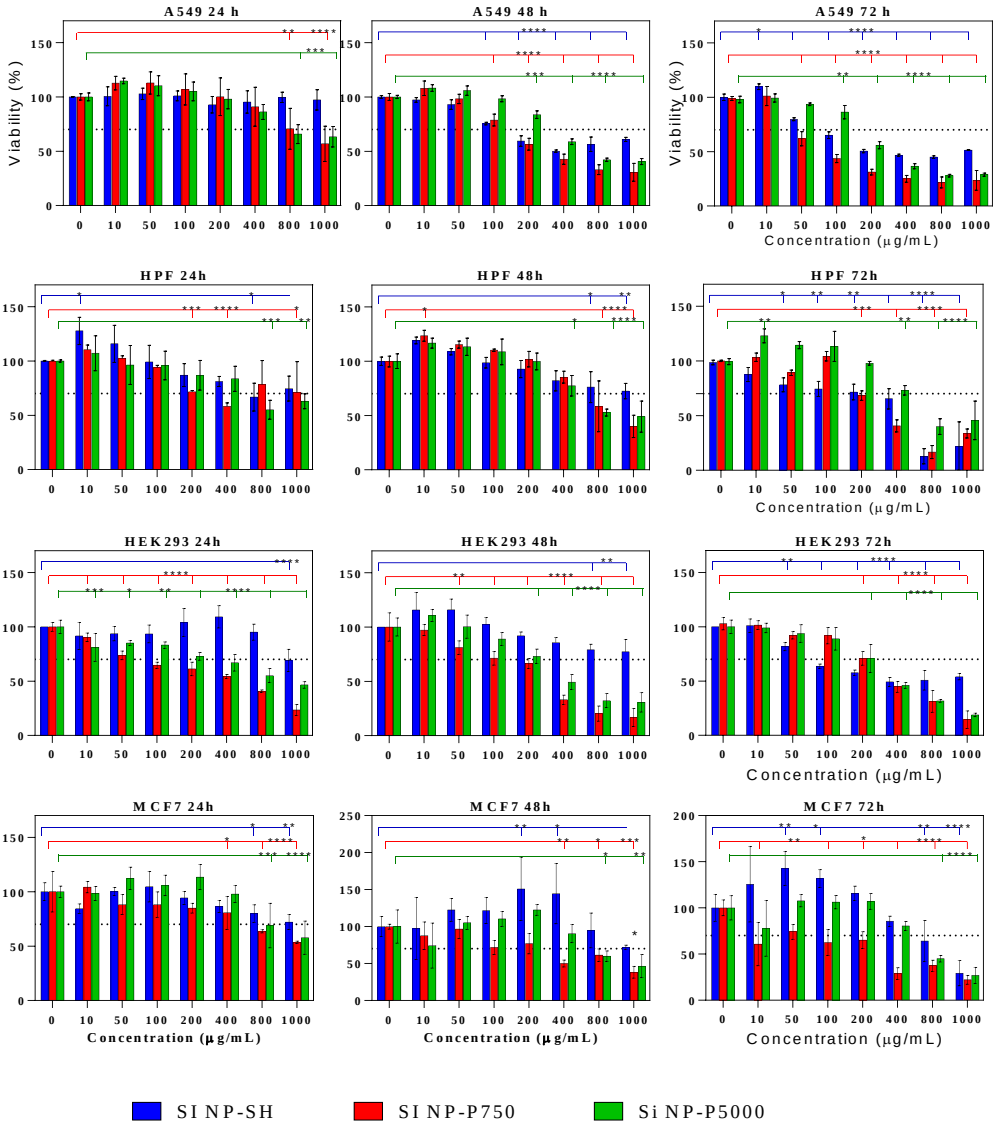

Figure 3.52. The cytotoxic effects of SiNP-SH, SiNP-PEG750, and SiNP-PEG5000 organosilica nanoparticles that depend on concentration were evaluated on four cell lines using the MTT assay. For 24, 48, and 72 hours, the cells were exposed to the nanoparticles (*P<0.05; **P≤0.01; ***P≤0.001; ****P≤0.0001).

Based on the MTT results, it can be inferred that SiNP-PEG750 exhibits more cytotoxicity towards all detected cell types than SiNP-SH and Si NP-PEG5000. In general, nanoparticles are considered safe for biomedical applications when used at low doses ranging from 10 µg/mL to 200 - 400 µg/mL and for short-term exposure.

To thoroughly assess nanoparticles' compatibility with living cells, we investigated their ability to cause hemolysis in human blood. Blood hemolysates can cause red blood cell deterioration or loss. This can increase free plasma haemoglobin levels, harming the body and putting stress on the kidneys or other organs (Neun, Ilinskaya and Dobrovolskaia, 2018). The assessment was conducted according to the ASTM standard, which states that "a material is considered hemocompatible" if its hemolytic index is below 5% (ASTM F 756-00, 2000). The red blood cells were subjected to nanoparticle treatment for 1 hour at a temperature of 37°C. Subsequently, we extracted the haemoglobin from the ruptured erythrocytes and quantified its absorbance. Our observation revealed that SiNP-SH induced a notable disruption of red blood cells (RBCs) at a concentration of 200 µg/mL (3.00.±2.26 %, $p < 0.05$).

Moreover, higher concentrations of SiNP-SH resulted in an additional rise in the quantity of free haemoglobin (Figure 3.6-E). It indicates that the SiNP-SH induces damage to red blood cells in a manner that is dependent on the concentration. However, the PEGylated nanoparticles yielded conflicting outcomes. Specifically, SiNP-PEG750 had a detrimental effect on the integrity of red blood cells (RBCs) at a concentration of 200 µg/mL, resulting in a 4.16±3.21% haemoglobin production. Interestingly, further increasing the concentration did not produce a proportional increase in hemolytic qualities, unlike SiNP-SH (Figure 3.6-E). The highest level of free haemoglobin was detected in samples treated with a concentration of 50 µg/mL of SiNP-PEG5000 (2.95±1.23, $p<0.05$). Increasing the concentration further did not significantly increase hemolysis compared to the control (Figure 3.6-E). However, the hemolysis assay demonstrated that all values obtained in the experiment, including the highest ones, are within the specified ASTM standard indicators.

Therefore, we may conclude that these nanoparticles are hemocompatible. The electron microscope images confirmed our hypothesis that at 200 µg/mL concentrations, SiNP-SH disrupts red blood cells by creating aggregates close to or around the erythrocytes, resulting in a more efficient cell membrane disruption. A scanning electron microscope (SEM) analysis showed that SiNP-SH produces enormous clusters around red blood cells (RBCs). In certain instances, it also caused erythrocytes to clump together,

which could result in thrombosis (Figure 3.6-A). PEGylated nanoparticles exhibited distinct behaviour, as they only partially adhered to the erythrocytes and no clumps were found on red blood cells (Figure 3.6-B). However, since they do not cause the burst of red blood cells, nanoparticles may be safe to use systemically in small amounts. However, it is imperative to consider the possibility of erythrocyte agglutination after SiNP-SH therapy.

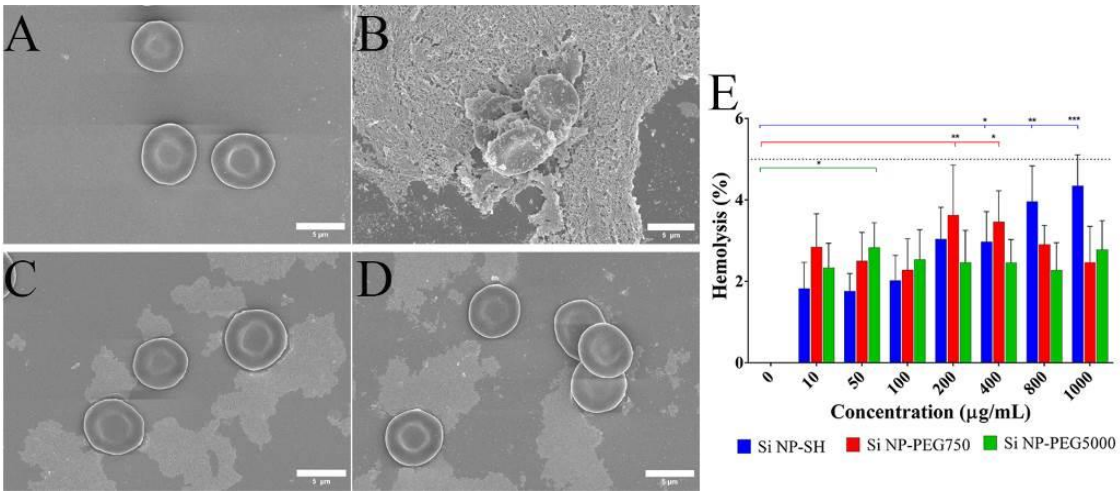

Figure 3.6. SEM pictures of red blood cells treated with A) PBS, B) SiNP-SH, C) SiNP-PEG750, and D) Si NP-PEG5000. The scale bar is 1 micron. Additionally, E) the results from the hemolysis assay are presented, with the dotted line corresponding to the 5% value (*P<0.05; **P≤0.01; ***P≤0.001; ****P≤0.0001).

Monitoring changes in the biomechanical properties of cells provides a means to evaluate the efficiency of pharmaceuticals delivery systems and their cytotoxic impact. Tumour formation and metastasis can induce modifications in the biomechanical characteristics of cells, including alterations in cell stiffness. Evaluating cell stiffness is crucial for understanding the impact of drug treatments and drug delivery systems and assessing their efficacy. Micro-indentation, utilising an Atomic Force Microscope (AFM), stands out as a reliable method for quantifying the stiffness of living cells. Despite being a relatively recent technique, AFM has been extensively employed to evaluate the rigidity of diverse materials, ranging from metal surfaces to delicate biological cells.

Increased tissue stiffness is a basic feature of solid tumours, and one of the main causes of this is the increased collagen fibre density in the extracellular matrix (ECM) (Wullkopf *et al.*, 2018; Deng *et al.*, 2022).

Our findings indicate that cell stiffness is notably influenced by the type of nanoparticles (Figure 3.7); for SiNP-SH and SiNP-PEG750, cell stiffness decreased after

24 hours, while cells treated with SiNP-PEG5000 exhibited increased stiffness. This phenomenon could be attributed to the ability of SiNP-PEG5000 to accumulate within cells, thereby altering their mechanical properties, a trend observed with magnetic nanoparticles (Perez *et al.*, 2021). Concurrently, SiNP-SH and SiNP-PEG750 also impacted cell mechanical properties, rendering them softer.

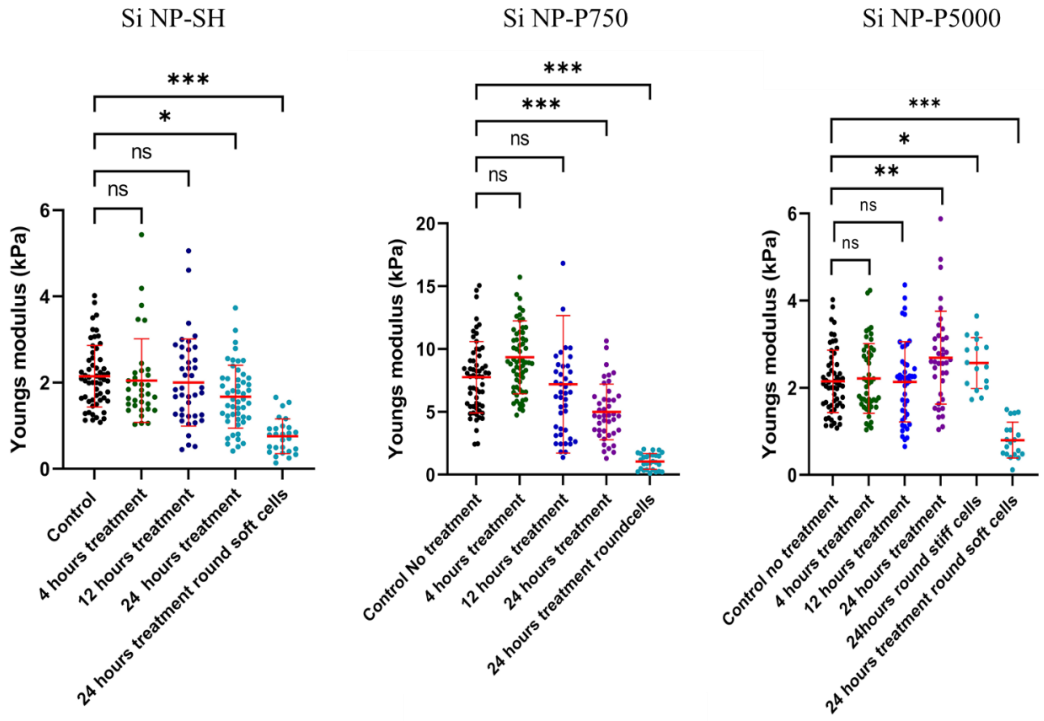

Figure 3.7. Cell stiffness change for A549 cells treated with SiNP-SH, SiNP-PEG750 and SiNP-PEG5000. SiNP-SH decreases the stiffness of A549 cells only at 24 hours, SiNP-PEG750 increases cell stiffness after 12 hours of treatment, and SiNP-PEG5000 increases cell stiffness of A549 cells only after 24 hours of treatment.

The cellular uptake of SiNP-SH, SiNP-PEG750, and SiNP-PEG5000 in the MCF7 cell line was investigated using laser scanning confocal microscopy based on the findings of the MTT and AFM tests. The cells were subjected to nanoparticles at a concentration of 400 µg/mL for various periods of 2, 4, 6, 12, and 24 hours in order to study the absorption process as it unfolded over time. Afterwards, the cells were immobilised and coloured using the methods specified in the section. The results indicated that nanoparticles penetrate the cell membrane in a manner that is affected by the duration of time. Furthermore, the capacity of SiNP-SH to infiltrate the cellular membrane and accumulate in the cytoplasm was compared to that of PEGylated nanoparticles. After a 24-hour incubation, thiolated nanoparticles experienced aggregation inside the cytoplasm

of the cells (Figure 3.8-A,B and C). The decrease in cell viability at this dosage is likely due to the formation of nanoparticle clusters both inside and on the cells. This observation is consistent with the results of the MTT experiment, which demonstrated a decrease in viability when the concentration reached 400 µg/mL.

In addition, the increased molecular weight of PEG extends the time it takes for nanoparticles to cross the cell membrane (Figure 3.8-C). The internalisation of SiNP-PEG5000 into the cell necessitated approximately 6 hours, while SiNP-SH and SiNP-PEG750 required a minimum of 2 hours. Furthermore, our objective was to ascertain the approximate quantity of NP absorbed by the cells. In order to accomplish this, we utilised ImageJ software to establish a correlation between the overall green fluorescence within the cells. The integrated density value (Figure 3.8-D) was obtained by subtracting the product of the area of selected cells and the background mean grey value. The findings demonstrated that SiNP-SH displayed a significantly greater capacity for internal uptake, as evidenced by the maximum amount of fluorescence observed within the cytoplasm of the cells after four hours. On the other hand, PEGylated nanoparticles exhibited the most intense fluorescence after being incubated for 24 hours, which is consistent with the results obtained from the cell stiffness investigations.

Thiolated nanoparticles are hypothesised to have rapid penetration of the cellular membrane and slow release from the cells, while PEGylated nanoparticles take longer to be taken up by the cells. The outcomes of our investigation corroborate the previous discoveries that the process of PEGylation diminishes the uptake of nanoparticles by cell lines, as documented in studies undertaken by Pelaz et al. in 2015 and Kim et al. in 2021. PEGylated nanoparticles exhibit a prolonged duration for cellular membrane integration, resulting in cell death demonstrated during the MTT experiment at high concentrations after 48 and 72 hours. The presence of sulfhydryl groups on the surface of SiNP-SH may impede the functioning of transmembrane proteins on the cell surface and enhance the permeability of nanoparticles (Hock *et al.*, 2022).

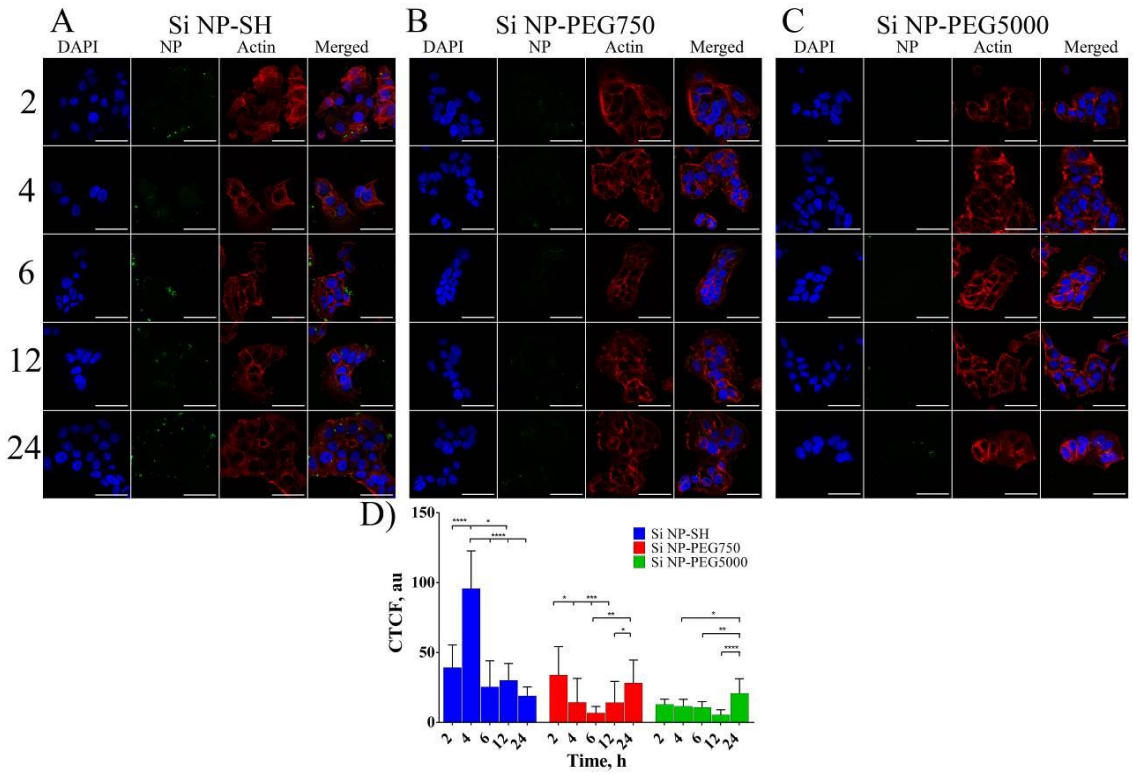

Figure 3.83. Images of MCF-7 cell line after the exposure to A) SiNP-SH, B) SiNP-PEG750, and C) SiNP-PEG5000 nanoparticles for 2, 6, 12 and 24 hours. In the images, blue denotes the nucleus, red signifies actin filaments, and green represents the nanoparticles. The scale bar is 50 μm. D) Quantitative analysis of absorbed nanoparticles inside the cells measuring the corrected fluorescence (*P<0.05; **P≤0.01; ***P≤0.001; ****P≤0.0001).

Previous studies did not demonstrate significant cytotoxicity of nanoparticles under controlled conditions. Consequently, the next logical step was to assess the toxicity of nanoparticles in animal models. Prior to conducting extensive in vivo research, our objective is to examine the biodistribution of nanoparticles and evaluate their histopathological effects on the primary organs of animals. In order to decrease the dependence on animals, we opted to investigate two different types of organosilica nanoparticles, SiNP-SH and SiNP-PEG5000, which exhibited varied results but showed reduced levels of toxicity in the MTT experiment.

The nanoparticles were labelled with a fluorescent dye, Alexa Fluor 750 C5 maleimide, to make them easier to see using the IVIS spectrum imaging station. The nanoparticles did not significantly increase in size after being labelled with fluorescent

markers. As stated before, PEGylation caused a slight rise in the size of nanoparticles, but it still stayed below the threshold of sub-100 nm.

Our study's main goal was to investigate nanoparticles' distribution in living organisms. Therefore, after administering SiNP-SH and SiNP-PEG5000 nanoparticles to mice through intravenous injection, we produced anaesthesia to make the animals fall asleep. Afterwards, we humanely put them to death in accordance with the ethical norms of the facility. The principal organs, such as the brain, spleen, lungs, heart, liver, kidneys and gastrointestinal tract organs, were extracted and examined for the presence of fluorescent signals utilising the IVIS Spectrum CT system. The fluorescence generated by the thiolated nanoparticles was first observed in the lungs till day 7 (Figure 3.9). Afterwards, the fluorescence signal disappeared from the lungs and reemerged in the spleen on days 14 and 28 and in the stomach on day 28 (Figure 3.9). Photobleaching poses a substantial problem when employing fluorescent dyes. In order to verify that the decrease in fluorescence was not responsible for the absence of signal in the lung, we performed thermogravimetric analysis (TGA). The aim of our study was to ascertain if there was a discrepancy in mass between the control and treatment groups. The TGA results confirmed that the nanoparticles did not persist in the lung (Figure 3.10).

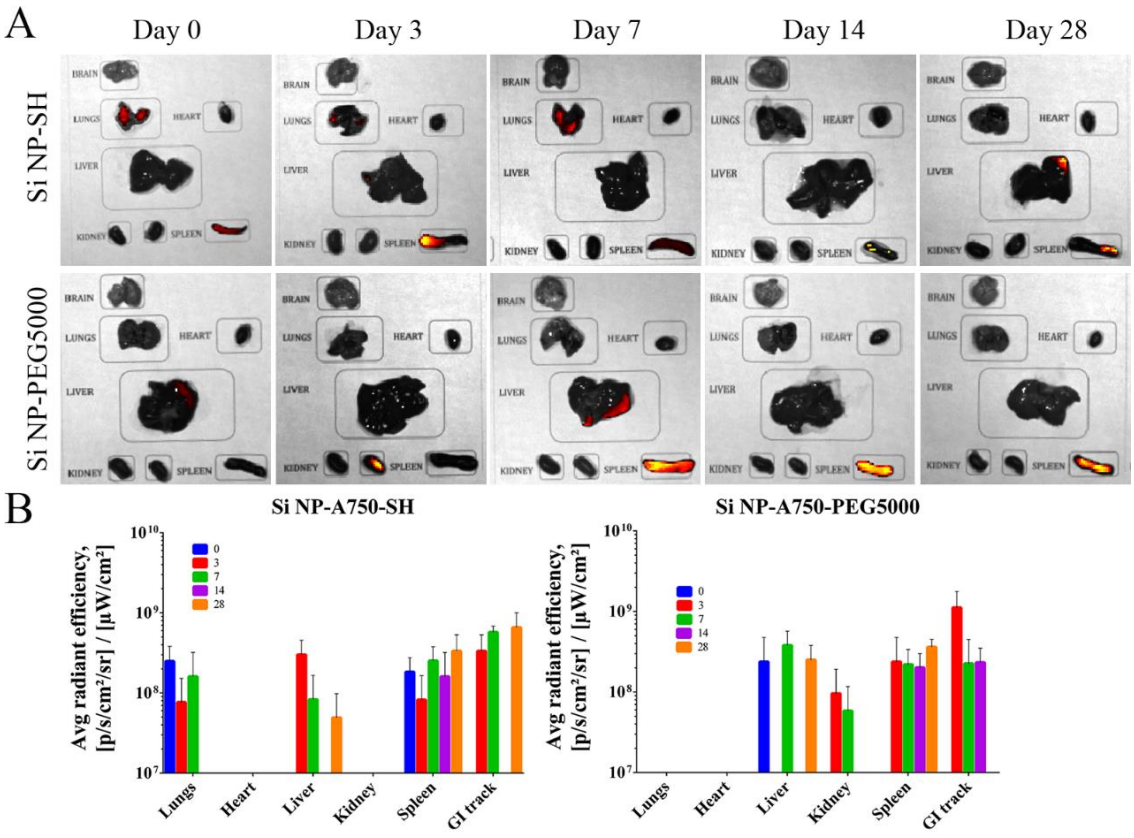

Figure 3.9. Distribution of organosilica nanoparticles ex vivo: A) Images of dissected organs from mice after the intravenous injection with SiNP-SH and SiNP-PEG5000 nanoparticles at 10

mg/kg of animal concentration. B) The average radiant efficiency (µW/cm2) of nanoparticles corresponding to dissected organs.

At first, only the liver showed light released by PEGylated nanoparticles on day 0. However, signals emerged in the kidney on the third day, followed by the spleen on the seventh day, and eventually in the stomach. However, the signal continues to exist in the spleen until day 28, despite the absence of nanoparticles in other organs (Figure 3.9). After being exposed to SiNP-PEG5000 nanoparticles for 3 and 7 days, the presence of the nanoparticles was detected in the kidney, suggesting that the renal clearance pathway removed some of the nanoparticles. He et al. (2011) found that PEGylated silica nanoparticles, specifically those conjugated with -OH, -COOH, and PEG, were excreted through the kidneys. However, they also observed that nanoparticles with -OH and -COOH groups had a higher uptake in the liver. This study provides evidence of renal excretion of these nanoparticles (Hadipour Moghaddam, Mohammadpour and Ghandehari, 2019). In a separate investigation, smaller silica particles evaded entrapment by liver and spleen tissues and underwent gradual biodegradation. Moreover, PEGylation of nanoparticles prevents them from being lodged in lung, spleen, and liver tissue (He *et al.*, 2011; Borak *et al.*, 2012).

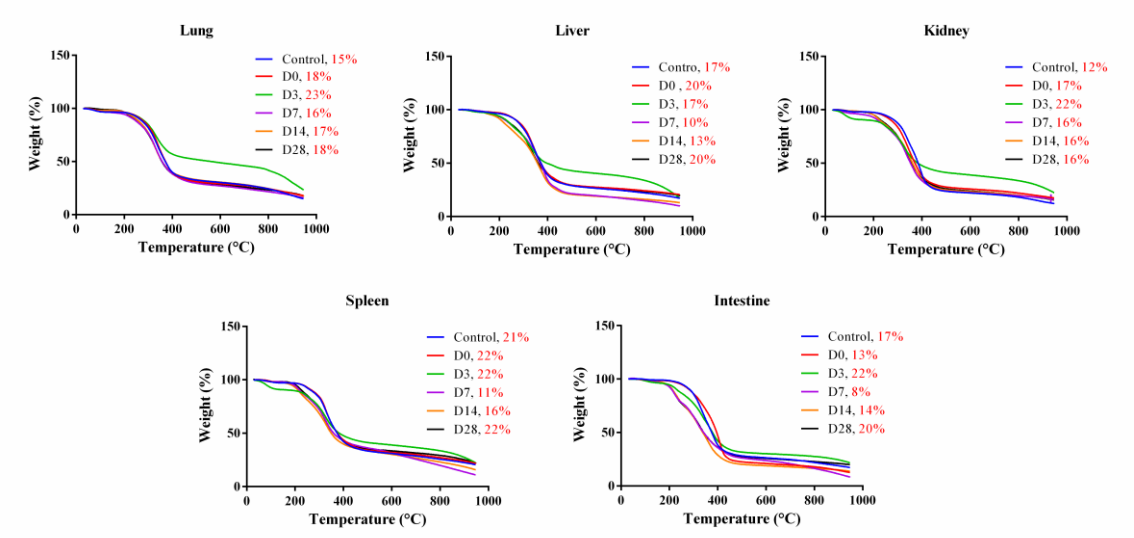

Figure 3.104. Graph of weight change after the thermogravimetric analysis (TGA) of dissected mice organs on 0, 3rd, 7th, 14th and 28th days post IV injections with Si NP-A750-SH nanoparticles. Organs were removed from a mouse, minced and sonicated to form homogenate.

Based on the distribution investigations, it is evident that thiolated nanoparticles exhibit adherence to the mucosal tissue, which has been previously documented in *ex vivo*

studies (Mun, Williams and Khutoryanskiy, 2016; Ways *et al.*, 2020). Hence, thiolated nanoparticles can be regarded as suitable candidates for drug delivery systems targeting the respiratory tract, urinary tract, or reproductive system organs, given their affinity for mucosal tissues lining them.

Fluorescence emitted by thiolated nanoparticles was detected in the gastrointestinal tract, liver, and the lining of the stomach and intestines on the third and seventh days. This indicates that the nanoparticles were eliminated from the body through hepatobiliary clearance (Souris *et al.*, 2010; Poon *et al.*, 2019). The fluorescent signal in the kidneys indicates that the clearance of PEGylated nanoparticles occurs through both the hepatobiliary and renal channels.

We conducted histological research on another cohort of mice to evaluate any potential tissue damage induced by the nanoparticles. The morphology of the examined organs remained largely unaltered following the intravenous delivery of nanoparticles. The liver's structure was maintained through the presence of a delicate capsule composed of fibrous connective tissue. The lobules maintained their hexagonal prism shape, characterized by the arrangement of hepatocytes in strands. Kuepfer cells adhere to the endothelium of the sinusoidal capillary, which is situated inside. Lymphocyte infiltrations were found in the liver on days 7 and 28 for both nanoparticles, as shown in Figure 3.11.

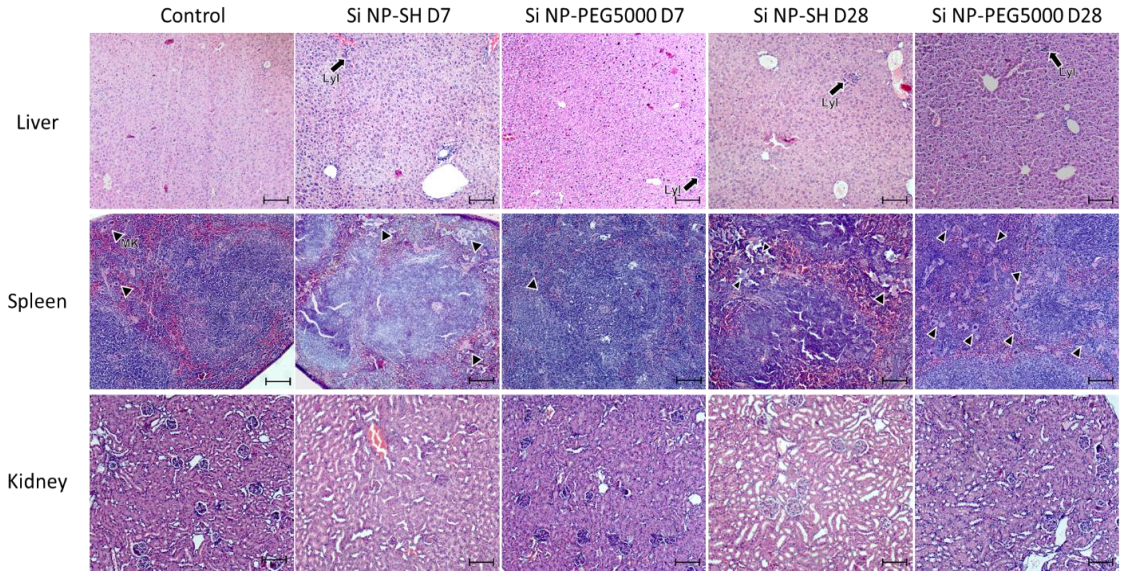

Figure 3.115. Hematoxylin and eosin-stained liver, spleen, and kidney slices under light microscopy following injection with SiNP-SH and Si NP-PEG5000. After an IV injection, organs were harvested one week and four weeks later. Triangles (MK) denote megakaryocytes, and arrows (LyI) indicate lymphocyte infiltration. The scale bar is 100 µm.

After four weeks of exposure to NP, the light microscopy images of the spleen showed that its composition remained unchanged, with clearly defined white and red pulp consisting of separate cells. The main downside of nanoparticles may be the degradation of the spleen composition (Awaad, 2015). In all groups, we noted a higher quantity of small and medium-sized lymphocytes in the mantle zone of the lymphoid. Megakaryocytes may be observed in the groups that had injections of both types of nanoparticles one week after the injection. The number of megakaryocytes rose further after four weeks. The number of megakaryocytes was greater in the spleen of mice subjected to Si NP-A750-PEG5000 treatment. The data corroborates prior research on mesoporous silica, indicating that the spleen and liver mainly capture nanoparticles (Chan *et al.*, 2017; Rascol *et al.*, 2018; Yu *et al.*, 2018; Yang, Chen and Shi, 2019a).

Due to the small size of nanoparticles, the possible elimination pathway via the kidney was also examined in the study; consequently, a histological evaluation of renal tissue was undertaken. Furthermore, we detected signals in the renal tissue of mice that were administered Si NP-PEG5000. The observations indicated the absence of significant disruptions to the kidneys' structure. However, we see the presence of lymphocytic infiltration in both the cortical area and medulla of the kidneys on days 7 and 28.

No necrotic regions were observed in histological samples, demonstrating that nanoparticles did not induce toxicity. Our discovery aligns with other research showing the favourable tissue compatibility of silica nanoparticles after their oral administration and intravenous injection into mice. Furthermore, Fu et al. (2013) proved that silica nanoparticles can be safely administered through hypodermic and intramuscular methods. Liu et al. (2011) also documented the little toxicity of intravenously injected silica nanoparticles, whether administered as a single dosage or repeatedly (Liu *et al.*, 2011; Fu *et al.*, 2013). In the study conducted by Fent et al. (2010), it was shown that there was no noticeable harm to the embryos of zebrafish while investigating the toxicity of silica nanoparticles (Fent *et al.*, 2010). This suggests that using these particles in medicinal applications has a minimal risk.

3.4. SUMMARY

This work conducted a comprehensive toxicological analysis to investigate the hazardous characteristics and distribution in the body of thiolated and PEGylated nanoparticles (SiNP-SH, SiNP-PEG750, and Si-NP-PEG5000) in various cell cultures, human blood, and animals — the investigation employed spectroscopy, optical imaging,

and electron microscopy techniques. Our objective was to make a substantial contribution to the current research on organosilica nanoparticles and collaborate with the scientific community to determine appropriate uses for both modified and non-modified nanoparticles. Laboratory investigations have shown that these nanoparticles may efficiently transport chemicals and serve as tools for medical imaging, given that they are suitably functionalised. Nanoparticle viability investigations typically occur between 0-100 µg/mL concentrations. Our analysis revealed no indication of cytotoxicity at doses of 100 µg/mL and lower for all varieties of nanoparticles.

Furthermore, the A549 and MCF-7 cell lines remained viable, with no decrease below 70%, even when exposed to a 400 µg/mL concentration of nanoparticles for 24 hours. Based on these observations, we can infer that the toxicity of nanoparticles is influenced by their concentration, exposure period, and the specific type of nanoparticle. In addition, it is crucial to consider the molecular mass of PEG for PEGylation. Our research indicates that SiNP-PEG750 exhibited higher toxicity when compared to SiNP-SH and Si NP-PEG5000.

Moreover, it has been observed that thiolated organosilica nanoparticles demonstrate enhanced and faster internalisation compared to their PEGylated counterparts. Furthermore, we have observed that PEG molecules with a greater molecular weight necessitate an extended period for internalisation. This suggests that the size of nanoparticles has a more significant influence on the process of cell internalisation compared to their surface features. Moreover, the ability of thiolated nanoparticles to adhere to the cell surface makes them an attractive choice for mucosal drug delivery systems.

The histology data indicates that both nanoparticles have had a minor effect on the spleen and liver, which was expected due to how these nanoparticles are eliminated from the body. The kidney structure did not suffer any substantial damage, and no necrotic tissues were detected after exposure to either type of nanoparticle.

Our thorough analysis has not only expanded our knowledge about the potential use of organosilica nanoparticles but has also demonstrated that MPTS-based nanoparticles are a highly effective type of nanoparticles for biological applications. Thiolated nanoparticles offer the benefit of being altered with various ligands and targeting agents, comparable to the process of PEGylation. MPTS-based nanoparticles are more versatile than other silica particles.

This study contributes to a better understanding of the potential applications of organosilica nanoparticles in biomedicine. In addition, it has ramifications for developing comprehensive analytical methods for any nanoparticles that are utilised in medical applications. It is essential to standardise methodologies for analysing nanotechnology instruments in the context of biomedical applications. In an effort to cover all of these different approaches, the National Cancer Institute made an effort. On the other hand, because there are many different kinds of nanoparticles, the data must be updated on a consistent basis. The data gathered in this chapter provides vital information regarding the essential study that must be carried out, underlining the demand for additional exploration of organosilica nanoparticles.

BLANK

CHAPTER 4. MODIFICATION OF ORGANOSILICA NANOPARTICLES WITH PEPTIDE

4.1. INTRODUCTION

Despite the progress and development of many different types of nanoparticles for drug delivery, two main drawbacks persist specificity and cellular membrane permeability. While a significant number of nanoparticles depend on passive targeting, leveraging the enhanced permeability and retention (EPR) effect facilitated by the inflammation and hypoxia associated with tumour sites, certain cancer types do not exhibit this effect. Moreover, within a single tumour, there may be high heterogeneity in vessel permeability, further complicating targeting strategies. Upon reaching the target site, nanoparticles encounter additional challenges, including crossing physical and biochemical barriers. Remarkably, approximately 1% of intravenously injected nanoparticles successfully reach the intended target site (Buddhiraju *et al.*, 2023). Therefore, numerous strategies for nanoparticle functionalisation are employed, among which conjugation with cell-penetrating peptides is prominent.

Before conducting experiments with targeting peptides, verifying the chemistry of peptide conjugation using a well-established peptide is prudent. Given the scope of our study, it is crucial to ascertain that nanoparticles accumulate in the cytoplasm. The selected cell-penetrating peptide for this purpose is TAT (trans-activating transcriptional transactivator). TAT-peptide is cationic and abundant in arginine residues. (Jhaveri and Torchilin, 2016), which allows it to be translocated inside the cell. Through binding to importin α and β (karyopherin), it can pass nuclear pore complexes and allow nanoparticles or drugs to accumulate in the nucleus (Pan, He, Liu, Chen, Zhang, *et al.*, 2012; Li, Zhang and Feng, 2019; Yang, Chen and Shi, 2019a).

The TAT-peptide was conjugated to thiolated organosilica nanoparticles through the maleimide moiety, modification on the peptide at its N-terminal, as provided by the manufacturer. Conjugation efficiency was assessed through various physicochemical characteristics such as zeta potential measurements, dynamic light scattering (DLS) and the Ellman assay. Furthermore, chemical analysis of the conjugation efficiency was conducted using NMR spectroscopy, SDS-PAGE, X-ray photoelectron spectroscopy (XPS) and Raman spectroscopy.

Our investigations resulted in the successful conjugation of TAT-peptide to the nanoparticles and the development of a robust method for analyzing the conjugation efficiency. Subsequently, the effectiveness of Si NP-TAT was evaluated *in vitro* to discern any alterations in cell viability and the impact on cellular translocation.

4.2. MATERIALS AND METHODS

Table 4.1. List of consumables, Chapter 4.

Name	Abbreviation	CAS-number	Manufacturer
(3-Mercaptopropyl)trimethoxysilane	MPTS	4420-74-0	Sigma-Aldrich
Sodium hydroxide	NaOH	1310-73-2	Sigma-Aldrich
Dimethyl sulfoxide	DMSO	67-68-5	Sigma-Aldrich
Dialysis tubing cellulose membrane	n/a	n/a	Sigma-Aldrich
Atto 488 maleimide	A488		Sigma-Aldrich
5,5-dithio-bis-(2-nitrobenzoic acid)	DTNB	69-78-3	Sigma-Aldrich
L-cysteine hydrochloride monohydrate	n/a	52-89-1	Sigma-Aldrich
Multicolor Low Range Protein Ladder ((1.7 to 40kDa))	n/a	n/a	Thermo Scientific
Dimethyl sulfoxide-d6	DMSO-d6	2206-27-1	Sigma-Aldrich
TAT-maleimide peptide	TAT-peptide	n/a	GenScript

4.2.1. Synthesis and characterization of thiolated organosilica nanoparticles

Organosilica nanoparticles were synthesized according to the protocol described in Chapter 3 (3.2). Silica precursor, MPTS, at volume 1.125 mL, was added to 30 mL DMSO and placed on a magnetic stirrer. The reaction started after adding 0.750 mL of 0.5M NaOH as a catalyst reagent. Reaction performed under air-bubbling conditions for 24 hours. After the synthesis completion, formed nanoparticles were purified with dialysis against diH_2O to remove unreacted composites for eight water changes.

The nanoparticles were prepared to measure size and sulfhydryl concentration. For dynamic light scattering (DLS) analysis, 50 µL of the nanoparticle suspension was diluted in 4.950 mL of ultrapure water. The suspension was then sonicated for 5 minutes to ensure uniform dispersion before being measured on a Nano-ZS series instrument (Malvern Instruments, U.K.) at 25°C. Analysis of sulfhydryl concentration was measured with Ellman's assay, which was described in the previous chapter. Briefly, 3 mg of freeze-dried nanoparticles were dissolved in PBS, and after 1 hour, the dissolved suspension was mixed with DTNB solution in a 1:1 ratio and absorbance of supernatant was measured at 420 nm on Microplate reader (Varioscan, Thermo Scientific, USA). The standard curve was produced with L-glutathione at a concentration range of 0.004 to 0.644 µmol/mL.

4.2.2. TAT peptide conjugation

Thiolated organosilica nanoparticles were functionalised by adding TAT-peptide to enhance cellular permeabilisation. TAT-maleimide (Genscript), with the sequence GRKKRRQRRRPQ, was employed in the experiment. Various concentrations of TAT-maleimide were tested to determine the optimal synthesis conditions. The amount of TAT-maleimide was calculated based on the molar ratio of peptide to the thiol content on the nanoparticles. Table 4.2 concisely overviews the synthesis conditions utilised.

Table 4.2. Conditions for TAT-maleimide conjugation to thiolated organosilica nanoparticle.

ID	C (SH), µmol	C (TAT), µmol	Conditions
SiNP-SH	-	-	-
Si NP-TAT_A	**1**	**1**	**18 h, rt**
SiNP-TAT_B	**1**	**2**	**18 h, rt**
SiNP-TAT_C	**1**	**4**	**18 h, rt**

In brief, TAT-maleimide was mixed with thiolated nanoparticles dissolved in 6 mM NaCl and stirred for 18 hours at room temperature. Subsequently, the functionalised nanoparticles were purified by dialysis against deionised water (diH_2O), with eight water changes conducted during the process.

4.2.3. DLS and Ellman's assay

The size and zeta potential of the functionalised nanoparticles were measured using the previously described method on a Nano-ZS series instrument (Malvern Instruments, U.K.) at 25°C. However, Ellman's assay was modified for protein assays due to the limited quantity of nanoparticles available. The new protocol involved preparing a DTNB stock solution containing two mM DTNB, 50 mM sodium acetate, and 1 M Tris base solution at pH 8. The procedure proceeded: 840 µL of ultrapure water, 100 µL of 1 M Tris solution, and 50 µL of DTNB solution were mixed in a 1.5 mL Eppendorf tube. Subsequently, 5 µL of the nanoparticle samples were added. 10 µL of water was added to another Eppendorf tube for the blank. The solution was thoroughly mixed and incubated for 5 minutes in the dark at room temperature. Following incubation, absorbance was measured on a Microplate reader (Varioscan, Thermo Scientific, USA) at 412 nm to determine the concentration of thiol compounds.

4.2.4. Elemental and Thermogravimetric Analysis

The nanoparticles were subjected to freeze-drying for CHNS elemental and thermogravimetric analysis. Freeze-dried nanoparticles weighing 5-7 mg were placed on a ceramic crucible for thermogravimetric analysis. The analysis was conducted using an STA6000 instrument (Perkin Elmer, USA), with temperatures ranging from 30 to 950 °C at a heating rate of 10 °C/min under a nitrogen flow of 30 mL/min. The obtained results were analysed using OriginPro software.

For CHNS analysis, freeze-dried nanoparticles weighing 2-3 mg were wrapped in a tin foil and placed into the wells of a CHNS-O unicube-organic elemental analyser (Elementar, Germany).

The measurements were performed by heating the samples to 1800 °C.

4.2.5. SDS-PAGE

SDS-PAGE for small molecular weight proteins was used to measure the presence of the peptide within nanoparticles qualitatively. The first steps consisted of a 3-layered gel preparation: 16% separating gel followed by 10% spacer gel and 4% stacking gel. Each solution was prepared right before the gel loading.

Initially, the casting frame was positioned on the casting stands, following which a 16% gel solution was meticulously loaded into the gap between the glass plates. A few

drops of water were then added to facilitate gel alignment. Subsequently, after 30 minutes of gelation, any remaining water was removed, and a 10% gel solution was added atop with a few additional drops of water. This mixture was left to gel for another 30 minutes. Upon removing excess water, a 4% stacking gel was added along with the insertion of a well-forming comb, and the entire setup was left to gel for an additional 30 minutes. The recipe for gel preparation can be found in Table 4.3.

Table 4.32. Gel composition for tricine SDS-PAGE for small molecular weight proteins and peptides. *AB-6: add 45.6 g acrylamide and 3 g bisacrylamide to 100 mL dH_2O.

	16%	**10%**	**4%**
AB-6*	5 mL	200 µL	500 µL
Gel buffer (3x)**	5 mL	300 µL	1.5 mL
Glycerol	1.5 mL	100 µL	-
Water	3.445 mL	394.5 µL	3.951 mL
10% APS	50 µL	5 µL	45 µL
TEMED	5 µL	0.5 µL	4.5 µL

To prepare functionalised nanoparticles for electrophoresis, they were first treated to break down the sulfhydryl groups using a DTT (dithiothreitol) solution. Specifically, 10 µL of 40 µM DTT was mixed with 10 µL of nanoparticles and incubated in a thermostat at 56°C for 30 minutes. As a control, 10 µL of TAT peptide at a concentration of 40 µM was mixed with 10 µL of water. Subsequently, the diluted nanoparticles and TAT peptide were mixed with an equal volume of Laemmli buffer (Sigma-Aldrich) and incubated in a thermostat for 5 minutes at 95°C. The prepared gels were then placed into an electrophoresis tank, with the inner chamber filled with 1X cathode buffer (6.055g Tris, 8.9585 g Tricine, 0.5 g SDS in 1000 mL dH_2O) and the outer chamber with anode buffer (pH 8.9, 6.05 g Tris in 500 mL dH2O). Subsequently, 20 µL of the prepared samples were added into each well, with the first well filled with 5 µL of a ladder (Fisher Scientific). The electrophoresis was initiated at an initial voltage of 30 V for approximately 30 minutes until the samples entered the separating gel, after which the voltage was increased to 120 V and continued for 2 hours.

Once the dye reached the bottom of the gel, electrophoresis was halted, and the gel was carefully transferred into a container with a fixative solution (50 mL H_2O, 40 mL methanol, 10 mL acetic acid) for 30 minutes. After fixation, the gel was washed with deionized water and stained with 0.025% Coomassie dye in 10% acetic acid for 30

minutes. After staining, the gel was washed several times with water and then destained in a 10% acetic acid solution for 1 hour before being visualized on a ChemiDoc system (Biorad, USA).

4.2.6. NMR and RAMAN spectroscopy

NMR and Raman spectroscopy analyses were conducted on Si NP-TAT, SiNP-SH, and TAT peptides to elucidate their structures and compare the functional groups.

For Raman spectroscopy, sample preparation was straightforward. The lid from a 1.5 mL Eppendorf tube was cut and utilized as a transparent mount, onto which 200 µL of the sample was added. Measurements were performed at room temperature using a laser with a wavelength (λ) of 532 nm, covering a spectral range from 4000 to 400 cm^{-1}.

Samples for NMR analysis were freeze-dried: 0.3 mL of nanoparticle suspension was placed into a 1.5 mL Eppendorf tube and frozen at -20°C overnight. The frozen sample was subsequently freeze-dried in a Lyotrap for two days to ensure complete water removal. In powder form, the nanoparticles were then dissolved in chloroform-D (CDCl3) to achieve a final concentration of 3 mg/mL. NMR characteristics included 1H proton analysis with 512 scans.

4.2.7. XPS

XPS measurements were conducted using the Nexsa XPS system equipped with a monochromated low-power Al Kα X-ray source emitting at 1486.6 eV alongside a charge neutralization gun. Freeze-dried nanoparticles were carefully positioned onto carbon tape affixed to the holder and pressed against the substrate using a clean spatula. Subsequently, the holder was inserted into the XPS chamber for analysis. Data analysis was carried out using the Avantage Data System, with a reference peak established at 284.2 eV corresponding to C1s (Mekaru et al., 2019).

4.2.8. MTT assay

Cell viability was assessed using the Thiazolyl blue tetrazolium bromide (MTT) (Thermo Scientific, USA). Before experimentation, nanoparticles were diluted to concentrations ranging from 0 to 400 µg/mL in a cell culture medium. A549 cell line was seeded in a 96-well plate at a density of $5*10^4$ cells per well and incubated overnight at 37°C with 5% CO_2 until reaching confluency. Upon achieving confluency, a fresh cell

medium containing nanoparticles was added to final concentrations of 25, 50, 100, 200 and 400 µg/mL. The cells were then further incubated for 24 hours in a humidified atmosphere at 37°C with 5% CO_2. Cells treated with cell media without nanoparticles served as the negative control.

Following incubation with nanoparticles, 15 µl of MTT dye solution was added to each well and incubated for 4 hours. Subsequently, 100 µl of 10% SDS was added to dissolve the formed formazan crystals. The absorbance was measured at 570 nm using a plate reader (Microplate reader Varioscan, Thermo Scientific, USA). Cell viability was calculated using the formula:

$$Cell\ viability\ \% = \frac{Absorbance\ of\ treated\ cells}{Absorbance\ of\ negative\ control} * 100\%$$

4.3. RESULTS AND DISCUSSION

Thiolated organosilica nanoparticles were synthesised according to the protocol developed by Irmukamedova and Mun (Irmukhametova, Mun and Khutoryanskiy, 2011; Mun, Williams and Khutoryanskiy, 2016). Upon completion of synthesis, their sulfhydryl content was quantified using Ellman's assay, and the amount of peptides was determined based on thiol concentration. Various concentrations were explored during conjugation, and subsequent investigations were conducted on the conjugated nanoparticles.

From Table 4.4, it is evident that the increase in size was dependent on the TAT concentration, with a corresponding increase in polydispersity index (PDI). However, TEM images revealed monodispersed nanoparticles in terms of size. SiNP-TAT_B and SINP-TAT_C significantly reduced thiol content, whereas SiNP-TAT_A did not. SiNP-TAT_A and SiNP-TAT_B displayed a size range below 100 nm with favourable PDI, indicating uniform size distribution, measured at 52±1 nm and 59±1 nm, respectively. In contrast, the size of SiNP-TAT_C nanoparticles was 517±65 nm, and the high polydispersity index suggests uneven size distribution. One possible explanation is the formation of TAT aggregates and modified nanoparticles, leading to the observed disparity.

Table 4.4. DLS and Ellman's assay of thiolated and TAT-conjugated nanoparticles.

ID	Size, nm	PDI	ζ-potential, mV	C (SH), µmol/L
SiNP-SH	49±1	0.134	-44.7±1.4	13±2.1/22±1.6
Si NP-TAT_A	52±1	0.212	-30.4±3.8	24.8±0.6
SiNP-TAT_B	59±1	0.282	-29.7±0.8	8.7±2.8
SiNP-TAT_C	517±65	0.802	-30±0.6	4.9±1.5

Further analysis via SDS-PAGE indicated no band corresponding to the TAT peptide in Si NP-TAT-A, while distinct bands corresponding to the TAT peptide were observed on SiNP-TAT_B and SiNP-TAT_C nanoparticles (Figure 4.1). Disrupting the bond between TAT and SiNP-SH was necessary to visualise the peptide. This was achieved by employing DTT as a reducing agent to denature the nanoparticles, followed by agarose gel electrophoresis analysis. From SDS-PAGE, the molecular weight of the peptide was calculated to be approximately 4.2 kDa. Notably, the size of TAT-maleimide purchased from GeneScript was reported as 1773.03 Da, which is lower than the observed value. This discrepancy may be attributed to the self-aggregation of the peptide (Macchi *et al.*, 2017).

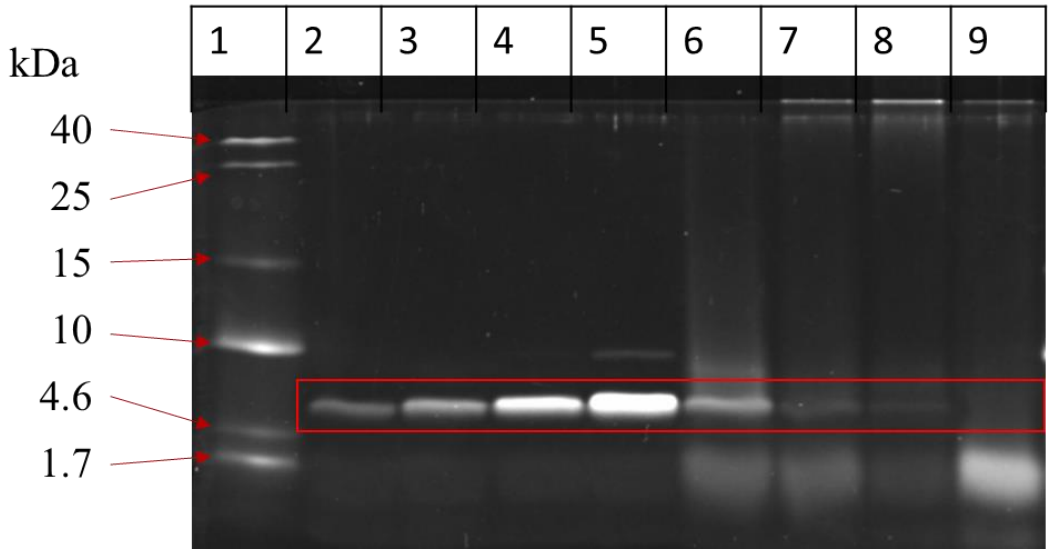

Figure 4.1. SDS-PAGE of TAT-maleimide at various concentrations 2)0.007 mM, 3) 0.014 mM, 4) 0.028 mM, 5) 0.056 mM and 6) SiNP-TAT_C; 7) SiNP-TAT_B, 8) SiNP-TAT_A and 9) SiNP-SH.

Following that, we performed a CHNS elemental analysis to determine the percentage of nitrogen (N) and other elements, such as carbon (C), hydrogen (H), and sulfur (S). Table 4.5 shows us that SiNP-SH and SiNP-TAT_A nanoparticles had no N within their structure. Regarding SiNP-SH, there are no N atoms present within the structure, while the absence of N in sample SiNP-TAT_A may represent that TAT-conjugation did not work or that the amount of the peptide is too low for the equipment's capabilities. However, the percentage of N in samples SiNP-TAT_B and SiNP-TAT_C is less than 1%, but it correlates with increasing the concentration of TAT peptide for each synthesis.

Table 4.53. CHNS elemental analysis results.

	N [%]	C [%]	H [%]	S [%]
SiNP-SH	0.00	24.23	5.95	23.75
Si NP-TAT_A	0.00	28.84	5.97	24.71
SiNP-TAT_B	0.23	27.88	6.02	24.59
SiNP-TAT_C	0.81	28.67	6.06	22.72

Thermogravimetric analysis revealed an uneven weight loss in thiolated and TAT-peptide-conjugated nanoparticles (Figure 4.2). Due to equipment limitations, the maximum temperature achievable was 950°C, preventing complete combustion of all organic residues. Based on calculations, if we consider the molecular mass of MPTS (196.34 g/mol) as 100%, the residual silicon dioxide (O=Si=O) should constitute approximately 31%. However, our study did not attain the temperature required for complete combustion of all organic matter. Despite this limitation, a clear trend in the weight loss of organic compounds in TGA was observed, which correlated with the concentration of TAT-peptide used for conjugation.

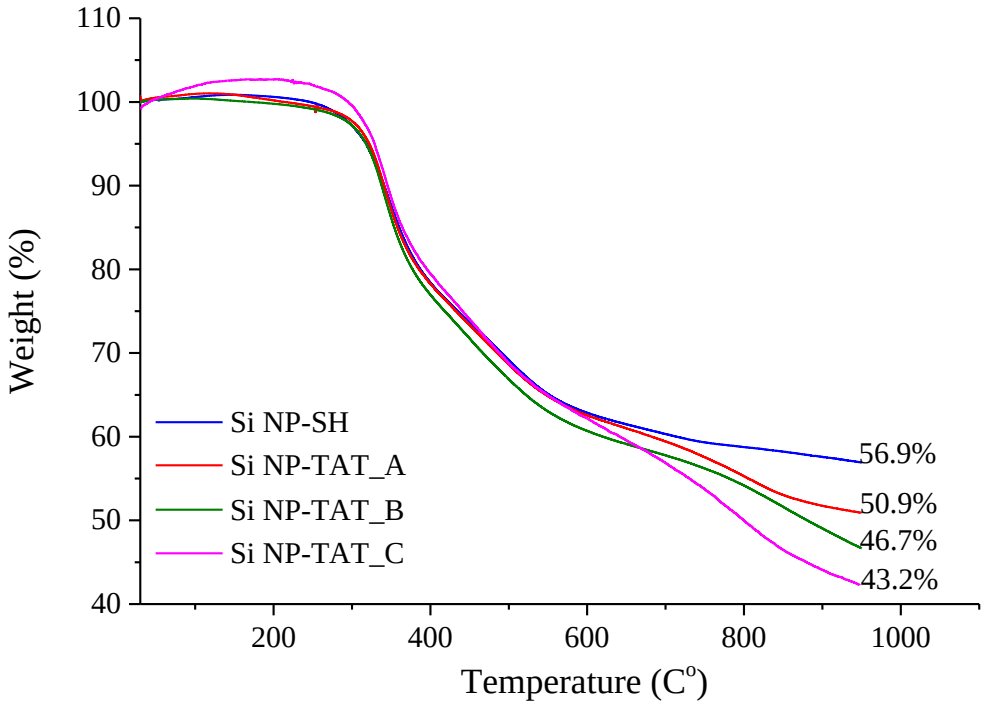

Figure 4.26. Thermogravimetric analysis, weight loss curve of thiolated and TAT-peptide modified organosilica nanoparticles upon heating from 30 °C to 950 °C.

The 1H NMR spectra of SiNP-SH, TAT-maleimide, and TAT-conjugated nanoparticles exhibited characteristic peaks for each compound. In the SiNP-TAT_B and SiNP-TAT_C spectra, peaks were observed at δ 1.10 ppm corresponding to the NH_2 group of glycine and at δ 1.65 ppm for NH_2 groups on other amino acids within the peptide structure (Figure 4.3). Additionally, a peak at δ 2.27 ppm was observed, indicating the presence of amino groups bonding amino acids of the peptide together. The presence of these peaks on SiNP-TAT_B and SiNP-TAT_C correlates with the data obtained from SDS-PAGE and CHNS analysis.

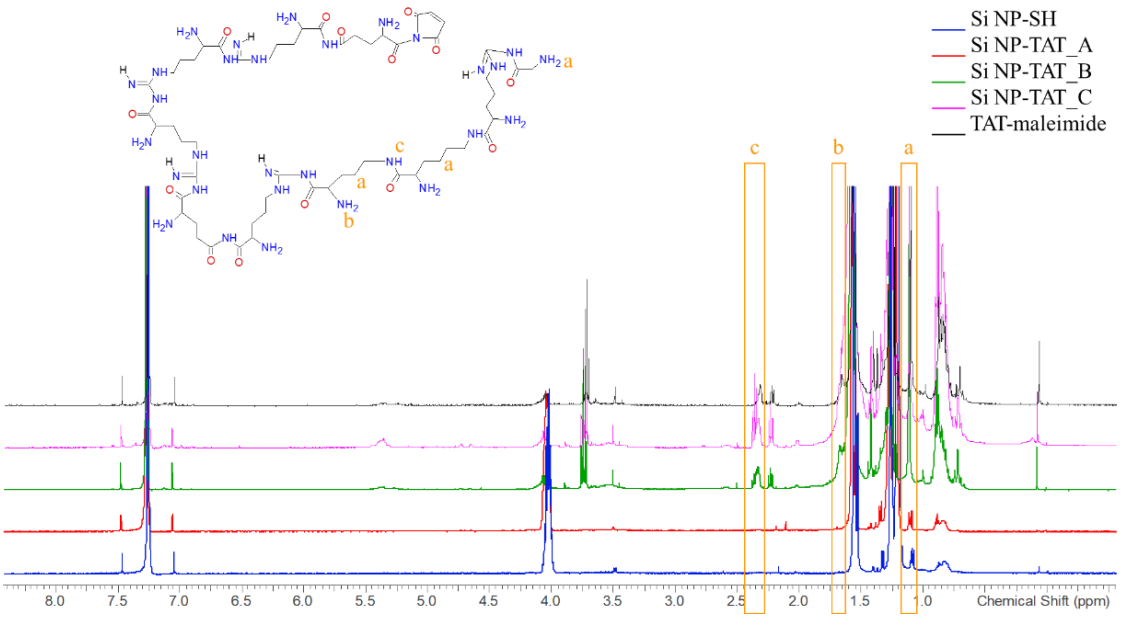

Figure 4.3. 1H MNR spectroscopy of thiolated and TAT-conjugated nanoparticles dissolved in CDCl3.

RAMAN spectroscopy performed on the liquid form of nanoparticles revealed the presence of peaks corresponding to the bonds present in the TAT-peptide (see Figure 4.4). For instance, a stretch between 1500-2000 cm^{-1} corresponds to the C=C bond found in the TAT-peptide, which is absent in the nanoparticles (Al Mahrooqi *et al.*, 2018c). Additionally, a peak at 3407 cm^{-1} corresponding to N-H and O-H bonds was observed, indicating the presence of these functional groups in both the conjugated and thiolated nanoparticles. While the peak of SiNP-SH could be attributed to water, the peaks observed for the TAT-conjugated nanoparticles were higher, suggesting successful conjugation.

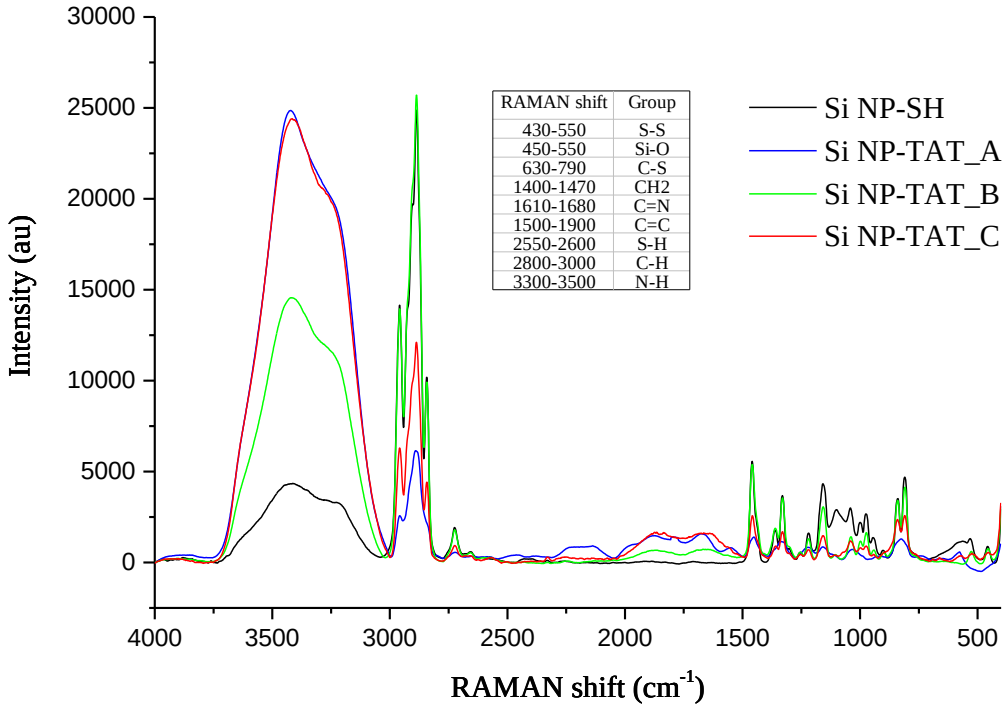

Figure 4.47. RAMAN spectroscopy of thiolated and TAT-peptide conjugated nanoparticles.

The nanoparticles were further analysed using X-ray photoelectron spectroscopy (XPS) to understand successful conjugation better. XPS is a valuable technique for determining the surface structure of compounds, providing insights into the composition of the outermost layers up to approximately 10 nm in depth. Although primarily used for thin film analysis, XPS can also be applied to nanoparticles.

In a study by Nakamura et al., the composition of thiolated organosilica nanoparticles synthesised from MPMS was examined using soft XPS (Mekaru et al., 2019). Interestingly, superior results were obtained with synchrotron radiation (SR), as the noise associated with an Al/Mg twin-anode X-ray gun hindered proper sample analysis. Our experiment obtained XPS data using a monochromated low-power Al Kα X-ray source with a photon energy (hν) of 1486.6 eV.

Five energy regions were selected for analysis: C 1s (279−297 eV), Si 2p (98−110 eV), O 1s (527−541 eV), S 2p (155-177 eV), and N 1s (380-410 eV). Following the measurements, the reference peak for C 1s was adjusted to 284.2 eV (Mekaru et al., 2019).

A survey of the entire spectra revealed the presence of C 1s, Si 2p, O 1s, and S 2p in all samples. However, only the SiNP-TAT_C exhibited a peak corresponding to N 1s (Figure 4.5).

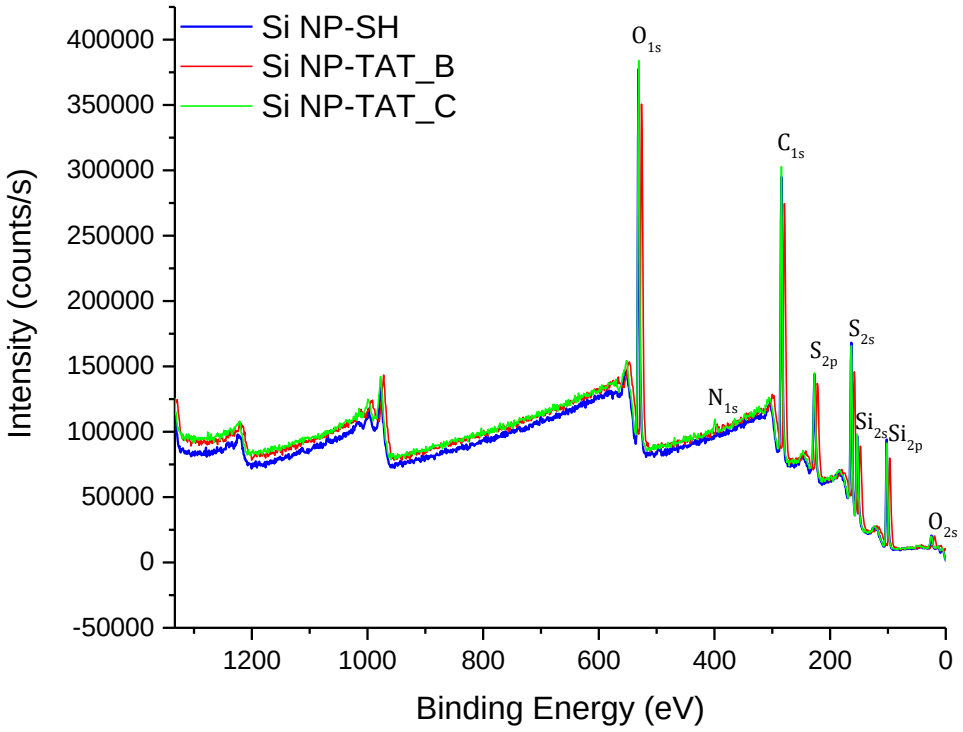

Figure 4.5. XPS spectroscopy survey of thiolated and TAT-conjugated nanoparticles

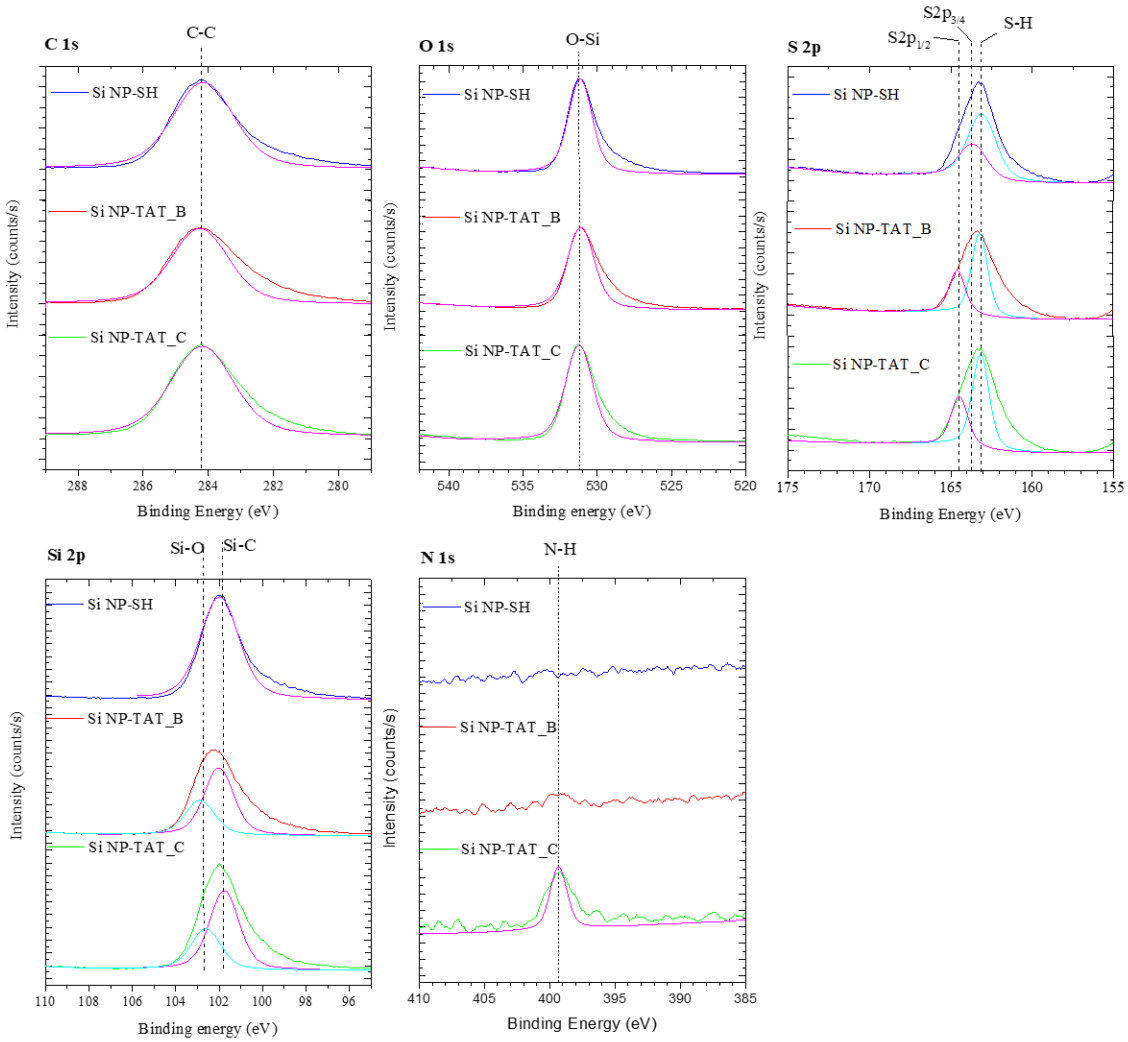

Figure 4.6. XPS spectroscopy of thiolated and TAT-conjugated nanoparticles at C 1s (279−297 eV), Si 2p (98−110 eV), O 1s (527−541 eV), S 2p (155-177 eV), and N 1s (380-410 eV)

The SiNP-SH contains organic groups, as described in the previous chapter. Therefore, it is easily charged at a high acceleration voltage during the measurements. Due to this feature of organosilica nanoparticles, results from all samples were adjusted by the binding energy for the C-C/C-H bonds in the C 1s spectra to 284.2 eV to calibrate the binding energy (Mekaru *et al.*, 2019). The characteristic peaks for the organosilica nanoparticles at C 1s, O 1s, S 2p and Si 2p were observed along all types of nanoparticles. However, the N 1s peak was spotted on sample SiNP-TAT_C at 398.95 eV, which aligns with the $–NH_2$ group on the TAT-peptide (Cho and Ivanisevic, 2005a, 2005b). Interestingly, we observed a peak for the Si-O bond on SiNP-TAT_B and SiNP-TAT_C, while at SiNP-SH, we observed a broad peak at Si-C (Figure 4.6).

Following the confirmation of the successful conjugation of peptides to organosilica nanoparticles, our objective was to investigate the potential effects of these modified nanoparticles on cell cultures. A549 cell lines were treated with SiNP-SH and Si NP-TAT_A/B/C at concentrations ranging from 25 µg/mL to 400 µg/mL for 24 hours. The results revealed that modified nanoparticles exhibited some toxicity at high concentrations. Surprisingly, even SiNP-TAT_A decreased cell viability compared to thiolated nanoparticles. Furthermore, this decline in viability was observed even at lower concentrations (25 µg/mL) for Si NP-TAT_A (Figure 4.7).

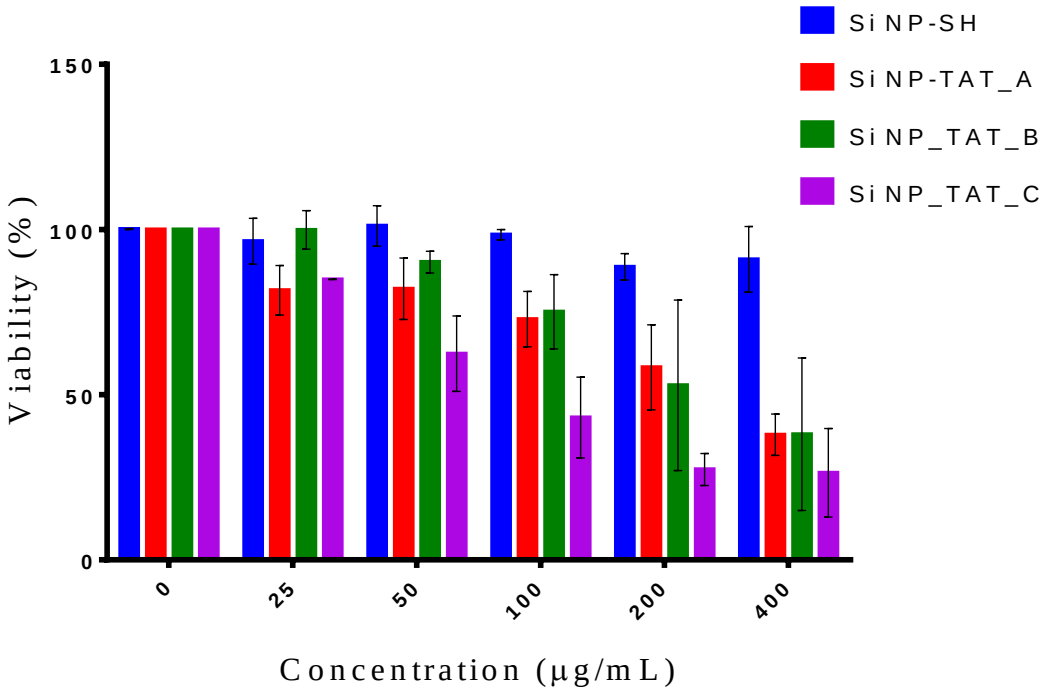

Figure 4.7. A549 cell line viability after the treatment with thiolated and TAT-conjugated nanoparticles for 24 hours

4.4. CONCLUSION

In this chapter, we meticulously demonstrated the successful conjugation of the TAT-peptide onto thiolated organosilica nanoparticles utilising thiol groups and maleimide chemistry. This conjugation approach holds substantial promise for its prospective application in forthcoming studies, wherein we plan to employ targeting peptides characterised by enhanced specificity towards particular types of cancer. Our conjugation method was validated through comprehensive analyses, including SDS-PAGE and TGA. These analyses unequivocally confirmed the successful conjugation of TAT-peptide, as evidenced by the distinct bands observed in SINP-TAT_B and SINP-TAT_C, corresponding to TAT-maleimide. Moreover, the observed uneven weight loss in TGA analysis, which correlated with the concentration of organic compounds, further supported the efficacy of our conjugation process.

However, it is noteworthy that although SiNP-TAT_C exhibited peaks at N 1s in XPS experiments, it did not align with our objective of fabricating suitably sized nanoparticles, as its size exceeded 100 nm, and the PDI value surpassed 0.210. Despite this, the concentrations utilised for synthesising SiNP-TAT_B hold significant promise for future applications. The observed size distribution and other experimental findings confirming the presence of TAT-peptide within the nanoparticle structure provide a compelling rationale for the continued exploration and utilisation of this chemistry in future endeavours.

BLANK

CHAPTER 5. DRUG CONJUGATION TO ORGANOSILICA NANOPARTICLES

5.1. INTRODUCTION

The advanced characteristics of nanoparticles have been identified as applicable in nanomedicine, a burgeoning field within biomedical science that leverages nanotechnology-based products for disease treatment and diagnosis. Notably, nanomedicine research is prominently focused on cancer therapy in the current landscape of biomedical studies.

Conventional cancer therapy currently relies on non-selective chemotherapeutic agents, which are widely accepted for their advantages in cancer treatment. However, these agents are notorious for their numerous adverse effects due to several limitations. One primary limitation is the lack of specificity, as most chemotherapeutic agents act on dividing cells. This results in harm not only to cancer cells but also to healthy cells, impacting the well-being of patients by inducing systemic toxicity, such as anaemia, fatigue, diarrhoea, constipation, bleeding, fertility issues, and hair loss. Moreover, chemotherapeutic drugs have a short circulation time, necessitating high dosages to ensure therapy effectiveness. This high dosage may contribute to another limitation — drug resistance. Over time, tumours may become unresponsive to the drug, leading to the administration of more chemotherapeutic agents to the patient and, ultimately, increased systemic toxicity or death (Dang and Guan, 2020; Rodríguez *et al.*, 2022; Thapa and Kim, 2023).

To enhance current therapy and improve patient well-being, nanoparticles have been employed to address issues related to specificity and dosage, aiming to strengthen drug effectiveness while reducing systemic toxicity. Approximately 100 nanomedicine-based drugs are available on the market, with over 500 undergoing clinical trials. These nanomedicines are not limited to cancer treatment; they are also being developed for treating various skin diseases, infections, blood disorders, cardiovascular diseases, and other conditions (Shan *et al.*, 2022).

In our study, we used the gold-standard drug doxorubicin for conjugation studies, as it has a higher molecular weight than other anti-cancer drugs and has fluorescence. Doxorubicin, as an anticancer drug, received FDA approval in 1974 and has been employed in the treatment of various cancer types, including breast, ovarian, sarcoma,

AIDS-related Kaposi's sarcoma, and more. It functions by causing DNA strand breakage, transcriptome alterations, and initiation of apoptosis (Tacar, Sriamornsak and Dass, 2013).

Our primary objective was to develop a drug-conjugated organosilica nanoparticle capable of releasing the drug at a targeted region upon exposure to endogenous stimuli. In nanomedicine studies, two types of stimuli-responsive nanoparticles are extensively researched: endogenous and exogenous stimuli.

Nanoparticles responding to external stimuli (exogenous) typically utilise or incorporate elements sensitive to light, heat, ultrasound, and magnetic fields. These nanoparticles may also find applications in diagnostic tools. Conversely, drug release in response to changes in pH, enzymes, or redox processes is associated with endogenous stimuli. Redox-responsive systems show promise for delivering therapeutic agents based on endogenous stimuli.

Tumour cells often exhibit elevated oxidative stress compared to healthy cells, creating a unique internal environment characterised by reactive oxygen species and, notably, glutathione (GSH). Moreover, the concentration of GSH in tumours is fourfold more significant than in healthy tissues. The intracellular levels, ranging from 2 to 10 mM, significantly surpass those in the extracellular compartment thousands of times (Sun *et al.*, 2023). The elevated levels of GSH are associated with proliferative responses and cell cycle progression (Traverso *et al.*, 2013). However, since GSH can cleave disulfide bonds, it can be utilised as a molecule that is crucial in releasing the drug from thiolated organosilica nanoparticles. Consequently, we conjugated doxorubicin and thioguanine to SiNP-SH through a disulfide bridge, specifically enabling elevated GSH to trigger a targeted drug release in tumour cells.

5.2. MATERIALS AND METHODS

Table 5.1. List of consumables, Chapter 5.

Name	Abbreviation	CAS-number	Manufacturer
(3-Mercaptopropyl)trimethoxysilane	MPTS	4420-74-0	Sigma-Aldrich
Sodium hydroxide	NaOH	1310-73-2	Sigma-Aldrich
Dimethyl sulfoxide	DMSO	67-68-5	Sigma-Aldrich
Dialysis tubing cellulose membrane	n/a	n/a	Sigma-Aldrich
5,5-dithio-bis-(2-nitrobenzoic acid)	DTNB	69-78-3	Sigma-Aldrich
L-cysteine hydrochloride monohydrate	n/a	52-89-1	Sigma-Aldrich
Doxorubicin hydrochloride	Dox	25316-40-9	Sigma-Aldrich
2-Iminothiolane hydrochloride	n/a	4781-83-3	Sigma-Aldrich
Triethylamine	TEA	121-44-8	Sigma-Aldrich
Dimethyl sulfoxide-d6	DMSO-d6	2206-27-1	Sigma-Aldrich

5.2.1. Doxorubicin thiolation and characterisation

Before conjugating with thiolated organosilica nanoparticles, Doxorubicin hydrochloride was chemically modified. The modification protocol employed was adapted from the work of Darwish et al. (Darwish *et al.*, 2019); fifty milligrams (0.09 mmol) of Doxorubicin hydrochloride (Dox-HCl) were reacted with 12 mg (0.09 mmol) of 2-iminothiolane hydrochloride in 40 mL of methanol, with the addition of 0.750 mL of TEA as a catalyst for 7 hours. Following the reaction, methanol was evaporated using a vacuum rotor evaporator for 1 hour. The resulting pellet was washed twice with diethyl ether through centrifugation at 1000 rpm for 5 minutes. The crude product was left overnight under a chemical hood to evaporate any remaining diethyl ether, and its mass was measured after evaporation.

Conjugation efficiency was assessed using NMR and FTIR spectroscopies. Fourier Transform Infrared (FTIR) analysis utilised a Nicolet iS10 FT-IR Spectrometer. Thiolated doxorubicin was placed on the stage and pressed against a high-refractive index prism with an attenuated total reflection accessory. Transmittance was measured between

400 and 4000 nm wavelength. Controls included Doxorubicin hydrochloride and thiolated organosilica nanoparticles.

1H nuclear magnetic resonance spectroscopy was conducted on a JNM-ECA FT NMR spectrometer. Thiolated doxorubicin, dox hydrochloride, and thiolated organosilica nanoparticles were dissolved in DMSO-d6 at a 1.5 mg/mL concentration. Undissolved suspended composites were filtered before recording the 1H NMR spectra at 500 MHz and room temperature. Spectral analysis was analysed using ACD/Labs software

5.2.2. Drug conjugation to thiolated organosilica nanoparticles

Organosilica nanoparticles were synthesised following protocols described in Chapters 3 and 4 (3.2 and 4.2). The silica precursor, MPTS, was added at a volume of 1.125 mL to 30 mL DMSO on a magnetic stirrer. The reaction commenced with adding 0.750 mL of 0.5M NaOH as a catalytic reagent and proceeded under air-bubbling conditions for 24 hours. After synthesis completion, the formed nanoparticles underwent purification against diH_2O through dialysis involving eight water changes.

Nanoparticles were prepared accordingly for size and sulfhydryl concentration measurements. For DLS analysis, 50 µL of nanoparticle suspension was diluted in 4.950 mL ultrapure water, sonicated for 5 minutes, and measured on a Nano-ZS series instrument (Malvern Instruments, U.K.) at 25°C to determine the hydrodynamic size and zeta-potential.

As explained in the preceding chapter, the sulfhydryl concentration was determined using Ellman's technique. In summary, a total of 3 mg of freeze-dried nanoparticles were dissolved in phosphate-buffered saline (PBS). Following a duration of 1 hour, the solution containing dissolved particles was combined with a solution of DTNB in a 1:1 proportion. The resulting mixture was then subjected to spectrophotometric analysis at a wavelength of 420 nm using a Microplate reader (Varioscan, Thermo Scientific, USA) to quantify the absorbance of the liquid above the sediment. A standard curve was generated using L-glutathione at concentrations ranging from 0.004 to 0.644 µmol/mL.

Thiolated doxorubicin was then conjugated to thiolated organosilica nanoparticles at concentrations dependent on the sulfur concentration of nanoparticles, with a ratio of 5 µmol of SH to 1 µmol of Dox-SH. The weighted mass of thiolated doxorubicin was added to 10 mL of thiolated nanoparticles and stirred for 24 hours under air-bubbling conditions at room temperature in the dark. Upon completion of synthesis, functionalised

nanoparticles were purified against diH_2O by dialysis involving six water changes in 4 L beakers.

Purified nanoparticles were used to measure the size and zeta potential of the Nano-ZS series (Malvern Instruments, UK). Samples, prepared according to the previously described protocol, involved mixing 50 µL of nanoparticles with 4.950 mL ultrapure water and were measured at room temperature.

Ellman's assay was conducted on a nanoparticle suspension, involving the preparation of a DTNB stock solution by mixing DTNB solution, Tris solution, and water. After mixing with a 10 µL sample, the solution was incubated for 5 minutes, and its absorbance was measured on Varioscan at 412 nm to determine thiol compound concentrations.

Thermogravimetric analysis was performed on SiNP-SH and drug-conjugated nanoparticles. Freeze-dried nanoparticles (5-7 mg) were placed on a ceramic crucible, and thermogravimetric analysis was done with STA6000 (Perkin Elmer, USA) from 30 – 950 °C at 10 °C/min with nitrogen flow at 30 mL/min. Results were analysed using OriginPro software.

Fourier Transform Infrared (FTIR) Analysis was performed on a Nicolet iS10 FT-IR Spectrometer. A few freeze-dried samples were placed in the centre of the stage and pressed against the high-refractive index prism using an attenuated total reflection accessory. Transmittance was measured in the range of 1400 – 4000 nm wavelength. Controls included doxorubicin hydrochloride and thiolated organosilica nanoparticles.

1H nuclear magnetic resonance spectroscopy was conducted on the JNM-ECA FT NMR spectrometer. Freeze-dried samples were dissolved in DMSO-d6 to a concentration of 3 mg/mL. Undissolved suspended composites were filtered via cotton wool before placing samples into the NMR tube. The 1H NMR spectra were recorded at 500 MHz at room temperature. Spectral analysis was performed using ACD/Labs software.

Doxorubicin-conjugated nanoparticles, diluted to a concentration of 1 mg/mL, had their fluorescence spectra measured at 450 – 700 nm on a 96-well plate reader Varioscan with an excitation wavelength of 470 nm. The fluorescence intensity of diluted nanoparticles was measured on a Biorad multiplex with excitation at 470 nm and emission at 575 nm. Data analysis was conducted using Origin Pro software.

5.2.3. Doxorubicin release and conjugation efficiency

The release of doxorubicin from nanoparticles was investigated in three different media:

- PBS with 0.2% Tween 80
- 10 mM glutathione in PBS with 0.2% Tween 80
- 20 µM glutathione in PBS with 0.2% Tween 80

The nanoparticles were diluted in water to achieve a 1 mg/mL concentration. Subsequently, 3 mL of the resulting solution was introduced into a dialysis bag with a 10,000 Da cut-off. The dialysis bag was submerged in 200 mL of the corresponding release medium. At designated time intervals (0, 1, 2, 3, 4, 5, 6, 24, 30, 48, 52, 72, 78, 96, and 102 hours), 200 µL of the release media was extracted for analysis, and the extracted volume was replaced with fresh release media. The experiment was replicated three times, and calculations were carried out using Graph/Pad Prism software.

5.2.4. *In vitro* toxicity of Doxorubicin conjugated organosilica nanoparticles

In vitro viability analysis was conducted using the MTT assay with Si NP-Dox. A549 cell lines were seeded in a 96-well plate at a density of 5×10^4 cells per well and incubated overnight at 37°C with 5% CO_2 to allow attachment to the bottom of the wells. The cell media (DMEM+10%FBS+1% PenStrep antibiotics) containing nanoparticles were added to cell cultures to final concentrations of 10, 50, 100, 200 and 400µg/mL. The cells were further incubated for 24, 48, and 72 hours in a humidified atmosphere at 37°C with 5% CO_2. Cells treated with cell media without nanoparticles served as the negative control. Following the nanoparticle incubation, 30 µL of MTT dye solution was added to each well and incubated for 4 hours. Subsequently, 100 µL of 10% SDS solution was added to dissolve the formed formazan crystals. Absorbance was measured on a plate reader at 570 nm (Microplate reader Varioscan, Thermo Scientific, USA). The viability of cells was calculated using the formula:

$$Cell\ viability\ \% = \frac{Absorbance\ of\ treated\ cells}{Absorbance\ of\ negative\ control} * 100\%$$

5.3. RESULTS AND DISCUSSION

Before the conjugation of doxorubicin with SiNP-SH, the compound was thiolated by reacting with Traut's reagent to introduce a thiol group to the amidin functional group.

The thiolation of doxorubicin (Dox-SH) was analysed through NMR and FTIR analyses (Figure 5.1 and Figure 5.2). For 1H NMR spectroscopy, Dox and Dox-SH were dissolved in DMSO-d6 and subsequently analysed using ACD/Lab software. Database-assisted spectral peak assignments revealed a peak at approximately 3.77 ppm in the Dox spectrum, corresponding to the -NH_2 functional group. In the Dox-SH spectrum, this peak was absent, while a new peak at 3.34 ppm emerged, indicative of the -SH functional group (Figure 5.1).

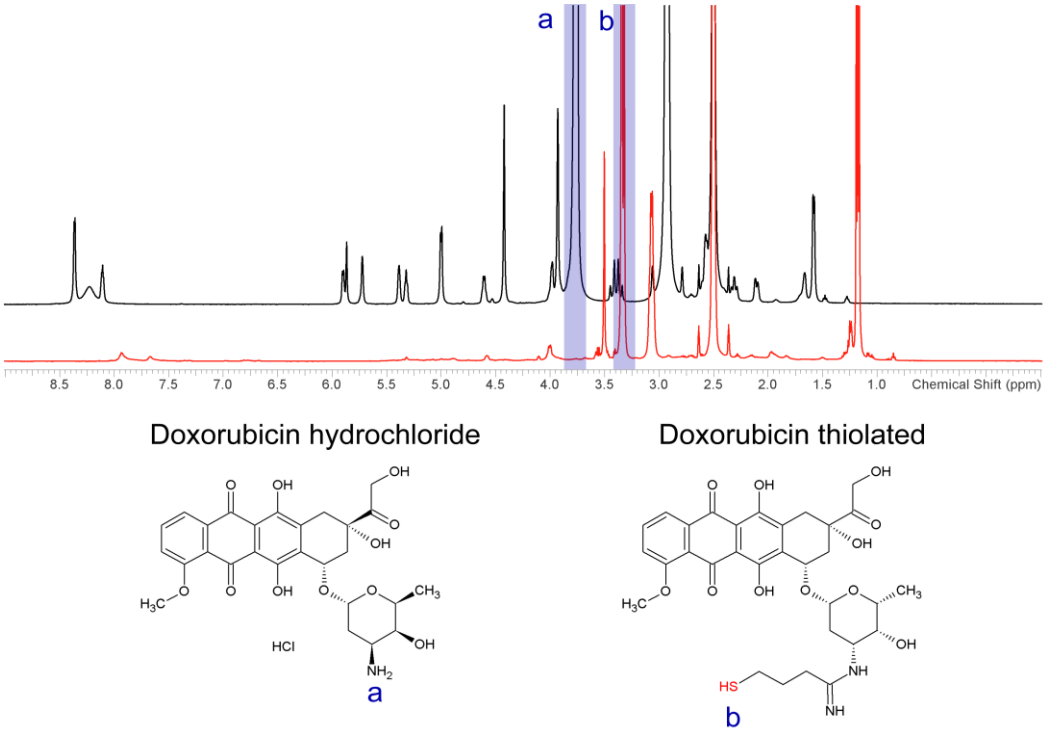

Figure 5.1. 1H NMR spectroscopy of doxorubicin and thiolated doxorubicin.

These findings were corroborated through FTIR, where the appearance of a peak at 2608 cm-1, corresponding to the -SH functional group, and the attenuation of peaks at 3308 and 3525 cm-1 (-NH) were observed (Figure 5.2).

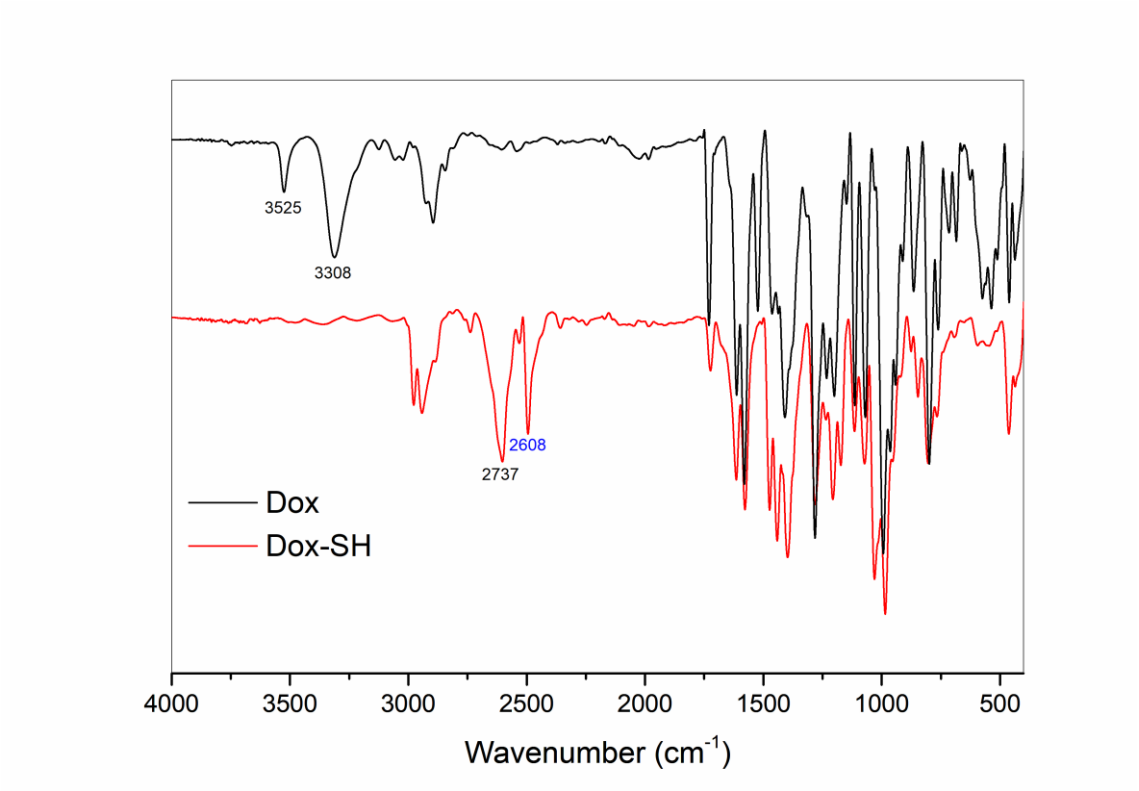

Figure 5.28. FTIR spectroscopy of doxorubicin and thiolated doxorubicin.

After the successful thiolation of Dox, it was conjugated to SiNP-SH by forming a disulfide bridge. The concentration of Dox-SH was calculated based on the results of Ellman's assay on SiNP-SH; in short, for every 5 µmol of thiol per particle, 1 µmol of Dox-SH was added. Subsequent analysis of the size, surface charge, and Ellman's assay revealed slight changes in the size and polydispersity of nanoparticles (p-value < 0.0001 and p-value < 0.001, respectively) (Table 5.2).

Table 5.2. DLS and Ellman's assay of thiolated and dox-conjugated nanoparticles.

	Si-NP-SH	**Si NP-Dox**
Size, nm	51±1	59±2
PDI	0.123	0.186
ζ-potential, mV	-59.1±12.9	-43.6±3.1
SH concentration, µmol/L	17.1±0.4	9.7±1.1

However, these changes do not conclusively indicate successful conjugation. Doxorubicin has a strong fluorescence and emits it upon excitation at 490 nm. After the synthesis, we observed a colour change of Si NP-Dox (Figure 5.3-A). Fluorescence spectroscopy showed Dox, and Si NP-Dox peaks after the excitation with 490 nm laser, and peaks were absent on SiNP-SH (Figure 5.3-B).

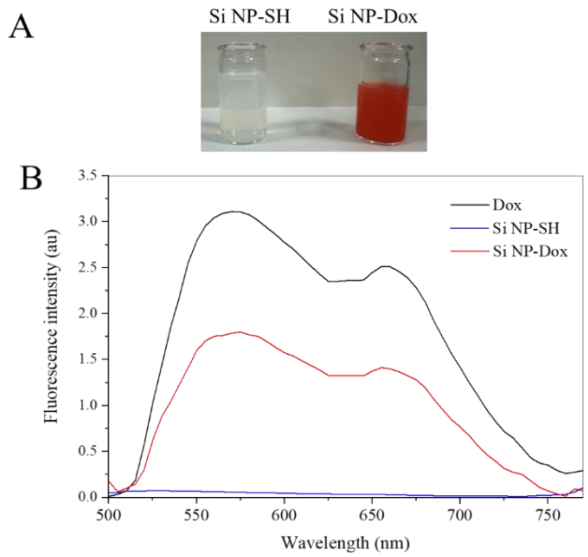

Figure 5.39. A) thiolated and dox-conjugated nanoparticles, B) Fluorescent emission of SiNP-SH, Si NP-Dox and dox after the excitation with a laser at a wavelength of 490 nm.

Next, thiolated and modified nanoparticles were characterised with NMR. The NMR results revealed aligned peaks between Si NP-Dox and Dox-SH (Figure 5.4). As nanoparticles do not contain amino groups, we were particularly interested in observing peaks corresponding to amine groups within the structure of Dox. The peak at approximately 3.5 ppm representing R-NH and the absence of ring structure in the nanoparticles' frame provides an option to detect these features in the structures of Dox (1.45 ppm, 2 ppm, and 4.57 ppm).

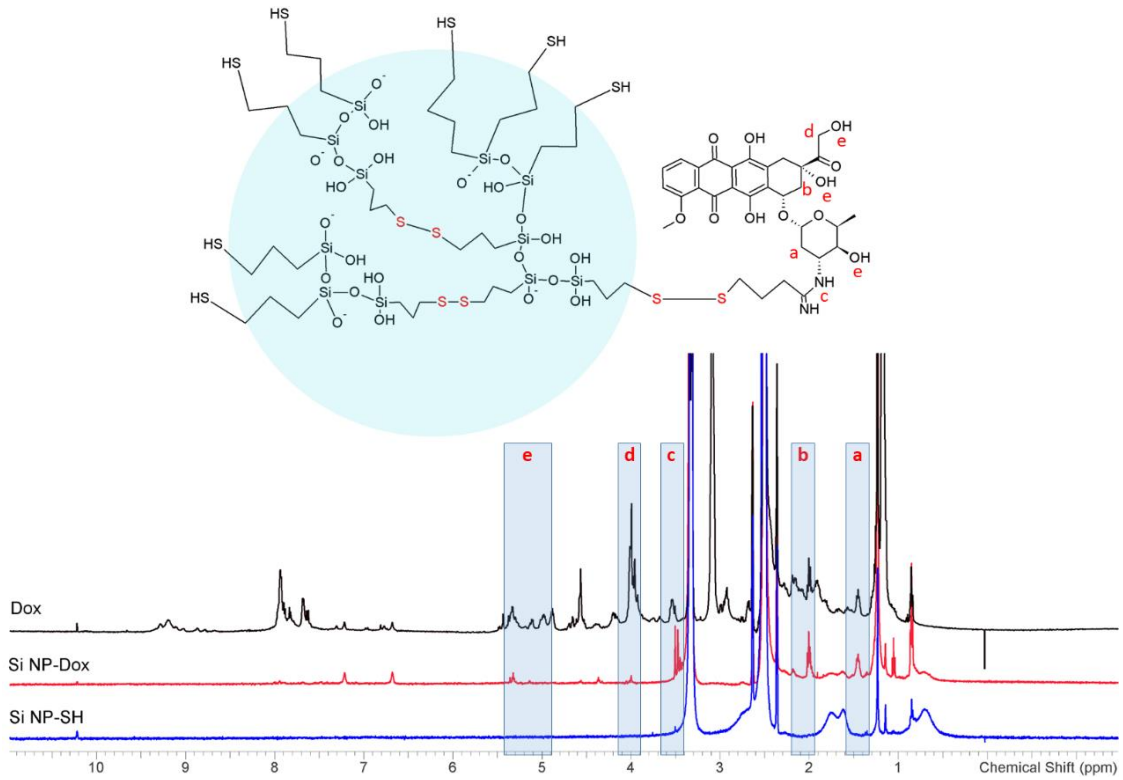

Figure 5.4. A schematic representation of Si NP-Dox and 1H NMR spectroscopy of dox, SiNP-SH and Si NP-Dox.

Subsequent elemental analysis using CHNS demonstrated the incorporation of nitrogen atoms in the samples of nanoparticles conjugated with doxorubicin (Table 5.3).

Table 5.3. CHNS elemental analysis results of SiNP-SH and Si NP-Dox.

	N [%]	**C [%]**	**H [%]**	**S [%]**
SiNP-SH	0.00	24.69	5.97	23.76
Si NP-Dox	0.34	29.74	6.51	23.45

TGA analysis further confirmed the successful conjugation of Dox-SH and SiNP-SH (Figure 5.5). The residue left after burning SiNP-SH constituted 56.9% of the initial mass. This data does not agree with the weight of the inorganic composition of MPTS; this could be due to limited temperature exposure. If we consider the molecular weight of MPTS (151.1 g/mol) as 100%, the residue of silanol, O=Si=O (60.1 g/mol), should be 39.8%. Even though we could not burn all organic residues, the curves show differing degradation rates. The higher weight loss of Si NP-Dox suggests that it contains more organic composites than SiNP-SH.

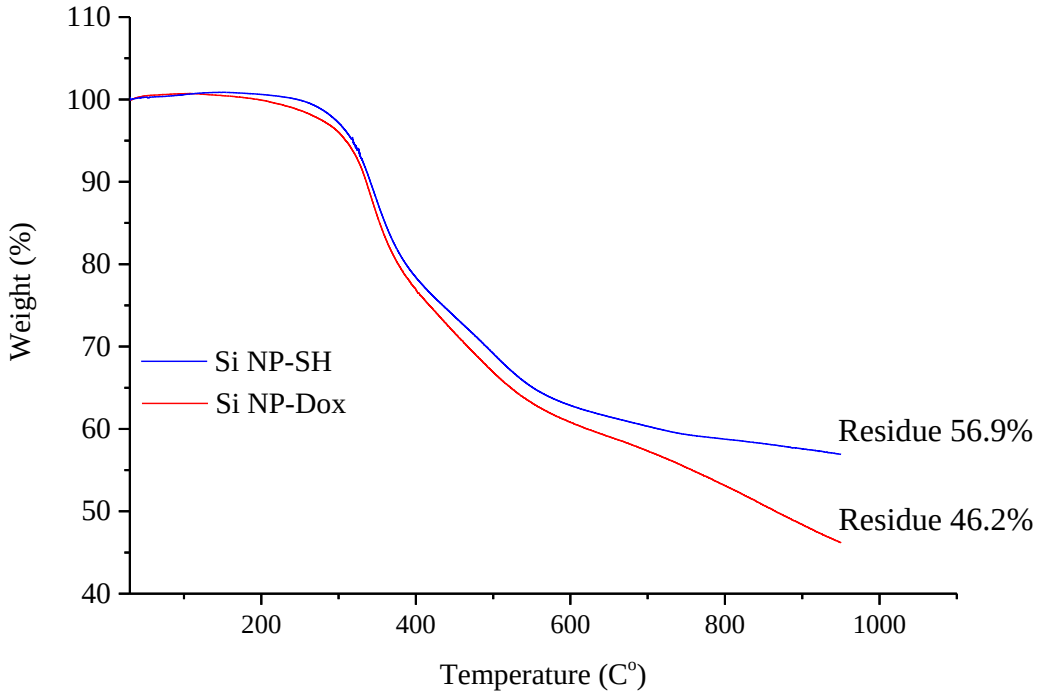

Figure 5.5. TGA results: weight loss of organic component of SiNP-SH and Si NP-Dox upon heating to 950°C.

We assessed the conjugation by using FTIR spectroscopy on SiNP-SH, Si NP-Dox, and Dox powder forms. The FTIR graph revealed a peak at 2358 cm^{-1} on Dox and Si NP-Dox, corresponding to the O=C=O bond stretch (Figure 5.6). However, no additional peaks were observed on Si NP-Dox corresponding to the peaks on Dox for N-H. This observation may be attributed to the low concentration of Dox on the nanoparticle. Despite the challenges posed by the small molecular weight of Dox for FTIR and Raman spectroscopy, results from TGA, NMR, and CHNS analyses conclusively demonstrated the association of doxorubicin with our nanoparticles. Therefore, we may confidently assert the success of the conjugation.

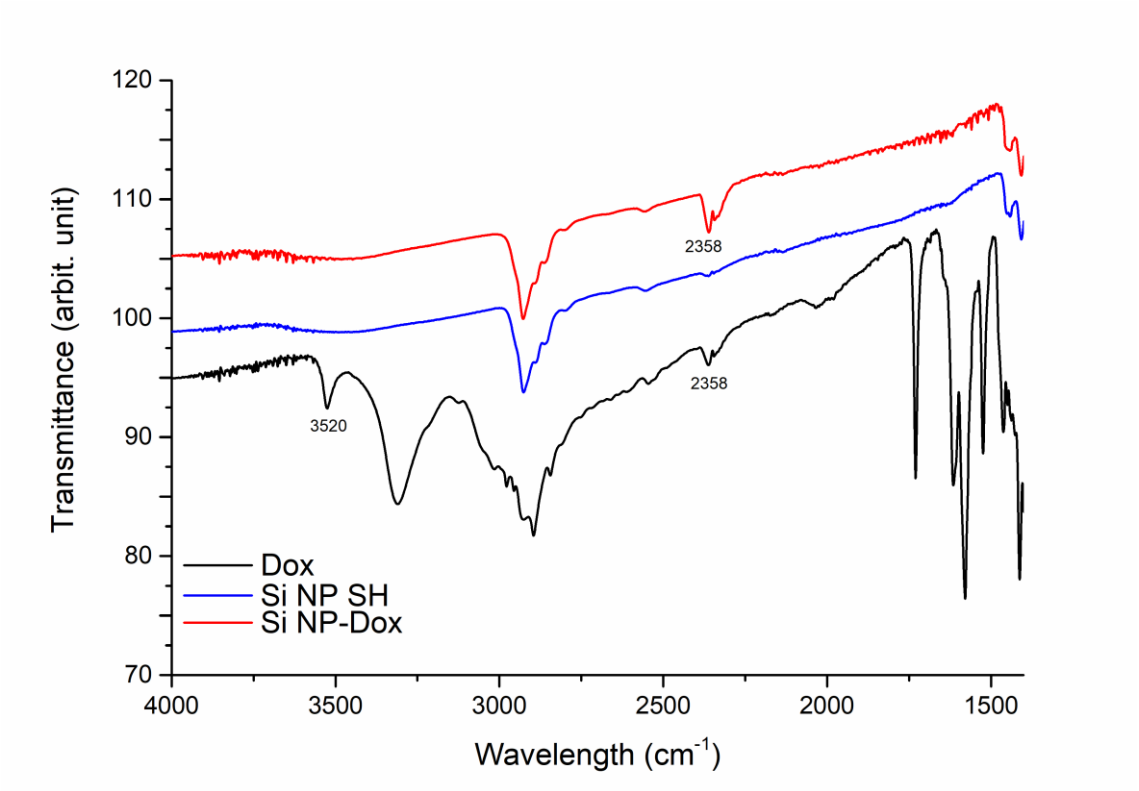

Figure 5.6. FTIR spectroscopy of Dox, thiolated and Dox conjugated nanoparticles.

Following the successful conjugation of Dox-SH to the nanoparticles, we analysed the conjugation efficiency and drug release in solutions containing glutathione. With a disulfide bridge in the conjugate and within the nanoparticle framework, we anticipate that nanoparticles will release Dox in cancer cells, given that their GSH concentration is 1000-fold higher compared to the extracellular matrix. Drug release was studied in three different media: PBS, 2 mM glutathione (simulating the cellular matrix of healthy cells), and 10 mM glutathione (mimicking the cancer cell environment). Our observations indicated that nanoparticles in 10 mM GSH exhibited higher drug release than in 2 mM GSH or PBS solution (Figure 5.7).

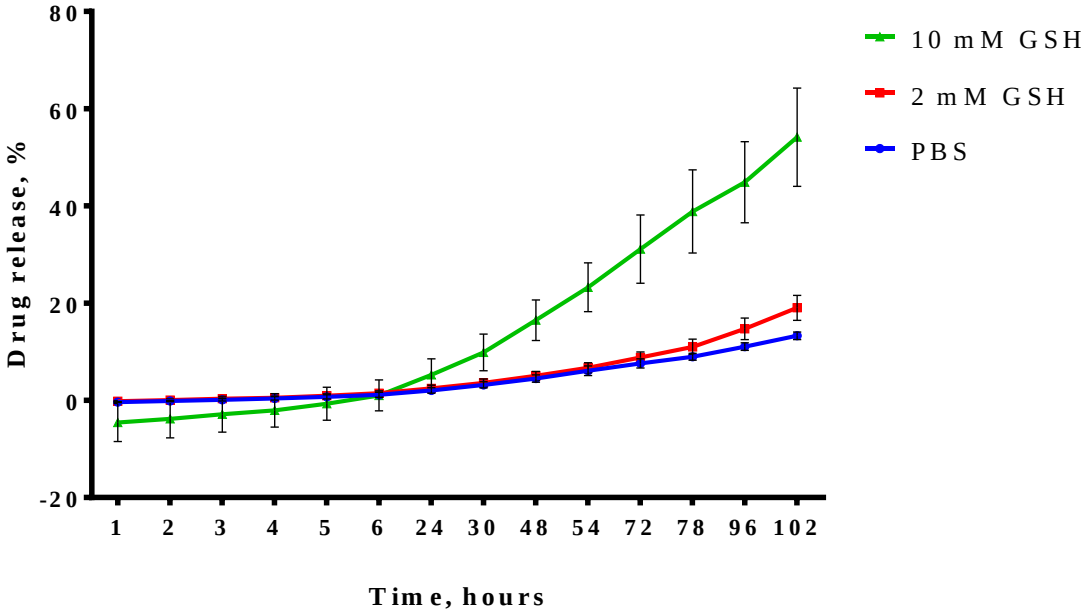

Figure 5.7. Doxorubicin release kinetics in different media for 102 hours.

As the doxorubicin in our samples underwent modification, a potential concern is the reactivity of the modified compound. To assess whether Dox-SH retained the same cytotoxic activity as unmodified doxorubicin, we treated cell lines with nanoparticles and evaluated cell viability using the MTT assay.

The viability assay revealed that Si NP-Dox exhibited significant toxicity compared to SiNP-SH, even at low concentrations (25 µg/mL) for the HEK293 cell line. Conversely, the A549 cell line showed some resistance at low concentrations after 24 hours of incubation, but the cytotoxic effect from Si NP-Dox became apparent at 200 µg/mL. However, cells treated for 48 and 72 hours displayed concentration-dependent cytotoxicity, including at 25 µg/mL. Here, it is essential to note that the A549 cell line is characterised to be highly resistant to many treatments, including some apoptosis-inducing drugs (Figure 5.8).

These results indicate that nanoparticles induce cell type-dependent toxicity, a phenomenon previously explored in Chapter 3.

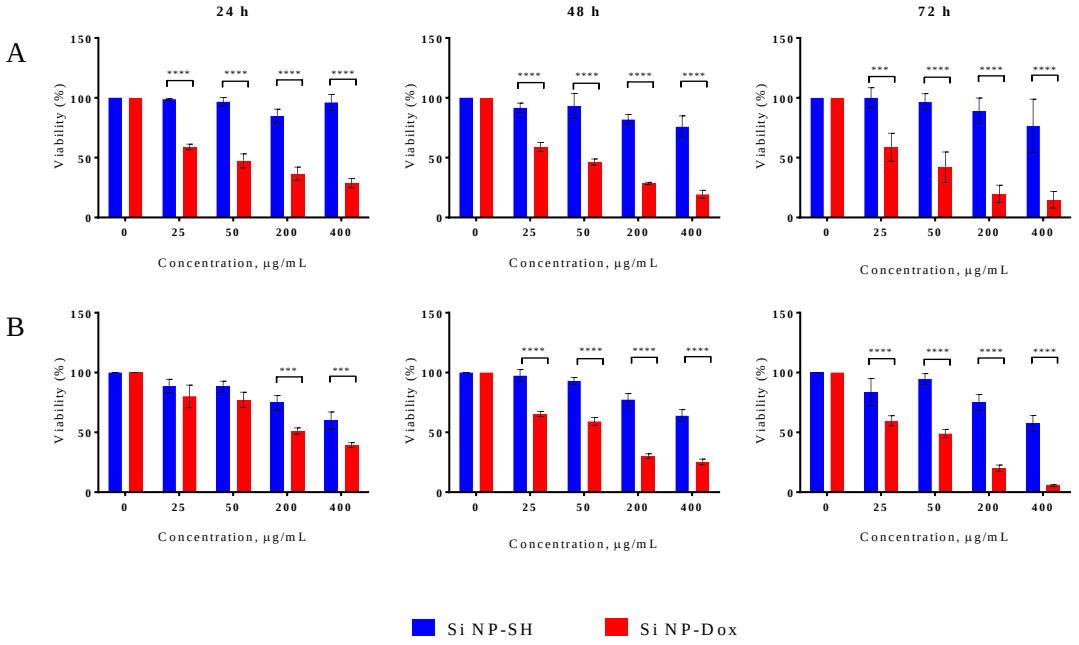

Figure 5.8. Cell viability assay after the treatment with SiNP-SH and SI NP-Dox for 24, 48 and 72 hours. The first is the HEK293 cell line, and the second is the A549 cell line. (*P<0.05; **P≤0.01; ***P≤0.001; ****P≤0.0001).

Therefore, we can conclude that SiNP-SH can be used for drug conjugation through disulphide bridge formation. Results from NMR, TGA, and FTIR confirm the successful conjugation, and the presence of nitrogen from elemental analysis is also in agreement. Next, we can use this chemistry to conjugate other thiol-containing drugs to SiNP-SH and use the developed method to analyse whether the synthesis was successful.

5.4. CONCLUSION

In this chapter, we described the modification of Dox by adding the thiol group to the amidin group of the drug. After the successful thiolation of doxorubicin, it was conjugated to SiNP-SH. Our study demonstrated that conjugation was successful according to TGA, NMR, RAMAN and FTIR results. Following that, we showed that drug release is environment-dependent and does not express rapid drug release. However, the drug release is slow, and after 6 hours after inserting in release media, it slowly de-attaches the drug. Moreover, the higher the glutathione concentration, the better the drug release kinetics. Furthermore, the thiolation of doxorubicin did not change the drug function, inducing cellular toxicity *in vitro.*

BLANK

CHAPTER 6. GENERAL CONCLUSION

Today, cancer, being one of the leading causes of death, exerts significant strain on the economic situation of a country. It necessitates the development of better tools for early diagnosis and improved treatment. While conventional cancer therapies have advanced considerably compared to the previous century, they still possess drawbacks that must be addressed to enhance treatment efficacy and patient survival while also ameliorating their condition during treatment. Nanomaterials could play a pivotal role in addressing these challenges. Due to their small size and large surface area, nanomaterials can efficiently absorb required drugs and deliver them to the site of inflammation through active or passive targeting. Furthermore, nanomaterials can serve not only as drug delivery vehicles but also for the delivery of genes, RNA, and proteins, as well as diagnostic tools.

In this study, organosilica nanoparticles were utilised as a model for future drug delivery systems in nanomedicine applications. Organosilica nanoparticles offer the advantage of possessing functional groups on their surface that can be exploited for future modifications. Moreover, thiol groups exhibit mucoadhesive properties that can benefit drug delivery to mucosal tissues, such as the bladder or ovary (Irmukhametova, Mun and Khutoryanskiy, 2011; Mun, Williams and Khutoryanskiy, 2016; Ways *et al.*, 2020).

This study demonstrated the safety of SiNP-SH on various mammalian cell lines (HEK293, A549, MCF7 and HPF) and BALB/C mice. Additionally, the PEGylation of nanoparticles was analysed, suggesting that PEGylation could enhance systemic drug administration by prolonging the circulation time of nanoparticles in animals.

Furthermore, thiol groups on nanoparticles were demonstrated to be valuable for coupling with TAT-peptide and doxorubicin without affecting their activity. In this study, we showcased the conjugation of TAT-peptide to thiolated organosilica nanoparticles and examined its impact on the A549 cell line. Additionally, the conjugation of doxorubicin via a disulfide bridge was demonstrated. The obtained results also confirmed our hypothesis that the disulfide bridge could trigger glutathione-mediated drug release under conditions of high glutathione concentration. Furthermore, the effect of Si NP-Dox was investigated on A549 and HEK293 cell lines, revealing a decrease in cell viability in both cell lines.

This research will significantly contribute to future endeavours to develop organosilica nanoparticles for drug delivery. The chemical strategies employed in this

study will serve as a foundation for future research that targets peptides and other anticancer drugs. Additionally, the initial steps in developing mesoporous nanoparticles have been initiated, and forthcoming studies will focus on further evaluating the formation of mesoporous nanoparticles, providing a more facile method for drug loading.

We firmly believe that this study, along with subsequent publications derived from it, will inspire and enable other researchers to make significant contributions to nanomedicine and the development of nanomaterials for cancer therapy.

BLANK

REFERENCES

Ahmadi, A. *et al.* (2022) 'Influence of Critical Parameters on Cytotoxicity Induced by Mesoporous Silica Nanoparticles', *Nanomaterials*, 12(12). doi: 10.3390/nano12122016.

Aminu, N. *et al.* (2020) 'The influence of nanoparticulate drug delivery systems in drug therapy', *Journal of Drug Delivery Science and Technology*. Elsevier B.V., 60(January), p. 101961. doi: 10.1016/j.jddst.2020.101961.

André Ilbawi, C. V. (2020) *WHO report on cancer: setting priorities, investing wisely and providing care for all, World Health Organization*. Geneva: doi: 10.1007/978-3-662-11496-4_24.

ASTM F 756-00 (2000) 'Standard practice for assessment of hemolytic properties of materials. Philadelphia', *American Society for Testing and Materials.*, (January), p. 5. doi: 10.1520/F0756-13.Copyright.

Attia, M. F. *et al.* (2019) 'An overview of active and passive targeting strategies to improve the nanocarriers efficiency to tumour sites', *Journal of Pharmacy and Pharmacology*, 71(8), pp. 1185–1198. doi: 10.1111/jphp.13098.

Avsievich, T. *et al.* (2020) 'Impact of nanocapsules on red blood cells interplay jointly assessed by optical tweezers and microscopy', *Micromachines*, 11(1), pp. 1–12. doi: 10.3390/mi11010019.

Awaad, A. (2015) 'Histopathological and immunological changes induced by magnetite nanoparticles in the spleen, liver and genital tract of mice following intravaginal instillation', *The Journal of Basic & Applied Zoology*. The Egyptian German Society for Zoology, 71, pp. 32–47. doi: 10.1016/j.jobaz.2015.03.003.

Von Baeckmann, C. *et al.* (2018) 'A Toolbox for the Synthesis of Multifunctionalized Mesoporous Silica Nanoparticles for Biomedical Applications', *ACS Omega*, 3(12), pp. 17496–17510. doi: 10.1021/acsomega.8b02784.

Böckelmann, L. C. and Schumacher, U. (2019) 'Targeting tumor interstitial fluid pressure: will it yield novel successful therapies for solid tumors?', *Expert Opinion on Therapeutic Targets*. Taylor and Francis Ltd, pp. 1005–1014. doi: 10.1080/14728222.2019.1702974.

Borak, B. *et al.* (2012) 'In vivo study on the biodistribution of silica particles in the bodies of rats', *Advances in Clinical and Experimental Medicine*, 21(1), pp. 13–18.

Bouchoucha, M. *et al.* (2017a) 'Antibody-conjugated mesoporous silica nanoparticles for brain microvessel endothelial cell targeting', *Journal of Materials Chemistry B*, 5(37),

pp. 7721–7735. doi: 10.1039/c7tb01385j.

Bouchoucha, M. *et al.* (2017b) 'Antibody-conjugated mesoporous silica nanoparticles for brain microvessel endothelial cell targeting', *Journal of Materials Chemistry B*. Royal Society of Chemistry, 5(37), pp. 7721–7735. doi: 10.1039/c7tb01385j.

Buddhiraju, H. S. *et al.* (2023) 'Advances in Peptide-Decorated Targeted Drug Delivery: Exploring Therapeutic Potential and Nanocarrier Strategies', *ACS Applied Bio Materials*. doi: 10.1021/acsabm.3c00711.

Burgess, R. (2012) *Understanding nanomedicine. An Introductory Textbook*. 1st edn. Jenny Stanford Publishing.

Castillo, R. R., Lozano, D. and Vallet-Regí, M. (2020) 'Mesoporous silica nanoparticles as carriers for therapeutic biomolecules', *Pharmaceutics*, 12(5). doi: 10.3390/pharmaceutics12050432.

Chan, W. T. *et al.* (2017) 'In vivo toxicologic study of larger silica nanoparticles in mice', *International Journal of Nanomedicine*, 12, pp. 3421–3432. doi: 10.2147/IJN.S126823.

Chen, F. *et al.* (2017) 'Organosilica Nanoparticles with an Intrinsic Secondary Amine: An Efficient and Reusable Adsorbent for Dyes', *ACS Applied Materials and Interfaces*, 9(18), pp. 15566–15576. doi: 10.1021/acsami.7b04181.

Cheng, C. S. *et al.* (2019) 'Codelivery of Plasmid and Curcumin with Mesoporous Silica Nanoparticles for Promoting Neurite Outgrowth', *ACS Applied Materials and Interfaces*. American Chemical Society, 11(17), pp. 15322–15331. doi: 10.1021/acsami.9b02797.

Cheng, Y. *et al.* (2020) 'Controllable synthesis of versatile mesoporous organosilica nanoparticles as precision cancer theranostics', *Biomaterials*. Elsevier Ltd. doi: 10.1016/j.biomaterials.2020.120191.

Cho, Y. and Ivanisevic, A. (2005a) 'Covalent attachment of TAT peptides and thiolated alkyl molecules on GaAs surfaces', *Journal of Physical Chemistry B*, 109(26), pp. 12731–12737. doi: 10.1021/jp0515737.

Cho, Y. and Ivanisevic, A. (2005b) 'TAT peptide immobilization on gold surfaces: A comparison study with a thiolated peptide and alkylthiols using AFM, XPS, and FT-IRRAS', *Journal of Physical Chemistry B*, 109(13), pp. 6225–6232. doi: 10.1021/jp045731q.

Dang, Y. and Guan, J. (2020) 'Nanoparticle-based drug delivery systems for cancer therapy', *Smart Materials in Medicine*. Elsevier Ltd, 1(April), pp. 10–19. doi: 10.1016/j.smaim.2020.04.001.

Darwish, S. *et al.* (2019) 'Synthesis and antiproliferative activities of doxorubicin thiol

conjugates and doxorubicin-SS-cyclic peptide', *European Journal of Medicinal Chemistry*. Elsevier Masson SAS, 161, pp. 594–606. doi: 10.1016/j.ejmech.2018.10.042.

Deng, B. *et al.* (2022) 'Biological role of matrix stiffness in tumor growth and treatment', *Journal of Translational Medicine*. BioMed Central, 20(1), pp. 1–15. doi: 10.1186/s12967-022-03768-y.

Douglas Hanahan and Robert A. Weinberg (2000) 'The Hallmarks of Cancer', *Cell*, 100, pp. 57–70. doi: 10.1016/s0092-8674(00)81683-9.

Eun Ji Chung, Lorraine Leon and Carlos Rinaldi (2020) 'Nanoparticles for biomedical application', in *Risk-based Energy Management*. Elsevier, pp. i–iii. doi: 10.1016/b978-0-12-817491-3.00014-3.

Farjadian, F. *et al.* (2019) 'Mesoporous silica nanoparticles: Synthesis, pharmaceutical applications, biodistribution, and biosafety assessment', *Chemical Engineering Journal*. Elsevier, 359, pp. 684–705. doi: 10.1016/J.CEJ.2018.11.156.

Feng, X. *et al.* (2022) 'TRAIL-modified, doxorubicin-embedded periodic mesoporous organosilica nanoparticles for targeted drug delivery and efficient antitumor immunotherapy', *Acta Biomaterialia*, 143, pp. 392–405. doi: 10.1016/j.actbio.2022.03.001.

Fent, K. *et al.* (2010) 'Assessment of uptake and toxicity of fluorescent silica nanoparticles in zebrafish (Danio rerio) early life stages', *Aquatic Toxicology*. Elsevier B.V., 100(2), pp. 218–228. doi: 10.1016/j.aquatox.2010.02.019.

Fu, C. *et al.* (2013) 'The absorption, distribution, excretion and toxicity of mesoporous silica nanoparticles in mice following different exposure routes', *Biomaterials*. Elsevier Ltd, 34(10), pp. 2565–2575. doi: 10.1016/j.biomaterials.2012.12.043.

G., S. *et al.* (2014) 'Mesoporous silica nanoparticles with tunable pore size for tailored gold nanoparticles', *Journal of Nanoparticle Research*, 16(2). doi: 10.1007/s11051-014-2245-1.

Golombek, S. K. *et al.* (2018) 'Tumor targeting via EPR: Strategies to enhance patient responses', *Advanced Drug Delivery Reviews*, 130, pp. 17–38. doi: 10.1016/j.addr.2018.07.007.

Griffon-Etienne, G. *et al.* (1999) 'Taxane-induced apoptosis decompresses blood vessels and lowers interstitial fluid pressure in solid tumors: Clinical implications', *Cancer Research*, 59(15), pp. 3776–3782.

Guimarães, R. S. *et al.* (2020) 'Overview of stimuli-responsive mesoporous organosilica nanocarriers for drug delivery', *Pharmacological Research*. Elsevier, 155(February), p.

104742. doi: 10.1016/j.phrs.2020.104742.

Guo, C. *et al.* (2015) 'Silica nanoparticles induce oxidative stress, inflammation, and endothelial dysfunction in vitro via activation of the MAPK/Nrf2 pathway and nuclear factor-κB signaling', *International Journal of Nanomedicine*. Dove Medical Press Ltd., 10, pp. 1463–1477. doi: 10.2147/IJN.S76114.

Hadipour Moghaddam, S. P. *et al.* (2017) 'Redox-Responsive Polysulfide-Based Biodegradable Organosilica Nanoparticles for Delivery of Bioactive Agents', *ACS Applied Materials and Interfaces*, 9(25), pp. 21133–21146. doi: 10.1021/acsami.7b04351.

Hadipour Moghaddam, S. P., Mohammadpour, R. and Ghandehari, H. (2019) 'In vitro and in vivo evaluation of degradation, toxicity, biodistribution, and clearance of silica nanoparticles as a function of size, porosity, density, and composition', *Journal of Controlled Release*. Elsevier, 311–312(May), pp. 1–15. doi: 10.1016/j.jconrel.2019.08.028.

Hadipour Moghaddam, S. P., Yazdimamaghani, M. and Ghandehari, H. (2018) 'Glutathione-sensitive hollow mesoporous silica nanoparticles for controlled drug delivery', *Journal of Controlled Release*. Elsevier, 282(April), pp. 62–75. doi: 10.1016/j.jconrel.2018.04.032.

Han, H. Y. *et al.* (2020) 'Amorphous silica nanoparticle-induced pulmonary inflammatory response depends on particle size and is sex-specific in rats', *Toxicology and Applied Pharmacology*. doi: 10.1016/j.taap.2020.114890.

Hanahan, D. and Weinberg, R. A. (2011) 'Hallmarks of cancer: The next generation', *Cell*. Elsevier Inc., 144(5), pp. 646–674. doi: 10.1016/j.cell.2011.02.013.

He, Q. *et al.* (2011) 'In vivo biodistribution and urinary excretion of mesoporous silica nanoparticles: Effects of particle size and PEGylation', *Small*, 7(2), pp. 271–280. doi: 10.1002/smll.201001459.

Heldin, C. H. *et al.* (2004) 'High interstitial fluid pressure - An obstacle in cancer therapy', *Nature Reviews Cancer*. Nature Publishing Group, pp. 806–813. doi: 10.1038/nrc1456.

Hock, N. *et al.* (2022) 'Thiolated Nanoparticles for Biomedical Applications: Mimicking the Workhorses of Our Body', *Advanced Science*, 9(1), pp. 1–24. doi: 10.1002/advs.202102451.

Hu, J. J., Xiao, D. and Zhang, X. Z. (2016) 'Advances in Peptide Functionalization on Mesoporous Silica Nanoparticles for Controlled Drug Release', *Small (Weinheim an der*

Bergstrasse, Germany), 12(25), pp. 3344–3359. doi: 10.1002/smll.201600325.

Irmukhametova, G. S. *et al.* (2012) 'Hydrogen-bonding-driven self-assembly of PEGylated organosilica nanoparticles with poly(acrylic acid) in aqueous solutions and in layer-by-layer deposition at solid surfaces', *Langmuir*, 28(1), pp. 299–306. doi: 10.1021/la2038735.

Irmukhametova, G. S., Mun, G. A. and Khutoryanskiy, V. V. (2011) 'Thiolated Mucoadhesive and PEGylated Nonmucoadhesive Organosilica Nanoparticles from 3-Mercaptopropyltrimethoxysilane', *Langmuir*. American Chemical Society, 27(15), pp. 9551–9556. doi: 10.1021/la201385h.

ISO 10993-5:2009(en), Biological evaluation of medical devices — Part 5: Tests for in vitro cytotoxicity (2009) *Biological evaluation of medical devices*. Available at: https://www.iso.org/obp/ui/#iso:std:iso:10993:-5:ed-3:v1:en (Accessed: 15 April 2021).

Jhaveri, A. and Torchilin, V. (2016) 'Intracellular delivery of nanocarriers and targeting to subcellular organelles', *Expert Opinion on Drug Delivery*. Informa Healthcare, 13(1), pp. 49–70. doi: 10.1517/17425247.2015.1086745.

Johann Kecht, Axel Schlossbauer, and T. B. (2008) 'Selective Functionalization of the Outer and Inner Surfaces in Mesoporous Silica Nanoparticles', *Chem. Mater.*, (20), pp. 7207–7214. doi: https://doi.org/10.1021/cm801484r.

Kang, Z. L. *et al.* (2021) 'The effects of sodium chloride on proteins aggregation, conformation and gel properties of pork myofibrillar protein Running Head: Relationship aggregation, conformation and gel properties', *Journal of Food Science and Technology*. Springer India, 58(6), pp. 2258–2264. doi: 10.1007/s13197-020-04736-4.

Kardys, A. Y., Bharali, D. J. and Mousa, S. A. (2013) 'Amino-functionalized silica nanoparticles: In vitro evaluation for targeted delivery and therapy of pancreatic cancer', *Journal of Nanotechnology*, 2013. doi: 10.1155/2013/768724.

Kim, H. L. *et al.* (2014) 'Enhanced tumor targetability of PEGylated mesoporous silica nanoparticles on in vivo optical imaging according to their size', *RSC Advances*. Royal Society of Chemistry, 4(59), pp. 31318–31322. doi: 10.1039/c4ra03905j.

Ko, J. W. *et al.* (2020) 'Silica dioxide nanoparticles aggravate airway inflammation in an asthmatic mouse model via NLRP3 inflammasome activation', *Regulatory Toxicology and Pharmacology*. Elsevier, 112(August 2019), p. 104618. doi: 10.1016/j.yrtph.2020.104618.

Kumar, R. *et al.* (2010) 'In vivo biodistribution and clearance studies using multimodal organically modified silica nanoparticles', *ACS Nano*, 4(2), pp. 699–708. doi:

10.1021/nn901146y.

Lee, J. G. *et al.* (2020) 'Adsorption of Myoglobin and Corona Formation on Silica Nanoparticles', *Langmuir*, 36(47), pp. 14157–14165. doi: 10.1021/acs.langmuir.0c01613.

Lee, K. I. *et al.* (2020) 'Ultrafine silicon dioxide nanoparticles cause lung epithelial cells apoptosis via oxidative stress-activated PI3K/Akt-mediated mitochondria- and endoplasmic reticulum stress-dependent signaling pathways', *Scientific Reports*, 10(1), pp. 1–13. doi: 10.1038/s41598-020-66644-z.

Leso, V. *et al.* (2019) 'Artificial Stone Associated Silicosis: A Systematic Review.', *International journal of environmental research and public health*. Multidisciplinary Digital Publishing Institute (MDPI), 16(4). doi: 10.3390/ijerph16040568.

Li, H., Raehm, L., Charnay, C., Durand, J. O., & Pleixats, R. (2020) 'Preparation and Characterization of Novel Mixed Periodic Mesoporous Organosilica Nanoparticles.', *Materials*, 13(7), pp. 1–16. doi: https://doi.org/10.3390/ma13071569.

Li, X. *et al.* (2020) 'Surface chemistry governs the sub-organ transfer, clearance and toxicity of functional gold nanoparticles in the liver and kidney', *Journal of Nanobiotechnology*. BioMed Central Ltd., 18(1). doi: 10.1186/s12951-020-00599-1.

Li, Z., Zhang, Y. and Feng, N. (2019) 'Mesoporous silica nanoparticles: synthesis, classification, drug loading, pharmacokinetics, biocompatibility, and application in drug delivery', *Expert Opinion on Drug Delivery*. Taylor & Francis, 16(3), pp. 219–237. doi: 10.1080/17425247.2019.1575806.

Liu, T. *et al.* (2011) 'Single and repeated dose toxicity of mesoporous hollow silica nanoparticles in intravenously exposed mice', *Biomaterials*. Elsevier Ltd, 32(6), pp. 1657–1668. doi: 10.1016/j.biomaterials.2010.10.035.

Luo, W. *et al.* (2019) 'Formation of enzymatic/redox-switching nanogates on mesoporous silica nanoparticles for anticancer drug delivery', *Materials Science and Engineering C*. Elsevier Ltd, 100, pp. 855–861. doi: 10.1016/j.msec.2019.03.028.

Macchi, S. *et al.* (2017) 'Self-aggregation propensity of the Tat peptide revealed by UV-Vis, NMR and MD analyses', *Physical Chemistry Chemical Physics*, 19(35), pp. 23910–23914. doi: 10.1039/c7cp04320a.

Al Mahrooqi, J. H. *et al.* (2018a) 'Controlling the Size of Thiolated Organosilica Nanoparticles', *Langmuir*. American Chemical Society, 34(28), pp. 8347–8354. doi: 10.1021/acs.langmuir.8b01556.

Al Mahrooqi, J. H. *et al.* (2018b) 'Controlling the Size of Thiolated Organosilica

Nanoparticles', *Langmuir*. American Chemical Society, 34(28), pp. 8347–8354. doi: 10.1021/acs.langmuir.8b01556.

Al Mahrooqi, J. H. *et al.* (2018c) 'Controlling the Size of Thiolated Organosilica Nanoparticles', *Langmuir*, 34(28), pp. 8347–8354. doi: 10.1021/acs.langmuir.8b01556.

Mai, N. X. D. *et al.* (2023) 'Engineering biodegradable periodic mesoporous functionalized-organosilica nanocarriers for efficient paclitaxel delivery', *Colloids and Surfaces A: Physicochemical and Engineering Aspects*. Elsevier B.V., 656(PA), p. 130405. doi: 10.1016/j.colsurfa.2022.130405.

Maurel, M. *et al.* (2021) 'Design of PEGylated Three Ligands Silica Nanoparticles for Multi-Receptor Targeting', *Nanomaterials*, 11(1), p. 177. doi: 10.3390/nano11010177.

Mebert, A. M. *et al.* (2017) 'Nanoengineered silica: Properties, applications and toxicity', *Food and Chemical Toxicology*. Elsevier Ltd, 109, pp. 753–770. doi: 10.1016/j.fct.2017.05.054.

Mekaru, H. *et al.* (2019) 'Biodegradability of Disulfide-Organosilica Nanoparticles Evaluated by Soft X-ray Photoelectron Spectroscopy: Cancer Therapy Implications', *ACS Applied Nano Materials*, 2(1), pp. 479–488. doi: 10.1021/acsanm.8b02023.

Mendoza, A. *et al.* (2014) 'Silica nanoparticles induce oxidative stress and inflammation of human peripheral blood mononuclear cells', *Cell Stress and Chaperones*. Cell Stress and Chaperones, 19(6). doi: 10.1007/s12192-014-0502-y.

Mohammadpour, R. *et al.* (2019) 'Subchronic toxicity of silica nanoparticles as a function of size and porosity', *Journal of Controlled Release*. Elsevier, 304(April), pp. 216–232. doi: 10.1016/j.jconrel.2019.04.041.

Moodley, T. and Singh, M. (2019) 'Polymeric Mesoporous Silica Nanoparticles for Enhanced Delivery of 5-Fluorouracil In Vitro', *Pharmaceutics*, 11(6), p. 288. doi: 10.3390/pharmaceutics11060288.

Mun, E. A. *et al.* (2014) 'On the Barrier Properties of the Cornea: A Microscopy Study of the Penetration of Fluorescently Labeled Nanoparticles, Polymers, and Sodium Fluorescein'. doi: 10.1021/mp500332m.

Mun, E. A., Williams, A. C. and Khutoryanskiy, V. V. (2016) 'Adhesion of thiolated silica nanoparticles to urinary bladder mucosa: Effects of PEGylation, thiol content and particle size', *International Journal of Pharmaceutics*, 512(1), pp. 32–38. doi: 10.1016/j.ijpharm.2016.08.026.

Murugadoss, S. *et al.* (2017) 'Toxicology of silica nanoparticles: an update', *Archives of Toxicology*. Springer Verlag, pp. 2967–3010. doi: 10.1007/s00204-017-1993-y.

Nakamura, M. *et al.* (2011) ‘One-pot synthesis and characterization of dual fluorescent thiol-organosilica nanoparticles as non-photoblinking quantum dots and their applications for biological imaging’, *Journal of Materials Chemistry*, 21(12), pp. 4689–4695. doi: 10.1039/c0jm04259e.

Nakamura, M. (2018) *Organosilica Nanoparticles and Medical Imaging*. 1st edn, *Enzymes*. 1st edn. Elsevier Inc. doi: 10.1016/bs.enz.2018.08.002.

Nakamura, M. and Ishimura, K. (2007) ‘Synthesis and characterization of organosilica nanoparticles prepared from 3-mercaptopropyltrimethoxysilane as the single silica source’, *Journal of Physical Chemistry C*, 111(51), pp. 18892–18898. doi: 10.1021/jp075798o.

Nakamura, M. and Ishimura, K. (2008) ‘One-pot synthesis and characterization of three kinds of thiol-organosilica nanoparticles’, *Langmuir*, 24(9), pp. 5099–5108. doi: 10.1021/la703395w.

Nenclares, P. and Harrington, K. J. (2020) ‘The biology of cancer’, *Medicine (United Kingdom)*. Elsevier Ltd, pp. 67–72. doi: 10.1016/j.mpmed.2019.11.001.

Neun, B. W., Ilinskaya, A. N. and Dobrovolskaia, M. A. (2018) ‘Updated method for in vitro analysis of nanoparticle hemolytic properties’, in *Methods in Molecular Biology*. Humana Press Inc., pp. 91–102. doi: 10.1007/978-1-4939-7352-1_9.

Niu, M. *et al.* (2016) ‘Shape-Dependent Genotoxicity of Mesoporous Silica Nanoparticles and Cellular Mechanisms’, *Journal of Nanoscience and Nanotechnology*. American Scientific Publishers, 16(3), pp. 2313–2318. doi: 10.1166/jnn.2016.10928.

P. V. Mohanan and Sudha Kappalli (2023) *Biomedical Applications and Toxicity of Nanomaterials*, *Biomedical Applications and Toxicity of Nanomaterials*. Springer Nature Singapore. doi: 10.1007/978-981-19-7834-0_20.

Pamukcu, A., Kaba, F. and Karaman, D. Sen (2019) ‘Tuning the tensile strength of electrospun fibers by mesoporous silica nanoparticle integration for tissue engineering applications’, in *TIPTEKNO 2019 - Tip Teknolojileri Kongresi*. Institute of Electrical and Electronics Engineers Inc. doi: 10.1109/TIPTEKNO.2019.8895193.

Pan, L., He, Q., Liu, J., Chen, Y., Ma, M., *et al.* (2012) ‘Nuclear-targeted drug delivery of tat peptide-conjugated monodisperse mesoporous silica nanoparticles’, *Journal of the American Chemical Society*, 134(13), pp. 5722–5725. doi: 10.1021/ja211035w.

Pan, L., He, Q., Liu, J., Chen, Y., Zhang, L., *et al.* (2012) ‘Nuclear targeting via TAT on Mesoporous NPs’, *Journal of the American Chemical Society*, 134(13), pp. 5722–5725. doi: 10.1021/ja211035w.

Park, J.-H. *et al.* (2016) 'The Effect of Silica Nanoparticles on Human Corneal Epithelial Cells.', *Scientific reports*. Nature Publishing Group, 6, p. 37762. doi: 10.1038/srep37762.

Passagne, I. *et al.* (2012) 'Implication of oxidative stress in size-dependent toxicity of silica nanoparticles in kidney cells', *Toxicology*. Elsevier Ireland Ltd, 299(2–3), pp. 112–124. doi: 10.1016/j.tox.2012.05.010.

Pérez-Herrero, E. and Fernández-Medarde, A. (2015) 'Advanced targeted therapies in cancer: Drug nanocarriers, the future of chemotherapy', *European Journal of Pharmaceutics and Biopharmaceutics*, 93(March), pp. 52–79. doi: 10.1016/j.ejpb.2015.03.018.

Perez, J. E. *et al.* (2021) 'Transient cell stiffening triggered by magnetic nanoparticle exposure', *Journal of Nanobiotechnology*. BioMed Central, 19(1), pp. 1–13. doi: 10.1186/s12951-021-00790-y.

Picchetti, P. *et al.* (2023) 'Responsive Nucleic Acid-Based Organosilica Nanoparticles', pp. 22896–22902. doi: 10.1021/jacs.3c00393.

Pietschnig, R. (2018) 'Advances and Properties of Silanol - Based Materials'.

Pillai, G. (2014) 'Nanomedicines for Cancer Therapy: An Update of FDA Approved and Those under Various Stages of Development', *SOJ Pharmacy & Pharmaceutical Sciences*. doi: 10.15226/2374-6866/1/2/00109.

Poon, W. *et al.* (2019) 'Elimination Pathways of Nanoparticles', *ACS Nano*, 13(5), pp. 5785–5798. doi: 10.1021/acsnano.9b01383.

R A Cairns, I Harris, S McCracken, T. W. M. (2011) 'Cancer cell metabolism', *Cold Spring Harb Symp Quant Biol*, 76, pp. 299–311. doi: 10.1101/sqb.2011.76.012856.

Rascol, E. *et al.* (2018) 'Biosafety of Mesoporous Silica Nanoparticles', *Biomimetics*. MDPI AG, 3(3), p. 22. doi: 10.3390/biomimetics3030022.

Rodríguez, F. *et al.* (2022) 'Nano-Based Approved Pharmaceuticals for Cancer Treatment: Present and Future Challenges', *Biomolecules*, 12(6), pp. 1–27. doi: 10.3390/biom12060784.

Rosenblum, D. *et al.* (2018) 'Progress and challenges towards targeted delivery of cancer therapeutics', *Nature Communications*. Springer US, 9(1). doi: 10.1038/s41467-018-03705-y.

Roy, I. *et al.* (2005) 'Optical tracking of organically modified silica nanoparticles as DNA carriers: A nonviral, nanomedicine approach for gene delivery', *Proceedings of the National Academy of Sciences*. Proceedings of the National Academy of Sciences, 102(2), pp. 279–284. doi: 10.1073/pnas.0408039101.

Rubio, L. *et al.* (2019) 'Safer-by-design flame-sprayed silicon dioxide nanoparticles: The role of silanol content on ROS generation, surface activity and cytotoxicity', *Particle and Fibre Toxicology*. Particle and Fibre Toxicology, 16(1), pp. 1–15. doi: 10.1186/s12989-019-0325-1.

Salekdeh, P. R. *et al.* (2021) 'Bi-functionalized aminoguanidine-PEGylated periodic mesoporous organosilica nanoparticles: a promising nanocarrier for delivery of Cas9-sgRNA ribonucleoproteine', *Journal of Nanobiotechnology*. BioMed Central, 19(1), pp. 1–16. doi: 10.1186/s12951-021-00838-z.

Shabbir, S. *et al.* (2023) 'Toxicity and Impact of Silica Nanoparticles on the Configuration of Gut Microbiota in Immunodeficient Mice', *Microorganisms*, 11(5). doi: 10.3390/microorganisms11051183.

Shan, X. *et al.* (2022) 'Current approaches of nanomedicines in the market and various stage of clinical translation', *Acta Pharmaceutica Sinica B*. Chinese Pharmaceutical Association and Institute of Materia Medica, Chinese Academy of Medical Sciences, 12(7), pp. 3028–3048. doi: 10.1016/j.apsb.2022.02.025.

Shinde, P. and Prasad, B. L. V. (2021) 'Amphifunctional Mesoporous Silica Nanoparticles with "Molecular Gates" for Controlled Drug Uptake and Release', *Particle and Particle Systems Characterization*, 38(12), pp. 1–10. doi: 10.1002/ppsc.202100185.

Siegel, R. L., Miller, K. D. and Jemal, A. (2020) 'Cancer statistics, 2020', *CA: A Cancer Journal for Clinicians*. Wiley, 70(1), pp. 7–30. doi: 10.3322/caac.21590.

Singh, N., Shi, S. and Goel, S. (2023) 'Ultrasmall silica nanoparticles in translational biomedical research: Overview and outlook', *Advanced Drug Delivery Reviews*. Elsevier B.V., 192, p. 114638. doi: 10.1016/j.addr.2022.114638.

Solorio-Rodríguez, A. *et al.* (2021) 'In vitro cytotoxicity study of superparamagnetic iron oxide and silica nanoparticles on pneumocyte organelles', *Toxicology in Vitro*, 72(November 2020). doi: 10.1016/j.tiv.2020.105071.

Song, H. *et al.* (2022) 'Glutathione-Sensitive Mesoporous Organosilica-Coated Gold Nanorods as Drug Delivery System for Photothermal Therapy-Enhanced Precise Chemotherapy', *Frontiers in Chemistry*, 10(February), pp. 1–10. doi: 10.3389/fchem.2022.842682.

Souris, J. S. *et al.* (2010) 'Surface charge-mediated rapid hepatobiliary excretion of mesoporous silica nanoparticles', *Biomaterials*. Elsevier Ltd, 31(21), pp. 5564–5574. doi: 10.1016/j.biomaterials.2010.03.048.

Spicer, C. D. *et al.* (2018) 'Peptide and protein nanoparticle conjugates: Versatile

platforms for biomedical applications', *Chemical Society Reviews*. Royal Society of Chemistry, pp. 3574–3620. doi: 10.1039/c7cs00877e.

Stöber, W., Fink, A. and Bohn, E. (1968) 'Controlled growth of monodisperse silica spheres in the micron size range', *Journal of Colloid And Interface Science*. Academic Press, 26(1), pp. 62–69. doi: 10.1016/0021-9797(68)90272-5.

Sun, L. *et al.* (2023) 'Smart nanoparticles for cancer therapy', *Signal Transduction and Targeted Therapy*. Springer US, 8(1). doi: 10.1038/s41392-023-01642-x.

Sweeney, A. E. (2015) 'Nanomedicine concepts in the general medical curriculum: Initiating a discussion', *International Journal of Nanomedicine*, 10, pp. 7319–7331. doi: 10.2147/IJN.S96480.

Tacar, O., Sriamornsak, P. and Dass, C. R. (2013) 'Doxorubicin: An update on anticancer molecular action, toxicity and novel drug delivery systems', *Journal of Pharmacy and Pharmacology*, 65(2), pp. 157–170. doi: 10.1111/j.2042-7158.2012.01567.x.

Tamanoi, F. *et al.* (2021) 'Construction of boronophenylalanine-loaded biodegradable periodic mesoporous organosilica nanoparticles for bnct cancer therapy', *International Journal of Molecular Sciences*, 22(5), pp. 1–13. doi: 10.3390/ijms22052251.

Teng, S. *et al.* (2023) 'Swellable hollow periodic mesoporous organosilica capsules with ultrahigh loading capacity for hydrophobic drugs', *Journal of Colloid and Interface Science*. Elsevier Inc., 630, pp. 266–273. doi: 10.1016/j.jcis.2022.10.017.

Thapa, R. K. and Kim, J. O. (2023) 'Nanomedicine-based commercial formulations: current developments and future prospects', *Journal of Pharmaceutical Investigation*. Springer Nature Singapore, 53(1), pp. 19–33. doi: 10.1007/s40005-022-00607-6.

Tian, Z., Xu, Y. and Zhu, Y. (2017) 'Aldehyde-functionalized dendritic mesoporous silica nanoparticles as potential nanocarriers for pH-responsive protein drug delivery', *Materials Science and Engineering C*, 71, pp. 452–459. doi: 10.1016/j.msec.2016.10.039.

Tran, A. V. *et al.* (2018) 'Targeted and controlled drug delivery by multifunctional mesoporous silica nanoparticles with internal fluorescent conjugates and external polydopamine and graphene oxide layers', *Acta Biomaterialia*. Acta Materialia Inc., 74, pp. 397–413. doi: 10.1016/j.actbio.2018.05.022.

Traverso, N. *et al.* (2013) 'Role of glutathione in cancer progression and chemoresistance', *Oxidative Medicine and Cellular Longevity*, 2013. doi: 10.1155/2013/972913.

Tsai, P. H. *et al.* (2019) 'Dual Delivery of HNF4α and Cisplatin by Mesoporous Silica Nanoparticles Inhibits Cancer Pluripotency and Tumorigenicity in Hepatoma-Derived

CD133-Expressing Stem Cells', *ACS Applied Materials and Interfaces*. American Chemical Society, 11(22), pp. 19808–19818. doi: 10.1021/acsami.9b04474.

Vega-Vásquez, P., Mosier, N. S. and Irudayaraj, J. (2020) 'Nanoscale Drug Delivery Systems: From Medicine to Agriculture', *Frontiers in Bioengineering and Biotechnology*. doi: 10.3389/fbioe.2020.00079.

Wang, W. *et al.* (2018) 'The size-dependent effects of silica nanoparticles on endothelial cell apoptosis through activating the p53-caspase pathway', *Environmental Pollution*. Elsevier Ltd, 233, pp. 218–225. doi: 10.1016/j.envpol.2017.10.053.

Ways, T. M. M. *et al.* (2018) 'Synthesis of thiolated, PEGylated and POZylated silica nanoparticles and evaluation of their retention on rat intestinal mucosa in vitro', *European Journal of Pharmaceutical Sciences*. Elsevier, 122(June), pp. 230–238. doi: 10.1016/j.ejps.2018.06.032.

Ways, T. M. M. *et al.* (2020) 'Silica nanoparticles in transmucosal drug delivery', *Pharmaceutics*, 12(8), pp. 1–25. doi: 10.3390/pharmaceutics12080751.

Wu, L. *et al.* (2016) 'Formation of mesoporous silica nanoparticles with tunable pore structure as promising nanoreactor and drug delivery vehicle', *RSC Advances*, 6(16), pp. 13303–13311. doi: 10.1039/c5ra27422b.

Wullkopf, L. *et al.* (2018) 'Cancer cells' ability to mechanically adjust to extracellular matrix stiffness correlates with their invasive potential', *Molecular Biology of the Cell*, 29(20), pp. 2378–2385. doi: 10.1091/mbc.E18-05-0319.

Xiao, D. *et al.* (2014) 'A dual-responsive mesoporous silica nanoparticle for tumor-triggered targeting drug delivery', *Small*, 10(3), pp. 591–598. doi: 10.1002/smll.201301926.

Xiong, L. and Qiao, S. Z. (2016) 'A mesoporous organosilica nano-bowl with high DNA loading capacity-a potential gene delivery carrier', *Nanoscale*. Royal Society of Chemistry, 8(40), pp. 17446–17450. doi: 10.1039/c6nr06777h.

Xu, J. H. *et al.* (2013) 'Gelatin-mesoporous silica nanoparticles as matrix metalloproteinases- degradable drug delivery systems in vivo', *Microporous and Mesoporous Materials*, 182, pp. 165–172. doi: 10.1016/j.micromeso.2013.08.050.

Yang, B., Chen, Y. and Shi, J. (2019a) 'Mesoporous silica/organosilica nanoparticles: Synthesis, biological effect and biomedical application', *Materials Science and Engineering R: Reports*, 137(February), pp. 66–105. doi: 10.1016/j.mser.2019.01.001.

Yang, B., Chen, Y. and Shi, J. (2019b) 'Mesoporous silica/organosilica nanoparticles: Synthesis, biological effect and biomedical application', *Materials Science and*

Engineering R: Reports, 137(January), pp. 66–105. doi: 10.1016/j.mser.2019.01.001.

Yang, H. *et al.* (2009) 'Comparative study of cytotoxicity, oxidative stress and genotoxicity induced by four typical nanomaterials: The role of particle size, shape and composition', *Journal of Applied Toxicology*, 29(1), pp. 69–78. doi: 10.1002/jat.1385.

Yang, H. *et al.* (2019) 'MiRNA-204-5p and oxaliplatin-loaded silica nanoparticles for enhanced tumor suppression effect in CD44-overexpressed colon adenocarcinoma', *International Journal of Pharmaceutics*. doi: 10.1016/j.ijpharm.2019.06.020.

Yanjun Jiang, Huan Liu, Lihui Wang, Liya Zhou, Zhihong Huang, Li Ma, Ying He, Lujing Shi, J. G. (2019) 'Virus-like organosilica nanoparticles for lipase immobilization: Characterization and biocatalytic applications', *Biochemical Engineering Journal*, 144, pp. 125–134. doi: https://doi.org/10.1016/j.bej.2019.01.022.

Yu, L. *et al.* (2018) 'Multifunctional Mesoporous Silica Nanoprobes: Material Chemistry–Based Fabrication and Bio-Imaging Functionality', *ADVANCED THERAPEUTICS*. Wiley, 1(8), p. 1800078. doi: 10.1002/adtp.201800078.

Zhang, H. *et al.* (2021) 'Co-delivery of nanoparticle and molecular drug by hollow mesoporous organosilica for tumor-activated and photothermal-augmented chemotherapy of breast cancer', *Journal of Nanobiotechnology*. BioMed Central, 19(1), pp. 1–13. doi: 10.1186/s12951-021-01025-w.

Zhang, Q. *et al.* (2014) 'Functionalized Mesoporous Silica Nanoparticles with Mucoadhesive and Sustained Drug Release Properties for Potential Bladder Cancer Therapy', *Langmuir*, 30(21), pp. 6151–6161. doi: 10.1021/la500746e.

Zhang, X. *et al.* (2018) 'Quantification of Lipid Corona Formation on Colloidal Nanoparticles from Lipid Vesicles', *Analytical Chemistry*. American Chemical Society, 90(24), pp. 14387–14394. doi: 10.1021/acs.analchem.8b03911.

Van Zundert, I. *et al.* (2021) 'Versatile and robust method for antibody conjugation to nanoparticles with high targeting efficiency', *Pharmaceutics*. MDPI, 13(12). doi: 10.3390/pharmaceutics13122153.